

AALBORG UNIVERSITY

FATIGUE BEHAVIOR AND RELIABILITY OF HIGH STRENGTH CONCRETE

MASTER THESIS
STRUCTURAL AND CIVIL ENGINEERING



TURNED IN:
10/06/2015
SCHOOL OF ENGINEERING AND SCIENCE

© Aalborg University, Spring 2015

René M. M. Slot, and Tias Andersen

The content of this report is freely accessible

Frontpage picture from <http://www.caer.uky.edu>

This report is typeset in Times New Roman 11pt.

Layout and typography by the authors using L^AT_EX.

AALBORG UNIVERSITY
STUDENT REPORT

Master Thesis
at the School of Civil Engineering

Sofiendalsvej 9-11
9200 Aalborg SV
Telephone 9940 8484
Fax 9940 8552
<http://www.ses.aau.dk/>

Synopsis:

In this report fatigue behavior and reliability of concrete, in compression-compression, is investigated and a failure surface for high strength concrete is developed. The report is divided into two parts, respectively: Fatigue in Concrete and Reliability and Uncertainty.

In part I a detailed description of how Eurocode, MC1990, MC2010 and DNV assesses fatigue in concrete loaded in compression-compression is made. Further the data that is acquired to develop the failure surface is presented, and the mathematical description of the developed failure surface is elucidated.

In part II the reliability levels of the presented codes are investigated. For this purpose two design cases are considered, namely the design of a bridge section and the design of a wind turbine foundation. Design equations for the chosen codes are presented, and two different limit state equations are presented. This leads to a calibration of the material partial safety factors for the codes.

A sensitivity study of the limit state equations are carried out to determine which stochastic variables are more important.

Lastly a discussion and a conclusion is presented, which sums up the choices, assumption and results of the report.

Title:

Fatigue Behavior and Reliability of Concrete

Project period:

Feb. 2015 - Jun. 2015

Supervisors:

John Dalgaard Sørensen
Henrik Stensgaard Toft

Report circulation: 5

Report page numbers: 114

Appendix page numbers: 35

Turned in: 10th june 2015

Participants:

René M. M. Slot

Tias Andersen

Sammenfatning

Idet styrken på beton hele tiden er i udvikling, er der en tendens til at de byggerier, der laves af beton, bliver slankere i forhold til tidligere. Dette gør, at udmattelse i beton i højere grad er en problemstilling, bygningsingeniører bliver nødt til at forholde sig til.

Denne rapport er rettet mod udmattelse og sikkerhed i højstyrke beton, der er udsat for tryk-tryk spændingscykler. Rapporten er opdelt i to dele hhv. "*Fatigue in Concrete*" og "*Reliability and Uncertainty*". I den første del af rapporten præsenteres der hvilke faktorer, der menes at have en indflydelse på udmattelsen af beton. Herefter undersøges der, hvordan fire udvalgte standarder anbefaler, at der dimensioneres for udmattelse af beton. De udvalgte standarder er hhv. Eurocode, MC1990, MC2010 og DNV. For at finde ud af forskelle og ligheder ved de fire standarder, laves der en sammenligning af de modeller, der bruges til at modelere udmattelsen af beton. Herudover sammenlignes de effekter der inkluderes ved design, for at undersøge om standarderne tager højde for det samme.

På baggrund af data, der repræsenterer over 400 udmattelses tests af højstyrke beton, vil der blive opstillet en matematisk model, der beskriver udmattelse af højstyrke beton. Modellen er baseret på den traditionelle teori bag *SN*-kurver, der også er brugt i de udvalgte standarder.

I den anden del af rapporten laves der en analyse af de sikkerheder, der opnåes ved at bruge de undersøgte standarder, til at designe for udmattelse i beton. Analysen er baseret på de data, der er presenteret i rapporten. I analysen undersøges to design tilfælde, hhv. en tofags bro udst for trafiklast og et fundament til en vindmølle, der er udsat for vindlast. I slutningen af rapporten er der en diskussion og en konklusion, der opsummerer, de resultater der er opnået igennem rapporten. I diskussionen vil der også være forslag til, hvordan undersøgelserne i rapporten kunne være forbedret.

Preface

This report presents the master thesis made by René M. M. Slot and Tias Andersen, at Aalborg University in the *Structural and Civil Engineering* master program. The subject is "*Fatigue Behavior and Reliability of Concrete*" with focus on high strength concrete. The project was made in the period 1-02-2015 to 10-06-2015. A show of gratitude is extended towards our supervisors, John Dalsgaard Sørensen and Henrik Stensgaard Toft.

Reading Guidelines

The project is divided into two parts: *Fatigue in Concrete* and *Reliability and Uncertainty*. At the start of each part a short introduction to the content is given.

Important appendixes coupled to the report are found at the back of the report. A digital appendix is placed on a CD attached to the report. The digital appendix contains *MATLAB* scripts and the report as a PDF version.

References throughout the report are collected in a bibliography at the back of the report, where all the sources of knowledge are mentioned with the needed data. Sources are presented using the *Harvard Method*, wherein a reference is given as: [Author, Year].

In this report "*CEB-FIP MODEL CODE 1990*" is referred to as MC1990 while while "*CEB-FIP MODEL CODE 2010*" is referred to as MC2010.

In each chapter of the main report, tables, pictures, and equations are used. They are given a reference numbers, starting with the number of the chapter. For equations the numbering will only occur if the equation has been referred to. Also commentary text is added below figures/tables for easier understanding for the reader.

Structure of Report

Figure 1 shows a flow chart of structure of the report to give an overview of the report.

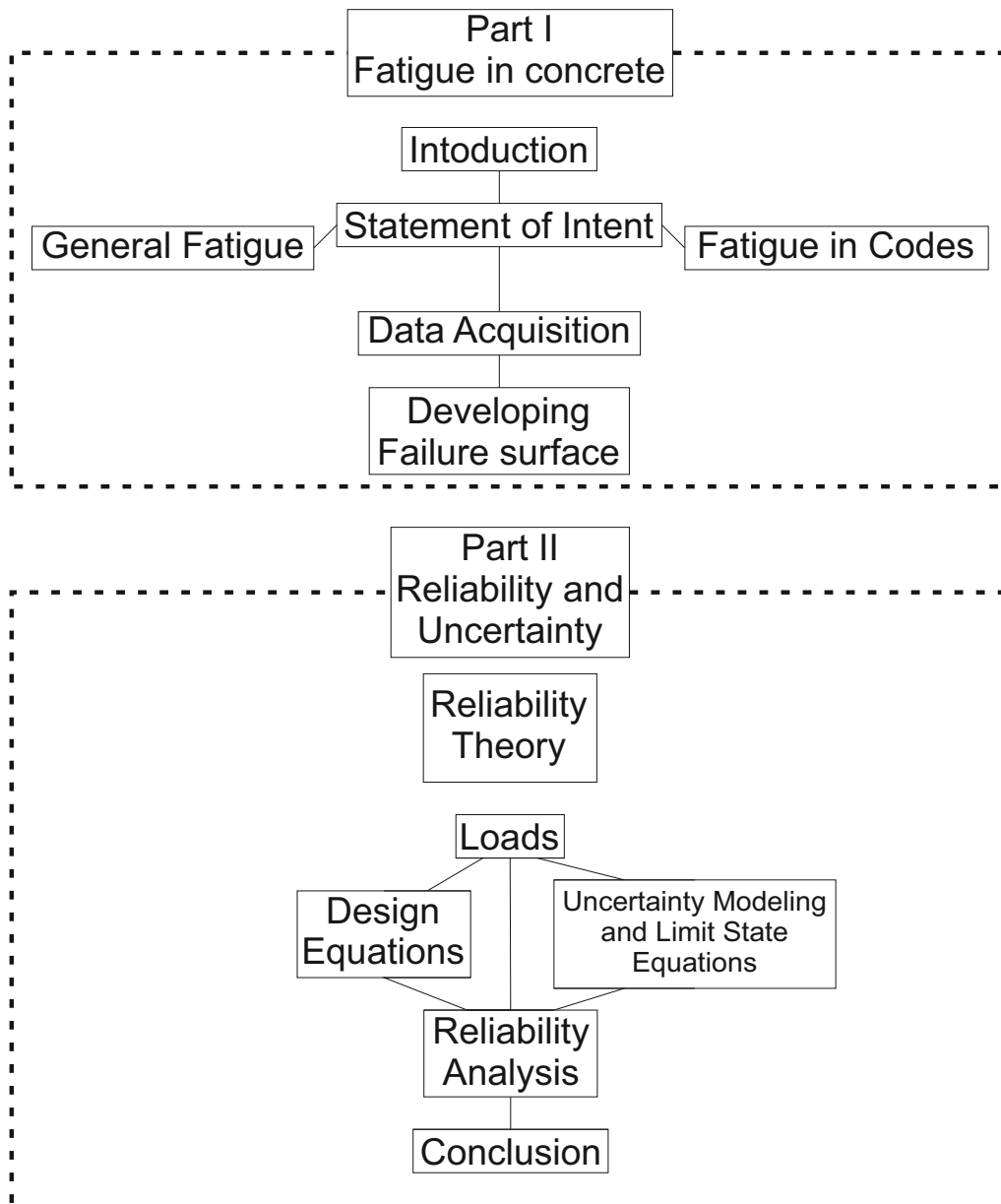


Figure 1. The structure of the report illustrated with a flow chart diagram.

Contents

Preface	v
Reading Guidelines	v
Part I - Fatigue in Concrete	1
1 Introduction	3
1.1 Statement of Intent	4
2 General fatigue in concrete	7
2.1 Factors Influencing Fatigue Behavior of Concrete	8
3 Fatigue of Concrete in Compression in Codes	11
3.1 Eurocode	11
3.2 MC1990	14
3.3 MC2010	17
3.4 DNV	20
3.5 IEC	23
3.6 Comparison	24
3.7 Comparison of <i>SN</i> -Curves	27
4 Data Acquisition	33
4.1 Data from "Structural Concrete"	33
4.2 Data series 3	39
4.3 Comparing Data with Material Models from Codes	40
5 Developing Fatigue Failure Surface of Concrete	43
5.1 Mathematical Description of the Failure Surface	43
5.2 Dependency of Concrete Strength	52
5.3 Validation of Failure Surface	54
5.4 Comparison Between Developed Surface and those used in the Investigated Codes	55

Part II - Reliability and Uncertainty	59
6 Reliability Theory	61
6.1 General reliability theory	61
7 Loads	67
7.1 Bridge	67
7.2 Wind Turbine Foundation	73
8 Design Equations	75
8.1 Effects that are not Considered in Design Equations	76
8.2 Eurocode	77
8.3 MC1990 and MC2010	78
8.4 DNV	80
8.5 Comparison	81
9 Uncertainty Modeling and Limit State Equations	83
9.1 General Stochastic Variables	83
9.2 Limit State Equation	86
9.3 Limit State Equation LSE 2	92
10 Reliability Analysis	95
10.1 Reliability Level in Codes	95
10.2 Target Design Parameters	99
10.3 Calibrating Partial Safety Factors	100
10.4 Sensitivity Analysis	102
11 Discussion	109
12 Conclusion	111
Bibliography	113
Appendix	117
A Maximum likelihood method	117
B Data	121
C Failure Surface	125
D Uncertainty Modeling	129

Part I

Fatigue in Concrete

In this part of the report general fatigue theory used throughout the report is presented, and factors effecting the fatigue life of concrete are outlined.

Furthermore selected codes are investigated with respect to how they assess fatigue in concrete, for stress cycles in compression-compression. This investigation is used as basis for the reliability investigation, that is to be carried out.

All the data that is used throughout the report is then presented. As some of the data is acquired through digitalizing plots it is validated against the original plots.

The acquired data is used to develop a failure surface, that aims to capture the data as accurately as possible. The failure surface is developed as it is used in the second part of the report, to assess the reliability of the presented codes.

Introduction

Concrete is an old building material. It was used by the Romans to erect their great buildings, where some still exists today e.g. the Pantheon. From the beginning of the use of concrete it was recognized as a versatile and cheap building material. Because of this it was used in great scale by the Romans. After the fall of the Roman empire the knowledge of how to produce concrete was lost, until 1824 where Portland cement was invented. Around 1890 concrete began to be used in civil engineering where reinforcement of the concrete was introduced. This gave birth to a revolution in architecture and structural engineering, where the nature of concrete was used to shape buildings as desired.[DANSKE, 2015]

To this day concrete is still recognized as a great building material, which plays an important role in the society we live in. It is present in everyday life for all of us as it is used to build our schools, apartment blocks, bridges, sewage systems, roads and much more.

Basically concrete is an "artificial stone" that is created by mixing cement, sand and aggregate with water. Concrete can withstand great compressive stresses, but is relatively weak for tensile stresses. Due to the poor tensile properties it is common to reinforce the concrete with steel rods.

In the more recent decades concrete has become stronger and stronger. Where the conventional concrete compressive strength varies from 20 MPa to 40 Mpa, the new ultra high strength concrete has compressive strengths that varies from 130 MPa to 150 MPa, and some concretes has an even higher compressive strength. [Manufacturers, 2015]

Due to the increase in concretes strength it has become even more effective as a building material for high-rise buildings and bridges. As an example parts of the Great Belt Bridge is made of concrete, e.g. the piers, anchor blocks and abutment were made with high performance concrete. Even the 254 m high pylons of the actual suspension bridge were made using high performance concrete and they are amongst the highest points in Denmark which is illustrated on figure 1.1.



Figure 1.1. Picture of the Great Belt Bridge [Storebaelt, 2015].

As the strength of concrete increases the structures has a tendency to become more slender and lighter, whereas concrete constructions traditionally were bulky structures. Due to the larger range of the uses of concrete as a building material and the increasing slenderness of the structures made of concrete, fatigue is more frequently a problem. This raises the attention of the fatigue behavior of high strength concrete, which will be the focus in this report.

1.1 Statement of Intent

In recent years there has been a rapid development in improving the strength of concrete. As the concrete has improved, the methods of designing fatigue loaded concrete structures has not necessarily developed accordingly. Due to this the safety of the design codes has to be assessed. This leads to the following statement of intent.

This report will investigate how the fatigue behavior of high strength concrete is assessed in different codes and evaluate the reliability level of these. To assess the reliability of the design from the codes an accurate fatigue failure surface is to be developed based on high strength concrete fatigue tests. The mathematical description of the failure surface should follow the the traditional fatigue theory of SN-curves. A reliability study is then to be carried out with focus on the partial safety factors that are used in the current standards.

1.1.1 Delimitation

Due to the data used in this report the developed failure surface will not take tension or shear of the concrete into consideration.

Fatigue behavior of reinforcement steel is not included in the report even though it can be important in practical applications.

All the loads are assumed time independent so an increase in e.g. traffic loads are not included in the load model.

For low cycle fatigue a stress analysis might not be sufficiently accurate, however a strain analysis is not included in the report.

When relevant design codes are evaluated only normal weight aggregates are considered.

General fatigue in concrete

In this chapter the general fatigue theory that is used in this report is presented. In any material a fatigue failure can be characterized as a failure that occurs below the static stress limit after being exposed to repeated loading. When evaluating the fatigue strength or fatigue life of a detail, the SN-curve is a useful tool. The SN-curve describes the relation between the stress ranges, ΔS , and the number of cycles to failure, N , see figure 2.1.

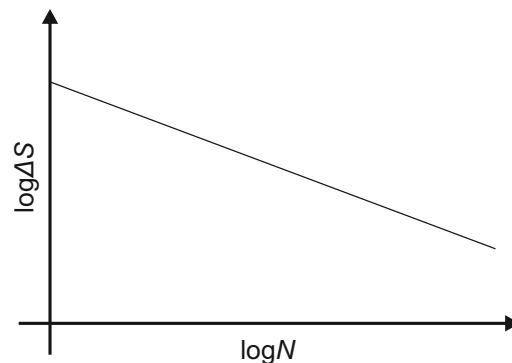


Figure 2.1. Sketch of a linear SN-curve depicted in a log-log diagram.

Often a structure is subjected to a number of different stress ranges or a spectrum of stress ranges. When this is the case, Miner's rule for damage accumulation can be used to combine the damage from each stress range, see eq. (2.1).

$$\Delta \geq \sum_{i=1}^k \frac{n_i}{N_i} \quad (2.1)$$

Where N_i is the number of cycles to failure for stress range i which can be determined using a SN-curve. n_i is the actual number of cycles which the system is subjected to at stress range i . Δ is the upper limit to the damage which the system can sustain before failure, which for a deterministic design is usually set to 1.0. It can be seen that Miner's rule accumulates the fatigue damage of the different stress states in a linear manner. It has to be noted that Miner's rule was determined on carved aluminium alloys and therefore it cannot be used on concrete without verification of its validity. Such verification has been pointed

out in [EuroLightCon, 2000], where variable amplitude tests with programmed loading have been executed. The results of the tests showed sufficient validity of Miner's rule when used on concrete. Furthermore the investigations made in [EuroLightCon, 2000] concludes that Δ is lognormal distributed for concrete and that the scatter is generally the same whether constant or variable amplitude loads are used in tests. This conclusion is important as it to some extent justifies using test results made at constant amplitude loading, to describe fatigue behavior of concrete structures subjected to e.g. wind- and waveloads that are random.

2.1 Factors Influencing Fatigue Behavior of Concrete

The fatigue behavior of concrete is influenced by many factors including frequency, environment, concrete strength, mean stresses, adding steel fibres and wave forms. Furthermore it is important if the fatigue loading is compression-compression, tension-tension or tension-compression, however in this report only uniaxial compression-compression is investigated.

2.1.1 Frequency

The frequency at which concrete is loaded is of most importance if the stress ratio with respect to the compressive strength is above 75 %. It has been shown that below this stress ratio frequencies in the range from 1 up to 15 Hz has almost no influence on the fatigue life. If the stress ratio is above 75 % of the compressive strength the fatigue strength will decrease with decreasing frequency. The effect occurs due to creep in the concrete, as the lower frequencies will induce a load on the concrete for a longer time period within each cycle.[EuroLightCon, 2000]

2.1.2 Environment

The environment where the concrete is tested is important, as studies has shown that concrete submerged in water has a lower fatigue life than dry concrete [Sørensen]. The decrease in fatigue life when the concrete is wet, can occur as stresses can build up in the micro cracks due to the presence of water. Additionally the water might initiate some transportation of sediment when the water moves through the cracks of the concrete. It is also shown in [Sørensen] that the load frequency have a larger effect on the fatigue life for wet concrete compared to dry concrete.

Furthermore, other external environmental processes can have an effect on the fatigue life, e.g. frost in the concrete, salinity etc.

2.1.3 Concrete strength

The fatigue life of concrete has in some research been shown to be dependent on its compressive strength. In e.g. [Kim and Kim, 1996] it is concluded that when the compressive strength rises the fatigue strength gets relatively lower. However it is not conclusive that the fatigue behavior of concrete is dependent on the compressive strength, as some research has not shown this effect.

2.1.4 Mean stresses

For concrete the mean stresses of the cyclic loading are of importance when calculating the fatigue life. As a result the SN -curves for concrete will be dependent on both the maximum and minimum stress ratio and the number of cycles. This effect is generally accepted and has been documented in various research papers.

2.1.5 Adding steel fibres

When adding steel fibres to a concrete mix the compressive strength will increase. However by adding steel fibres the fatigue strength of the concrete can be lower compared to the same type of concrete without fibres. This is e.g. shown in [Lohaus et al., 2012].

2.1.6 Wave forms

In a test program it has been proved that the fatigue behavior of concrete is dependent on whether the waveform of the load is sinusoidal, rectangular or triangular, see figure 2.2.

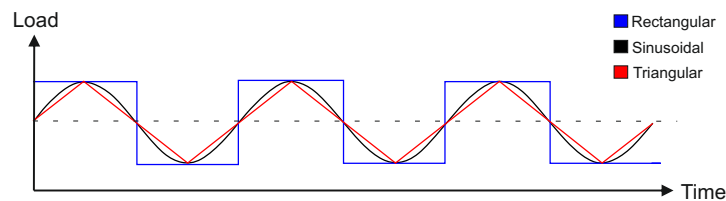


Figure 2.2. Illustration of a rectangular, sinusoidal and triangular wave. The dotted line represents the mean value of the waves.

In the test it was found that the rectangular waveform is more damaging than the sinusoidal, and the triangular was least damaging. The explanation for the rectangular waveform to be the worst is that it is exposed to high load levels for a longer time period, compared to the sinusoidal or triangular [EuroLightCon, 2000]. It is noted that only in some special cases the load form will be different than a sinusoidal. Traffic load over a bridge, wave loads and wind loads are all examples of sinusoidal loads which are all very common in design.

Fatigue of Concrete in Compression in Codes

In this chapter the models used to calculate the assess the fatigue limit state, of concrete under uniaxial compression-compression fatigue actions, in various codes are presented and compared. The investigated codes are also used throughout the reliability analysis that is presented in part II of the report.

3.1 Eurocode

In EN 1992-1-1 a simplified procedure is presented to verify the fatigue limit state of concrete for buildings which is outlined in this section. Furthermore EN 1992-2 presents an expression for a failure surface that can be used to evaluate the fatigue life of concrete bridges, which is also described in this section. As this report is prepared in Denmark the Danish National Annexes are used in addition to the relevant Eurocodes.

3.1.1 EN 1992-1-1

In EN 1991-1-1 it is stated that the fatigue limit state of concrete buildings is satisfied if eq. (3.1) is fulfilled.

$$\frac{\sigma_{c,max}}{f_{cd,fat}} \leq 0.5 + 0.45 \frac{\sigma_{c,min}}{f_{cd,fat}} \leq \begin{cases} 0.9 & \text{for } f_{ck} \leq 50 \text{ MPa} \\ 0.8 & \text{for } f_{ck} > 50 \text{ MPa} \end{cases} \quad (3.1)$$

where

$\sigma_{c,max}$	Maximum stress
$\sigma_{c,min}$	Minimum stress
f_{ck}	Characteristic compressive strength of the concrete taken as the 5th percent quantile of the 28 days cylinder compressive strength [MPa]
$f_{cd,fat}$	The fatigue design strength determined by eq. (3.2)

$$f_{cd,fat} = k_1 \beta_{cc}(t_0) f_{cd} \left(1 - \frac{f_{ck}}{250} \right) \quad (3.2)$$

Where

$\beta_{cc}(t_0)$	Coefficient that takes the age of the concrete into account, see eq. (3.3)
t_0	
f_{cd}	
k_1	
	Time where the cyclic loading starts [days]
	Design compressive strength of the concrete found by eq. (3.4) [MPa]
	Coefficient that takes long term effects into account. Recommended value in EN 1992-1-1 and EN 1992-2 is 0.85

It can be seen from eq. (3.2), that if the characteristic strength of the concrete is larger than 125 MPa the fatigue strength will decrease. It is noted that the input strengths in eq. (3.2) has to be in MPa as f_{ck} is divided by 250 which implicitly has this unit.

$$\beta_{cc}(t) = e^s \left(1 - \left(\frac{28}{t}\right)^{0.5}\right) \quad (3.3)$$

Where

s | Coefficient that take the cement type into account

$$f_{cd} = \alpha_{cc} \frac{f_{ck}}{\gamma_{C,fat}} \quad (3.4)$$

Where

$\gamma_{C,fat}$	Partial safety factor for concrete
α_{cc}	
	Factor taking into account long term effects on compressive strength and unfavorable effects from the way the load is applied

In accordance with EN 1992-1-1 and DK NA EN 1992-2 α_{cc} can be set to 1.0. For normal reinforced concrete structures $\gamma_{C,fat}$ can found by eq. (3.5) in accordance with DK NA EN 1992-1-1.

$$\gamma_{C,fat} = 1.1 \cdot 1.45 \gamma_3 \quad (3.5)$$

Where

γ_3 | Partial safety factor taking account of the control class.
The recommended value in DK NA EN 1992-1-1 for normal control class is 1.0

3.1.2 EN 1992-2

In EN 1992-2 an expression of a failure surface is given for verification of fatigue, in compression-compression, for concrete bridges. The model uses Miner's rule with $\Delta = 1$ to account for damage accumulation, where the number of allowed cycles for a given stress state, i , can be found by eq. (3.6).

$$N_i = 10 \left(14 \frac{1 - E_{cd,max,i}}{\sqrt{1 - R_i}} \right) \quad (3.6)$$

Where

$E_{cd,max,i}$	Maximum stress in bin i normalized with the fatigue strength, found by eq. (3.7)
$E_{cd,min,i}$	Minimum stress in bin i normalized with the fatigue strength, found by eq. (3.8)
R_i	Ratio between minimum stress and maximum stress in bin i , found by eq. (3.9)

$$E_{cd,max,i} = \frac{\sigma_{cd,max,i}}{f_{cd,fat}} \quad (3.7)$$

$$E_{cd,min,i} = \frac{\sigma_{cd,min,i}}{f_{cd,fat}} \quad (3.8)$$

$$R_i = \frac{E_{cd,min,i}}{E_{cd,max,i}} \quad (3.9)$$

Where

$f_{cd,fat}$	Defined as in EN 1992-1-1
$\sigma_{cd,max,i}$	Maximum design stress in bin number i found by eq. (3.10)
$\sigma_{cd,min,i}$	Minimum design stress in bin number i found by eq. (3.11)

$$\sigma_{cd,max,i} = \gamma_{F,fat} \sigma_{c,max,i} \quad (3.10)$$

$$\sigma_{cd,min,i} = \gamma_{F,fat} \sigma_{c,min,i} \quad (3.11)$$

Where

$\gamma_{F,fat}$	Partial safety factor for fatigue loads. Recommended value found as 1.0 in EN 1992-1-1
------------------	---

On figure 3.1 design SN -curves from Eurocode are shown for two different concrete strengths. For simplicity it is assumed that it is a normal reinforced concrete structure with normal control class. All values are taken as the recommended ones, the stress ratio, R , is set to 0.2 and $\beta_{cc} = 1.0$.

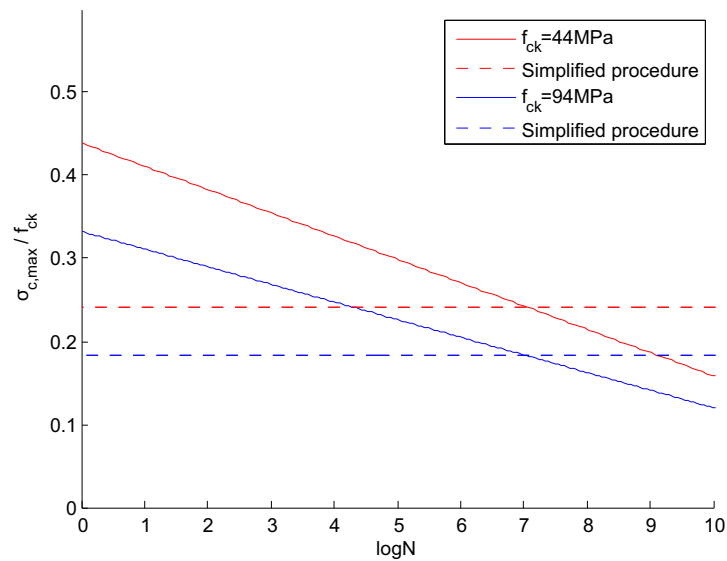


Figure 3.1. Design SN-curves from EN 1992-2 for the chosen example using two different concrete strengths. The dotted lines represent the procedure from EN 1992-1-1.

On the y -axis $\sigma_{c,max}$ normalized with f_{ck} is depicted to clearly show how the fatigue strength of concrete decreases relatively as the compressive strength increases. $\sigma_{c,max}$ is used instead of $\sigma_{cd,max}$ to efficiently comparing the SN-curves from different codes, which is explained further in section 3.6.

For the chosen example it can be seen that the simplified procedure presented in EN 1992-1-1 is safer than the SN-curves from EN 1992-2, as long as the amount of cycles does not exceed approximately 10^7 . It is noted that only the first limit in eq. (3.1) is shown on the figure as the second limit shown in eq. (3.1) is above 1.0 on the y -axis which is not relevant.

3.2 MC1990

MC1990 is intended to serve as a basis for the design of buildings and civil engineering structures using structural concrete with normal weight aggregate. It does not treat any particular types of civil engineering works specifically, and due to its international character, it can be considered more general than national codes.

Three methods are introduced in MC1990 to verify the fatigue limit state of concrete in uniaxial compression-compression. First a simplified procedure is described. Then a verification by means of a single load level is introduced if the simplified method is not adequate. Last a method is introduced that can estimate the fatigue damage if the fatigue life has to be evaluated for a spectrum of load levels.

3.2.1 Simplified procedure

The simplified procedure states that if eq. (3.12) is satisfied no further fatigue investigations are necessary. This procedure has a limited use as only one load level can be represented, and it is also a requirement that there are less than 10^8 cycles.

$$\gamma_{Sd} \sigma_{c,max} \eta_c \leq 0.45 f_{cd,fat} \quad (3.12)$$

Where

γ_{Sd}	Partial safety factor for maximum design stress. Recommended value in MC1990 is 1.1
$\sigma_{c,max}$	Maximum compressive stress
η_c	Stress gradient factor found by eq. (3.13)
$f_{cd,fat}$	Fatigue design reference strength of the concrete

$$\eta_c = \frac{1}{1.5 - 0.5 \frac{\sigma_{c1}}{\sigma_{c2}}} \quad (3.13)$$

Where

σ_{c1}	Minimum compressive stress within 300 mm from the surface, see figure 3.2
σ_{c2}	Maximum compressive stress within 300 mm from the surface, see figure 3.2

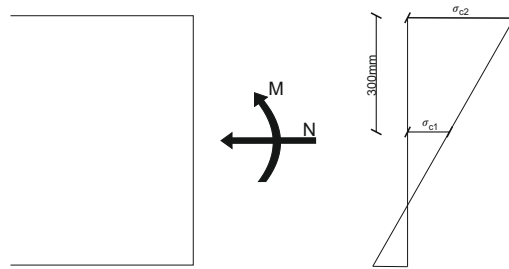


Figure 3.2. Definition of the stresses, σ_{c1} and σ_{c2} .

The fatigue design reference strength $f_{cd,fat}$ can be found by eq. (3.14).

$$f_{cd,fat} = 0.85 \beta_{cc}(t) \frac{f_{ck} \left(1 - \frac{f_{ck}}{25 f_{ck0}}\right)}{\gamma_c} \quad (3.14)$$

Where

$\beta_{cc}(t)$	Coefficient that takes the age of the concrete into account. Determined by eq. (3.15) which is similar to that of Eurocode
f_{ck}	Characteristic compressive strength of the concrete taken as the 5th percent quantile of the 28 days cylinder compressive strength [MPa]
f_{ck0}	Reference strength of 10 MPa
γ_c	Partial safety factor for concrete strength. Recommended value in MC1990 is 1.5

$$\beta_{cc}(t) = e^s \left(1 - \left(\frac{28}{t/t_1}\right)^{0.5}\right) \quad (3.15)$$

Where

s	Coefficient that depends on the type of cement
t_1	1 day
t	Age of concrete [given in days] adjusted with eq. (3.16)

$$t = \sum_{i=1}^n \Delta t_i e^{\left(13.65 - \frac{4000}{273 + \frac{T(\Delta t_i)}{T_0}}\right)} \quad (3.16)$$

Where

t	Temperature adjusted concrete age
Δt_i	Number of days where temperature T prevails
$T(\Delta t_i)$	Temperature during time period Δt_i [$^{\circ}\text{C}$]
T_0	1 $^{\circ}\text{C}$
n	Number of intervals with constant temperature

It is noted that the strength increase from β_{cc} is neglected after start of fatigue loading.

3.2.2 Verification by means of a single load level

If it cannot be shown that a concrete detail satisfy the limit of the simplified procedure a second more refined method is introduced in MC1990. However as for the simplified procedure this method is limited to a repetition of a single load level only.

In Eq. (3.17) a failure surface is described which should be used for the second method. If $S_{cd,min} \geq 0.8$ the relations for $S_{cd,min} = 0.8$ should be used.

For $0 < S_{cd,min} < 0.8$

$$\log(N) = \begin{cases} \log N_1 & \text{if } \log N_1 \leq 6 \\ \log N_2 & \text{if } \log N_1 > 6 \text{ and } \Delta S_{cd} \geq 0.3 - 0.375 S_{cd,min} \\ \log N_3 & \text{if } \log N_1 > 6 \text{ and } \Delta S_{cd} < 0.3 - 0.375 S_{cd,min} \end{cases} \quad (3.17)$$

Where

$$\begin{aligned} \log N_1 &= (12 + 16 S_{cd,min} + 8 S_{cd,min}^2) (1 - S_{cd,max}) \\ \log N_2 &= 0.2 \log N_1 (\log N_1 - 1) \\ \log N_3 &= \log N_2 \frac{0.3 - 0.375 S_{cd,min}}{\Delta S_{cd}} \end{aligned}$$

Where

$$S_{cd,max} = \frac{\gamma S_d \sigma_{c,max} \eta_c}{f_{cd,fat}} \quad (3.18)$$

$$S_{cd,min} = \frac{\gamma S_d \sigma_{c,min} \eta_c}{f_{cd,fat}} \quad (3.19)$$

$$\Delta S_{cd} = S_{cd,max} - S_{cd,min}$$

In figure 3.3 SN -curves from MC1990 are shown for the same concrete strengths that was used to illustrate the SN -curves from Eurocode. All coefficients are taken as the recommended and β_{cc} is set to 1.0. Furthermore η is set to 1.0 for uniform compression and the stress ratio, R , is set to 0.2.

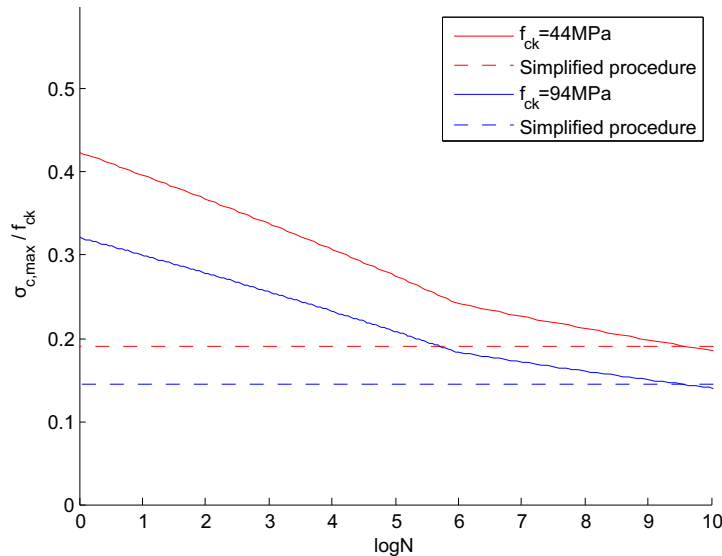


Figure 3.3. SN -curves from MC1990 for two different concrete strengths. The dotted lines represent the simplified procedure for the two strengths.

As for Eurocode it can be seen that, in the chosen example, the fatigue strength is relatively decreasing as the compressive strength increases. Furthermore it can be seen that for the chosen example the simplified procedure gives a sufficiently safe result as it crosses the SN -curves after $\log N = 8$. However it is noted that by decreasing the R -value, the $\log N$ value of the crossings will decrease as well. In this example if R were decreased below approximate 0.05 the crossing would be below $\log N = 8$.

3.2.3 Verification by means of spectrum of load levels

If a spectrum of load levels is acting on the concrete detail MC1990 uses Miner's rule to accumulate the damage. If an appropriate counting method, e.g. Rain-flow counting, has been chosen the damage limit, Δ , can normally be set to 1.0 [fip, 1990].

3.3 MC2010

MC2010 has the same purpose and application as the MC1990 model code. In MC2010 the same three procedures are introduced as in MC1990, and the characteristic compressive strength of concrete is defined as in MC1990 and Eurocode.

3.3.1 Simplified procedure

The simplified procedure can only be used for $\log N < 8$ which was also a requirement in MC1990. For the simplified procedure eq. (3.20) is used which is

similar to that in MC1990.

$$\gamma_{Ed} \sigma_{c,max} \eta_c \leq 0.45 f_{cd,fat} \quad (3.20)$$

γ_{Ed} is the same as γ_{Sd} from MC1990 just with a different notation. The fatigue reference strength, $f_{cd,fat}$, is changed compared to MC1990, see eq. (3.21)

$$f_{cd,fat} = 0.85 \beta_{cc}(t) \frac{f_{ck} \left(1 - \frac{f_{ck}}{40 f_{ck0}}\right)}{\gamma_{c,fat}} \quad (3.21)$$

Where

$$\gamma_{c,fat} \left| \begin{array}{l} \text{Partial safety factor for fatigue strength of concrete with a value of 1.5} \\ \text{according to MC2010} \end{array} \right.$$

With this change to $f_{cd,fat}$ the fatigue strength of concrete will be increasing until 200 MPa instead of only 125 MPa as in Eurocode and MC1990.

3.3.2 Verification by means of a single load level

For this method the only thing that has changed in MC2010 compared to MC1990 is the failure surface used to find N , see eq. (3.22)

$$\log(N) = \begin{cases} \log N_2 = 8 + \frac{8 \ln(10)}{Y-1} (Y - S_{cd,max}) \log \left(\frac{S_{cd,max} - S_{cd,min}}{Y - S_{cd,min}} \right) & \text{if } 8 \leq \log N_1 \\ \log N_1 = \frac{8}{Y-1} (S_{cd,max} - 1) & \text{if } 8 \geq \log N_1 \end{cases} \quad (3.22)$$

$S_{cd,min}$ and $S_{cd,max}$ are found as in MC1990. Y describes the relation between $S_{cd,min}$ and $S_{cd,max}$ at $\log N = 8$ and is given by eq. (3.23).

$$Y = \frac{0.45 + 1.8 S_{cd,min}}{1 + 1.8 S_{cd,min} - 0.3 S_{cd,min}^2} \quad (3.23)$$

On figure 3.4 design SN -curves from MC2010 are shown for the same two concrete strengths used in the other codes. For comparison β_{cc} is set to 1.0, η is set to 1.0 for uniform compression and an R -value of 0.2 is used. All coefficients are taken as recommended in MC2010.

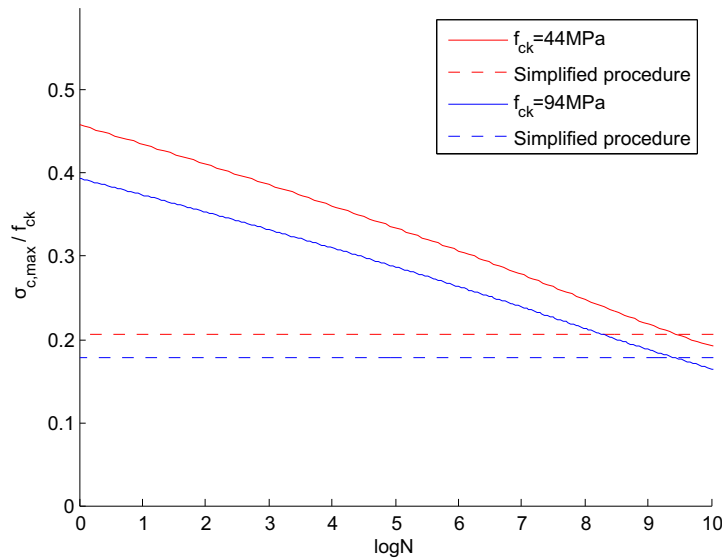


Figure 3.4. Design SN -curves from MC2010 for two different characteristic concrete strengths. The dotted lines represent the simplified procedure.

As with the other codes it is seen that the fatigue life decreases relatively as the compressive strength increases in the chosen example. Furthermore the simplified procedure is always on the safe side for the two chosen concrete strengths as it crosses the SN -curves after $\log N = 8$ for relevant R -values ranging from 0 to 1.

3.3.3 Verification by means of a spectrum of loads

Verification of a spectrum of loads is done with Miner's rule where Δ may normally be set to 1.0. This is similar to what has been proposed in MC1990.

3.3.4 Construction of MC2010 material model

The material model used in MC2010, is described in detail in [Lohaus et al., 2012]. To construct this model some fatigue tests on high strength concrete were conducted and the results were used to set up a mathematical description of a failure surface for concrete in fatigue loading. The following assumptions were also taken into consideration:

- $S_{c,max} = 1$ at $\log N = 0$ for all $S_{c,min}$.
- Linear SN -relationship until $\log N = 8$.
- Deviation between the mathematical model and the test results should be on the safe side.
- The description should be continuous for all $S_{c,max}$.
- After $\log N = 8$ an asymptotic approach is considered for $S_{c,max}$ going towards the respective $S_{c,min}$.

The mathematical description of the failure surface will not be described in detail, in this section, as it is very similar to the one that is developed in chapter 5. In that chapter the main differences between the two models are also pointed out, and in section 5.3 some comparisons are made between the models.

3.4 DNV

In this section the fatigue models from DNV-OS-C502 and DNV-OS-J101 are presented. They both apply to offshore concrete structures however DNV-OS-J101 is specifically intended towards offshore wind turbines.

3.4.1 DNV-OS-C502

DNV-OS-C502 is a standard which provides principals, technical requirements and guidelines for design of offshore concrete structures.

DNV-OS-C502 uses Miner's rule as basis for their design equations and the characteristic compressive cylinder strength is defined as a 5th percent quantile, as in the other investigated codes. The upper limit to the damage threshold, Δ according to eq. (2.1), depends on the access for inspection and repair of the detail. The recommended values by DNV-OS-C502 are listed in table 3.1 below.

Upper limit to damage ratio Δ		
No access for inspection and repair	Below or in the splash zone	Above splash zone
0.33	0.5	1.0

Table 3.1. Recommended values for Δ found in [DNV, 2015].

The number of cycles to failure N_i is estimated by the failure surface in eq. (3.24).

$$\log N = C_1 \frac{\left(1 - \frac{\sigma_{max}}{C_5 f_{rd,fat}}\right)}{\left(1 - \frac{\sigma_{min}}{f_{rd,fat}}\right)} \quad (3.24)$$

Where

C_1	Factor that takes the stress situation and environment of the concrete into account
$f_{rd,fat}$	Reference design fatigue strength for the type of failure estimated by eq. (3.25)
σ_{max}	Largest compressive stress
σ_{min}	Least compressive stress

$$f_{rd,fat} = C_5 f_{rd} \quad (3.25)$$

Where

C_5	Fatigue strength coefficient. Recommended value for concrete is 1.0
-------	---

Even though it is not specified directly in the DNV it is assumed that $\sigma_{max} = \sigma_{cd,max}$ and $\sigma_{min} = \sigma_{cd,min}$. As such the compressive stresses are represented by design values found through eq. (3.26) and (3.27).

$$\sigma_{cd,max} = \sigma_{max} \gamma_F \quad (3.26)$$

$$\sigma_{cd,min} = \sigma_{min} \gamma_F \quad (3.27)$$

Where

γ_F | Partial safety factor for the load. Recommended value in DNV-OS-C502 is 1.0 for FLS

For structures in air C_1 can be set to 12. For uniform compression f_{rd} can be set as f_{cd} , and if the detail is in bending f_{rd} can be found by eq. (3.28).

$$f_{rd} = \alpha f_{cd} \quad (3.28)$$

$$\alpha = 1.3 - 0.3\beta \geq 1$$

Where β can be found as η_c in eq. (3.13). It has to be noted that f_{cd} is defined differently in DNV-OS-C502 than in the other codes that has been presented. In eq. (3.29) the definition of f_{cd} is shown.

$$f_{cd} = \frac{f_{cn}}{\gamma_c} \quad (3.29)$$

Where

f_{cn} | Normalized compression strength, considering transition of test strength into in situ strength, ageing effects due to high-sustained stresses etc.
 γ_c | Partial safety factor for concrete

The normalized compression strength is lower than the characteristic 28 days cylinder strength and can be found by eq. (3.30) for concrete grades between C25 and C90. However it is noted that in this report the equation is used for stronger concrete as well as a best approximation.

$$f_{cn} = f_{ck} \left(1 - \frac{f_{ck}}{600}\right) \quad (3.30)$$

The partial safety factor, γ_c , varies between 1.0 and 1.5 depending on tolerance limits and whether the concrete is reinforced or not.

If the calculated fatigue life $\log N$ is larger than the value X , the fatigue life may be increased by the factor C_2 see eq. (3.31).

$$\begin{aligned} & \text{if } \log N > X \\ \log N &= C_2 \log N \end{aligned} \quad (3.31)$$

Where

X | Found by eq. (3.32)
 C_2 | Found by eq. (3.33)

$$X = \frac{C_1}{1 - \frac{\sigma_{min}}{f_{rd,fat}} + 0.1 C_1} \quad (3.32)$$

$$C_2 = (1 + 0.2(\log N - X)) > 1.0 \quad (3.33)$$

Furthermore it can be found in DNV-OS-C502 that the fatigue capacity of a concrete detail subjected to randomly variable actions such as wind, waves and/or traffic is adequate if the calculated design life for the largest acting load-amplitude corresponds to $2 \cdot 10^6$ cycles. This corresponds to assuming a cut-off in the failure surface at $2 \cdot 10^6$ cycles.

Design SN -curves from DNV-OS-C502 are made for the same two strengths as was used to illustrate the other codes. As these strengths were given in characteristic compressive cylinder strengths the corresponding normalized strengths are found and listed in table 3.2.

Cylinder strength, f_{ck}	Normalized strength, f_{cn}
44 MPa	40.8 MPa
94 MPa	79.3 MPa

Table 3.2. Cylinder and normalized strength for the two chosen concrete strengths.

C_1 is set to 12 for concrete in air and γ_c is set to 1.5 which corresponds to reinforced concrete with normal tolerances. α is set to 1.0 corresponding to η_c being 1.0 in MC1990 and MC2010. As C_5 is recommended as 1.0 for concrete this value is used.

The design SN -curves are shown on figure 3.5.

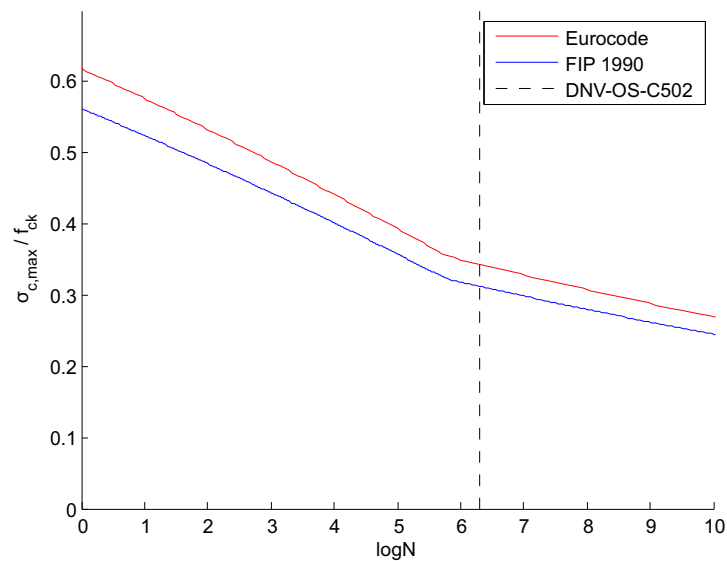


Figure 3.5. Design SN -curves from DNV-OS-C502 for two different characteristic concrete strengths. The dotted line represents $N = 2 \cdot 10^6$ cycles.

It is noted that the y -axis on figure 3.5 is extended from 0.6 to 0.7 compared to figures showing the SN -curves from the other codes.

As for the other investigated codes it can be seen that the fatigue life is relatively decreasing with increasing strength, for the chosen example. The discontinuity on the curves at $\log N \approx 6$ is due to $\log N > X$ so the factor C_2 is introduced.

It is important to note that the SN -curves would be on top of each other until $\log N > X$ if the y -axis had been normalized with f_{rd} instead of f_{ck} . This indicates that the lower relative fatigue life with increasing cylinder strength stems from the relation between f_{cn} and f_{ck} .

Furthermore it can be seen that there is no cut-off in the SN -curve at $2 \cdot 10^6$ cycles, which is implicitly assumed when designing for the largest acting load-amplitude. However as the slope is relatively flat after $2 \cdot 10^6$ cycles it is very unlikely that the smaller load-amplitudes will contribute significantly to fatigue damage.

3.4.2 DNV-OS-J101

In DNV-OS-J101, which covers offshore wind turbines, it is recommended to follow the fatigue verification specified in DNV-OS-C502. The material partial safety factor γ_c should be 1.5 partial safety factor for the load should be 1.0 for normal tolerances. However these are the same partial safety factors that are suggested in DNV-OS-C502 therefore the design equations are the same.

3.5 IEC

In this section the draft CD IEC 61400-6 and IEC 61400-1 are outlined. It is noted that IEC does not provide its own failure surface for fatigue of concrete in compression-compression. Therefore IEC is not included in the comparison of failure surfaces between the codes.

3.5.1 draft CD IEC 61400-6

The draft CD IEC 61400-6 is a draft for a code that is specified for tower and foundation design requirements of wind turbines. In this draft it is recommended to use the failure surface from MC1990 to estimate the fatigue behavior of concrete. The material model should be used in combination with the partial safety factors from IEC 61400-1.[IEC, 2015]

3.5.2 IEC 61400-1

The international standard IEC 61400-1 specifies design requirements for wind turbines of all sizes. To ensure sufficient safety IEC 61400-1 makes recommendations for the partial safety factors applied to both the strength of the material and the load. The material partial safety factor can be found by eq. (3.34) for reinforced concrete in FLS.[IEC, 2005]

$$\gamma_m = 1.2 \gamma_n \quad (3.34)$$

Where

γ_n | Partial safety factor related to the consequence of failure for the investigated component. The values for γ_n are listed in table 3.3

It is noted that the value 1.2 requires that the used failure surface is based on 95% survival, which is assumed to be the case for the failure surfaces in the presented codes.

However it is noted that the value of 1.2 should be exchanged with 1.5 for failure surfaces based on 50% survival and COV less than 15%. For larger COV the value should be increased to at least 1.7.

	γ_n	Description
Component class 1	1.0	Used for fail-safe components whose failure does not result in failure of a major part of the wind turbine
Component class 2	1.15	Used for non fail-safe components whose failure may result in failure of a major part of the wind turbine
Component class 3	1.3	Used for non fail-safe components that link actuators and brakes to the main structural components.

Table 3.3. γ_n values from IEC 61400-1.

The partial safety factor for the load should be set to $\gamma_f = 1.0$ according to the recommendations in IEC 61400-1 for FLS.

3.6 Comparison

By comparing the investigated codes the following observation are made:

- None of the investigated codes take frequency, steel fibres or waveforms into account.
- all investigated codes take mean stresses into account.
- For all the investigated codes Miner's rule is used to take damage accumulation into account, and the threshold, Δ , is generally set to 1.0.
- All codes introduce some limit to when fatigue of concrete in compression-compression has to be investigated, except for EN 1992-2.
- All codes use the 5th percent quantile of the 28 days cylinder strength as characteristic strength, f_{ck} .
- DNV, MC1990 and MC2010 are taking account of the stress gradient in the concrete.
- DNV is the only code to account for the environment surrounding the concrete, tolerances and accessibility. This is probably because it is intended towards offshore structures.

Furthermore some similarities were observed in the way $f_{cd,fat}$ is calculated in Eurocode, MC1990 and MC2010. The different ways of obtaining $f_{cd,fat}$ in those

codes are shown below for easy comparison.

$$f_{cd,fat} = \begin{cases} k_1 \beta_{cc}(t) f_{cd} \left(1 - \frac{f_{ck}}{250}\right) & \text{for Eurocode} \\ 0.85 \beta_{cc}(t) f_{cd} \left(1 - \frac{f_{ck}}{250}\right) & \text{for MC1990} \\ 0.85 \beta_{cc}(t) f_{cd} \left(1 - \frac{f_{ck}}{400}\right) & \text{for MC2010} \end{cases}$$

Based on the similarities following assumptions are considered in this report:

- The fixed value of 0.85 in MC1990 and MC2010 is modeling the same long term effects as k_1 from Eurocode.
- The fatigue life relative to concrete strength is modelled in each code by the last term in parenthesis, which is denoted α_{fat} for future reference.

In DNV the fatigue design reference strength is obtained quite differently. However the description of C_5 in the DNV leads to the assumption that it models the same effect as α_{fat} in the other codes. It is noted though that the reduction in in fatigue life relative to concrete strength was traced back to f_{cn} when evaluation the design SN -curves from DNV. This is however not expected by the description of f_{cn} which states that it accounts for "transition of test strength into in situ strength, ageing effects due to sustained stresses etc.". The only thing that can be recognized in f_{cn} which is mentioned in the other codes is ageing effects which is modelled by k_1 and β_{cc} . Therefore it seems plausible that f_{cn} covers these coefficients as they are not found elsewhere in DNV.

Furthermore DNV includes the effects of stress gradients by increasing the material strength with the factor α . This should be comparable with η from MC1990 and MC2010 however these codes reduce the load rather than increase the material strength.

As conclusion it is found difficult to compare Eurocode, MC1990 and MC2010 with DNV however for further use in the report the following assumption are taken into account:

- Time depended effects are modelled though the relation between f_{ck} and f_{cn} , which is fully comparable with β_{cc} and k_1 .
- The stress gradient factor α is fully comparable with η .
- Fatigue life relative to concrete strength is modelled through C_5 which is comparable with α_{fat} .

3.6.1 Fatigue life relative to concrete strength

In MC1990, MC2010 and Eurocode the fatigue life relative to concrete strength is taken into account in a similar manner by α_{fat} , as shown in eq. (3.35).

$$\alpha_{fat} = \begin{cases} 1 - \frac{f_{ck}}{250} & \text{for Eurocode} \\ 1 - \frac{f_{ck}}{25 f_{ck0}} & \text{for MC1990} \\ 1 - \frac{f_{ck}}{40 f_{ck0}} & \text{for MC2010} \end{cases} \quad (3.35)$$

On figure 3.6 the fatigue reference strength is shown as a function of the characteristic cylinder strength, f_{ck} , for Eurocode, MC1990 and MC2010. All partial

safety factors and coefficients are taken as those recommended in the codes and β_{cc} is set to 1.0.

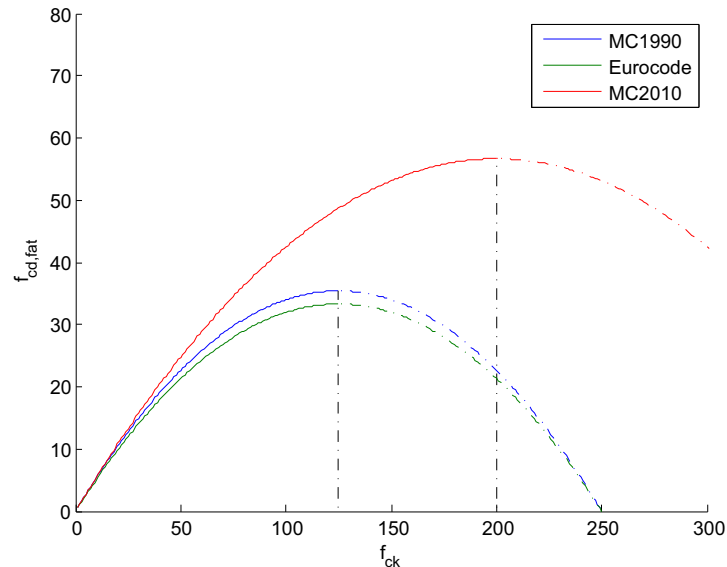


Figure 3.6. Comparison between design strength used in the different codes and the characteristic cylinder strength. The dotted lines shows where the curves gets regressive.

The following observation are made:

- Characteristic compressive strengths higher than 125 MPa leads to a regressive curve for Eurocode and MC1990.
- Characteristic compressive strengths higher than 200 MPa leads to a regressive curve for MC2010.

As result it can be concluded that Eurocode and MC1990 are not viable to use for characteristic concrete strengths higher than 125 MPa, even though this is not specified in the codes.

It is noted that the difference between the curves from Eurocode and MC1990 stems from a small difference in the partial safety factors.

For MC2010 it can be concluded that a characteristic concrete strength up to 200 MPa can be used.

In DNV the C_2 factor which is multiplied with $\log N$ if $\log N > X$ depends on the concrete strength. To determine if this factor leads to a reduction of fatigue life for higher strengths two cases are investigated.

In the first case f_{rd} is found where σ_{max} is constant at 25 MPa and for the other cases σ_{max} is set to respectively 10%, 30% and 50% of f_{rd} . For both cases σ_{min} is chosen constant at 5 MPa representing a dead load and C_1 is set to 12. The results are shown in figure 3.7.

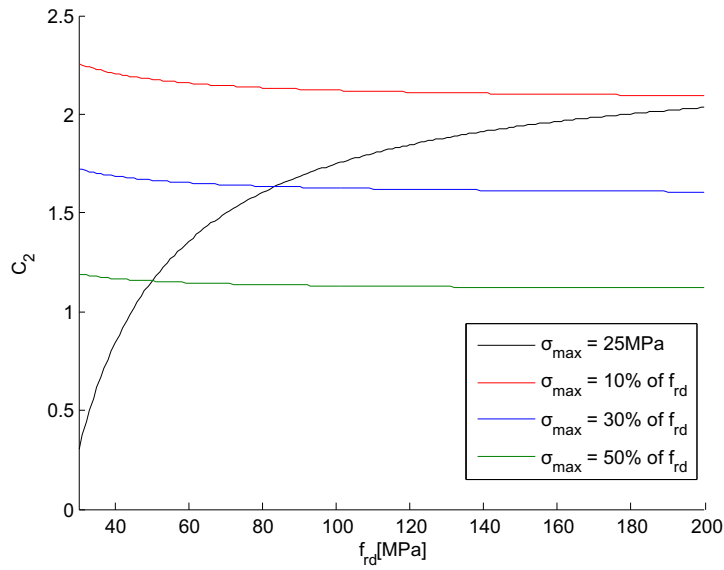


Figure 3.7. C_2 as function of concrete strength for the different cases.

On the figure it can be seen that C_2 is increasing with concrete strength, if σ_{max} is constant and decreasing if σ_{max} is a fraction of f_{rd} . As such it is situational whether or not C_2 is relatively increasing or decreasing the fatigue life with respect to the concrete strength. However it seems most appropriate to model σ_{max} as a fraction of the concrete strength as a higher strength would usually be due to a higher load.

3.7 Comparison of SN-Curves

On figure 3.8 and 3.9 the design SN-curves for the chosen examples used earlier are compared.

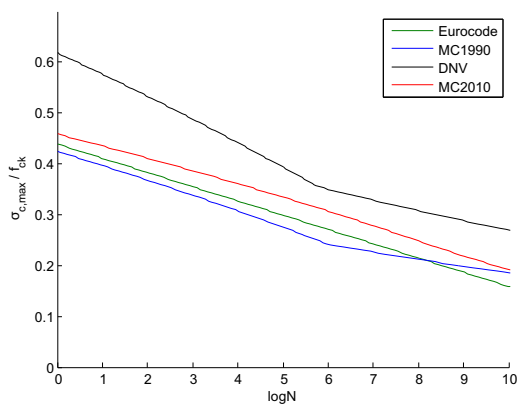


Figure 3.8. Comparison of SN-curves for $f_{ck} = 44$ MPa.

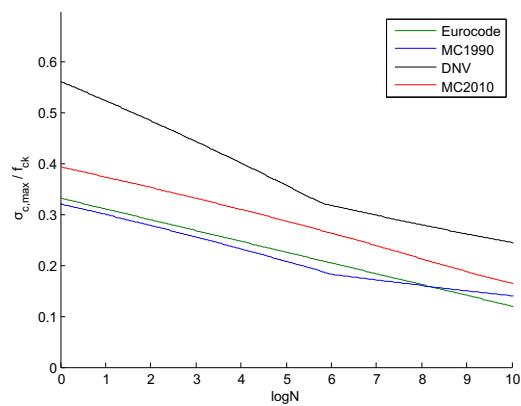


Figure 3.9. Comparison of SN-curves for $f_{ck} = 94$ MPa.

For the chosen example the following observations are made:

- MC1990 and Eurocode has the most conservative approach to fatigue behavior of concrete for both concrete strengths, while DNV has the most non-conservative approach.
- The SN -curve from MC2010 becomes more non-conservative compared to the SN -curves from MC1990 and Eurocode for stronger concrete, as expected from figure 3.6.
- Both the SN -curve from Eurocode and MC2010 are continuous in their description.

As the chosen example that has been used to create the design SN -curves from the different codes has been for uniform compression another comparison is made for pure bending as well. This is done to evaluate how much the stress gradients are weighted in design.

It is chosen to show the design SN -curves from the different codes for $\eta = \frac{2}{3}$ as this corresponds to pure bending in a slender structure. This way it represents the other extreme of η as it can range between $\frac{2}{3}$ and 1.0. The design SN -curves for pure bending are shown on figures 3.10 and 3.11 for the same examples used earlier.

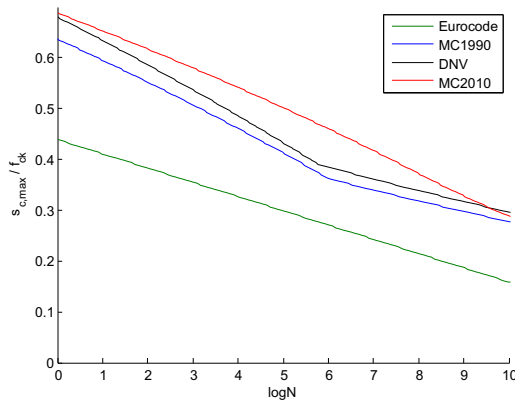


Figure 3.10. Comparison of SN -curves for $f_{ck} = 44$ MPa for pure bending.

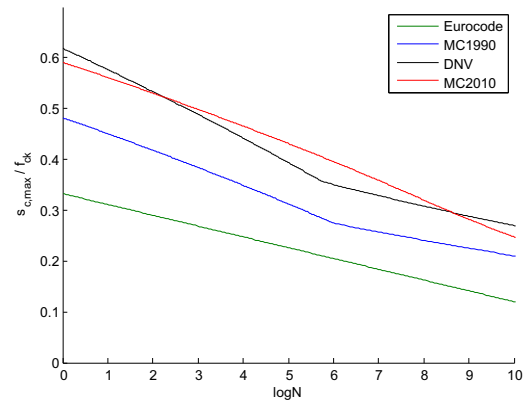


Figure 3.11. Comparison of SN -curves for $f_{ck} = 94$ MPa for pure bending.

For the example with pure bending the following observations are made:

- MC2010 has the most non-conservative approach to fatigue in concrete for both strengths.
- The SN -curve from DNV is in between the two curves from MC1990 and MC2010 for both strengths whereas it was the most non-conservative at pure compression.
- As Eurocode does not increase the fatigue life in concrete based on the type of failure mode it becomes the most conservative.
- Compared with the example of uniform compression MC1990, MC2010 and DNV has become far less conservative.

As a result of the investigation it can be concluded that the stress gradient factor is increasing the fatigue life significantly for the codes that includes it. Therefore it is an important factor to investigate further, especially to see if it can be incorporated in Eurocode as well.

By looking at the figures in this section it can not conclusively be determined which code is the most non-conservative in the chosen example, as it depends on the failure mode whether or not it is DNV or MC2010. However it can be seen that for both failure modes and both investigated concrete strengths the SN-curves from Eurocode are conservative compared to DNV and MC2010.

3.7.1 Comparison of mean failure surfaces

The mean failure surfaces that are incorporated in the investigated codes will be compared, to evaluate the difference of these. This is done as the effects of stress gradients, α_{fat} and time effects are accounted for differently for each code. Therefore the design SN-curves shown earlier are influenced a lot by the choices of how to incorporate the mentioned effects.

The mean failure surfaces are assumed to be obtained by replacing the design values with mean values for the strengths and loads. It is noted that this assumption might be inaccurate as some safety could be accounted for in the constants of the failure surfaces, e.g. 14 in eq. 3.6. Furthermore the assumption implies that the obtained mean failure surfaces are unbiased with respect to the data it is based on. This is e.g. not the case for MC2010 which is shown in section 9.3.

The equation that is assumed to represent the mean failure surface from Eurocode is presented in equation (3.36).

$$N = 10^{14} \frac{1 - E_{cm,max}}{\sqrt{1 - R_m}} \quad (3.36)$$

Where

$E_{cm,max}$	Mean maximum stress ratio found by eq. (3.37)
R_m	Mean ratio between minimum and maximum stress found by eq. (3.38)

$$E_{cm,max} = \frac{\sigma_{c,max}}{f_{cm}} \quad (3.37)$$

$$R_m = \frac{E_{cm,min}}{E_{cm,max}} \quad (3.38)$$

Where

$E_{cm,min}$	Mean minimum stress ratio found by eq. (3.37)
f_{cm}	Mean compressive cylinder strength of the concrete

To predict the mean failure surface from MC1990 eq. (3.39) is used.

For $0 < S_{cm,min} < 0.8$

$$\log(N) = \begin{cases} \log N_1 & \text{if } \log N_1 \leq 6 \\ \log N_2 & \text{if } \log N_1 > 6 \text{ and } \Delta S_{cm} \geq 0.3 - 0.375 S_{cm,min} \\ \log N_3 & \text{if } \log N_1 > 6 \text{ and } \Delta S_{cm} < 0.3 - 0.375 S_{cm,min} \end{cases} \quad (3.39)$$

Where

$$\begin{aligned} \log N_1 &= (12 + 16 S_{cm,min} + 8 S_{cm,min}^2) (1 - S_{cm,max}) \\ \log N_2 &= 0.2 \log N_1 (\log N_1 - 1) \\ \log N_3 &= \log N_2 \frac{0.3 - 0.375 S_{cm,min}}{\Delta S_{cm}} \end{aligned}$$

Where

$$\begin{aligned} S_{cm,max} &= \frac{\sigma_{c,max}}{f_{cm}} \\ S_{cm,min} &= \frac{\sigma_{c,min}}{f_{cm}} \\ \Delta S_{cm} &= S_{cm,max} - S_{cm,min} \end{aligned}$$

To describe the mean failure surface from MC2010 eq. (3.40) is used. This corresponds directly to the mean failure surface that is presented in [Lohaus et al., 2012].

$$\log(N) = \begin{cases} \log N_2 = 8 + \frac{8 \ln(10)}{Y-1} (Y - S_{cm,max}) \log \left(\frac{S_{cm,max} - S_{cm,min}}{Y - S_{cm,min}} \right) & \text{if } 8 \leq \log N_1 \\ \log N_1 = \frac{8}{Y-1} (S_{cm,max} - 1) & \text{if } 8 \geq \log N_1 \end{cases} \quad (3.40)$$

Where Y is found by eq. (3.41)

$$Y = \frac{0.45 + 1.8 S_{cm,min}}{1 + 1.8 S_{cm,min} - 0.3 S_{cm,min}^2} \quad (3.41)$$

Lastly the mean material model from DNV is assumed to be described by eq. (3.42).

$$\log N = C_1 \frac{\left(1 - \frac{\sigma_{max}}{f_{cm}}\right)}{\left(1 - \frac{\sigma_{min}}{f_{cm}}\right)} \quad (3.42)$$

It is noted that C_1 is kept as it takes into account whether it is dry environment or not. To effectively compare the codes and due to the scope of the report the mean failure surface for DNV is predicted for dry environment corresponding to $C_1 = 12$.

In figure 3.12 mean SN -curves from the different codes are compared for an R -value of 0.2 corresponding to the comparison of the design SN -curves.

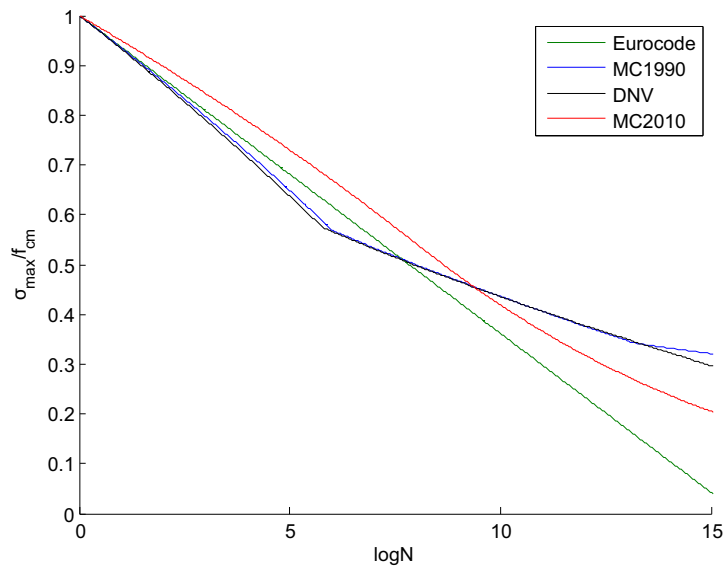


Figure 3.12. Comparison of mean SN-curves from the investigated codes.

For the chosen example the following observations are made:

- The mean SN-curves from MC1990 and DNV are very similar until very high cycle fatigue.
- Until $\log N \approx 8$ The mean SN-curve from Eurocode is more non-conservative than those from MC1990 and DNV.
- The mean SN-curve from MC2010 is the most non-conservative until $\log N \approx 10$.

By comparing figure 3.12 with figures 3.8 and 3.9 it can be concluded, that the effects of α_{fat} is very important in design for the chosen example. This is seen as DNV has one of the most conservative mean SN-curves, but becomes the most non-conservative in design.

Data Acquisition

In this chapter the data that is used throughout this report is presented. The data is collected from the two papers [Lohaus et al., 2012] and [Sørensen]. All data stems from uniform compression-compression tests, thus the effect of stress gradients can not be investigated based on the data.

The data from [Sørensen] was directly available, as it was listed in tables within the article. The data from [Lohaus et al., 2012] was not directly available so it was acquired through digitalizing plots using the program "GetDataGraphDigitizer". This way of retrieving the data may introduce some difference between the acquired data and the original data, both in amount of data points and the value of each data point. These differences are discussed in this chapter, and comparisons are made to validate the quality of the acquired data. In the end of the chapter selected data is compared to the mean failure surfaces from the investigated codes.

In [Lohaus et al., 2012] two data series were documented. The first data series was used to make the mathematical description of the failure surface that is incorporated in MC2010. In this report this data series is referred to as "*data series 1*".

The second data series is from test specimens with different concrete strengths, and in [Lohaus et al., 2012] it is used for verification of the mathematical model. In this report the data series is referred to as "*data series 2*".

In [Sørensen] data is available from tests in both dry and wet environment, where only the data from dry environment is presented. In this report the data from [Sørensen] is referred to as "*data series 3*".

4.1 Data from "Structural Concrete"

In this section the two data series from [Lohaus et al., 2012] are presented. The available information about the concretes that has been used for the tests is also shortly described as the composition of the concrete might have some influence on the fatigue behavior, that is not investigated further in this report.

4.1.1 Data series 1

Two different ultra high strength concretes were used to make *data series 1* that is used for the mathematical model in [fib, 2010]. A fine grained concrete(M2Q) with a maximum grain size of 0.5 mm and a coarse grained concrete(B4Q) with a maximum grain size of 8.0 mm with compressive strengths of $f_{c,cube,100} = 160MPa$ and $f_{c,cube,100} = 180MPa$. Both mixtures contained steel fibres and were heat treated at $120^\circ C$ for two days. On figure 4.1 all the data from *data series 1* is shown as it is presented in [Lohaus et al., 2012] where regression lines are plotted as well. It is noted that the stress ratios in [Lohaus et al., 2012] are taken relative to the mean compressive strength, f_{cm} , which was found using at least three cylindrical specimens, with dimensions $D \cdot H = 60mm \cdot 180mm$ which are the same as the specimens used for fatigue tests, from the same batch of concrete. The stress ratios $S_{c,min}$ and $S_{c,max}$ are defined in equations (4.1) and (4.2).

$$S_{c,min} = \frac{\sigma_{min}}{f_{cm}} \quad (4.1)$$

$$S_{c,max} = \frac{\sigma_{max}}{f_{cm}} \quad (4.2)$$

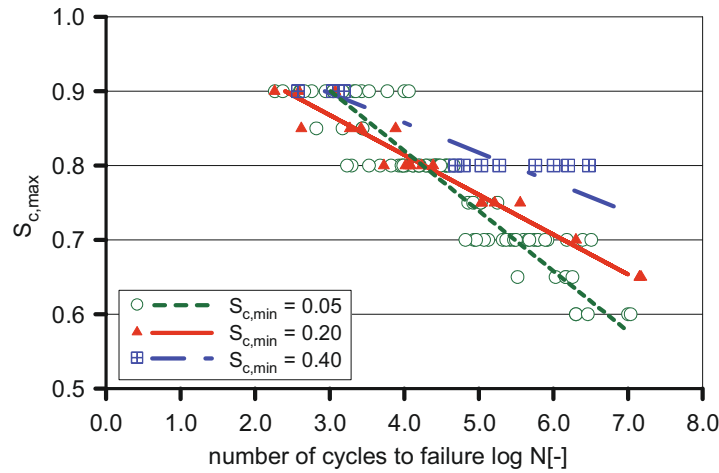


Figure 4.1. Data as presented in [Lohaus et al., 2012] with regression lines. The figure is taken directly from the article.

According to [Lohaus et al., 2012] 88 tests were made at $S_{c,min} = 0.05$, 21 tests at $S_{c,min} = 0.20$ and 12 tests at $S_{c,min} = 0.40$. For tests with an expected number of cycles to failure up to $N = 2.0 \cdot 10^6$ the test frequency was 10 Hz. For tests where a higher number of cycles was expected a frequency of 60 Hz were used. It is noted that a frequency of 60 Hz is not within the frequency range, where the fatigue behavior is expected to be independent. However the influence from frequency on *data series 1* is not investigated any further in this report, as it is not pointed out which data points belong to which frequency.

To extract the data points from figure 4.1 the program *GetDataGraphDigitizer* was used. All the retrieved data points are listed in appendix B.

In tables 4.1 to 4.3 the amount of retrieved data points are listed with the mean and standard deviation to compare to figure 4.1.

$S_{c,max}$	Extracted data points	$\bar{x}_{\log N}$	$s_{\log N}$
0.90	16	3.10	0.56
0.85	3	3.13	0.31
0.80	22	4.12	0.42
0.75	4	5.01	0.17
0.70	20	5.57	0.47
0.65	4	5.99	0.33
0.60	4	6.70	0.38
Total	73		

Table 4.1. General information about the data retrieved for $S_{c,min} = 0.05$.

$S_{c,max}$	Extracted data points	$\bar{x}_{\log N}$	$s_{\log N}$
0.90	3	2.63	0.42
0.85	4	3.29	0.52
0.80	6	4.08	0.22
0.75	3	5.27	0.26
0.70	1	6.31	0.00
0.65	2	7.17	0.18
Total	19		

Table 4.2. General information about the data retrieved for $S_{c,min} = 0.20$.

$S_{c,max}$	Extracted data points	$\bar{x}_{\log N}$	$s_{\log N}$
0.90	3	2.93	0.33
0.80	8	5.53	0.68
Total	11		

Table 4.3. General information about the data retrieved for $S_{c,min} = 0.40$.

In table 4.4 a comparison is shown between the retrieved and original amount of data.

	Original data points	Retrieved data points
$S_{c,min} = 0.05$	88	73
$S_{c,min} = 0.20$	21	19
$S_{c,min} = 0.40$	12	11

Table 4.4. Comparison of amount of retrieved and original data.

On figure 4.2 the retrieved data are shown with corresponding regression lines.

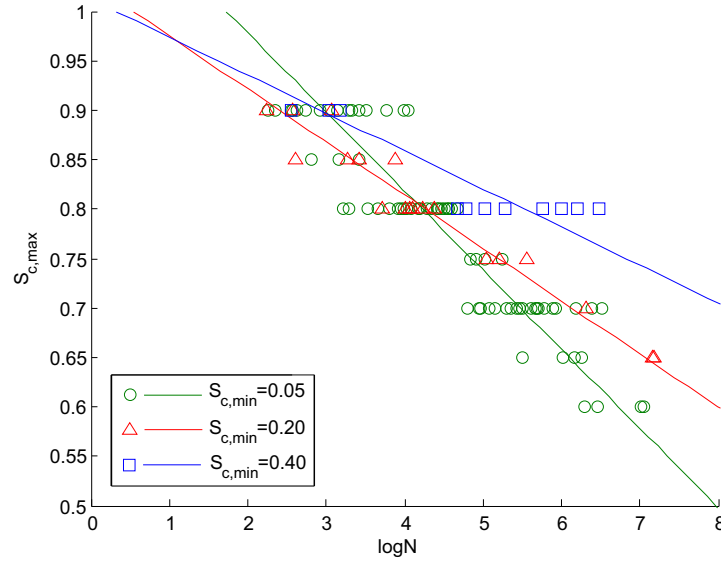


Figure 4.2. Retrieved data with regression lines.

Validating Data

To validate the retrieved data the regression lines from the original and retrieved data are compared. The regression lines from [Lohaus et al., 2012] follows the expression shown in eq. (4.3).

$$\log N = k_1 S_{c,max} + k_2 \quad (4.3)$$

Whereas the regression lines found in this report are found by using maximum likelihood method, or MLM, and follows the expression shown in eq. (4.4). An introduction to MLM is given in appendix A.

$$\log N = k_1 S_{c,max} + k_2 + \epsilon \quad (4.4)$$

Where ϵ is an error term assumed normal distributed with a mean value of zero and a standard deviation, σ_ϵ .

In table 4.5 a comparison is made between the regression lines for each $S_{c,min}$, which is also shown graphically on figure 4.3.

Min. stress ratio	Data	k_1	k_2	σ_ϵ	μ_ϵ
$S_{c,min} = 0.05$	Original	-12.4	14.1	-	-
	Retrieved	-12.5	14.2	0.46	0.00
$S_{c,min} = 0.20$	Original	-18.7	19.2	-	-
	Retrieved	-18.7	19.2	0.32	0.00
$S_{c,min} = 0.40$	Original	-24.9	25.4	-	-
	Retrieved	-26.0	26.4	0.56	0.00

Table 4.5. Comparison of constants from regression lines between the original and retrieved data.

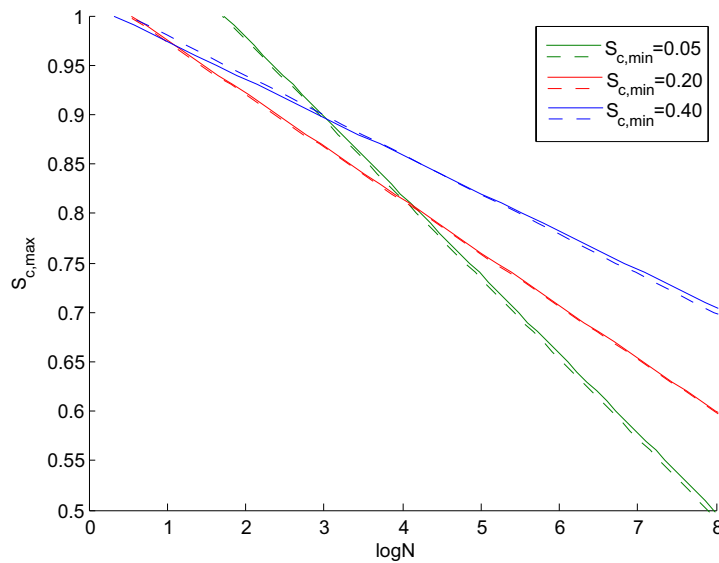


Figure 4.3. Comparison of regression lines from retrieved and original data. The dotted lines represent the original data and the full lines represent the retrieved data.

It is seen that the regression lines for the retrieved data matches those from [Lo-haus et al., 2012] very well so no further effort is done in order to improve the quality of the data.

As it was evident from table 4.4 less data were retrieved than the original amount. However by looking in appendix B table B.1 to B.3 it can be seen that far most of the missing data points are from the clusters of data near the mean values. As a result all the outlying data that leads to high uncertainty is taken into account. Given the presented analysis it is expected that the mean regression lines are accurately captured. However due to the missing points near the mean values, it is expected that the standard deviations presented in table 4.5 are slightly overestimated. In order to improve the results the last data should be extracted, however this would rely partly on guessing due to the density of the data near the mean values. As conclusion no further effort was done to improve the quantity of the data.

4.1.2 Data series 2

data series 2 represents a total of 272 experimental tests conducted on specimens of different concrete strength. In figure 4.4 the data is shown as it is presented in [Lohaus et al., 2012]. A data point that contains an right upwards pointing arrow represents run-out. all tests are made at $S_{c,min} = 0.05$ and each data point represents a mean value.

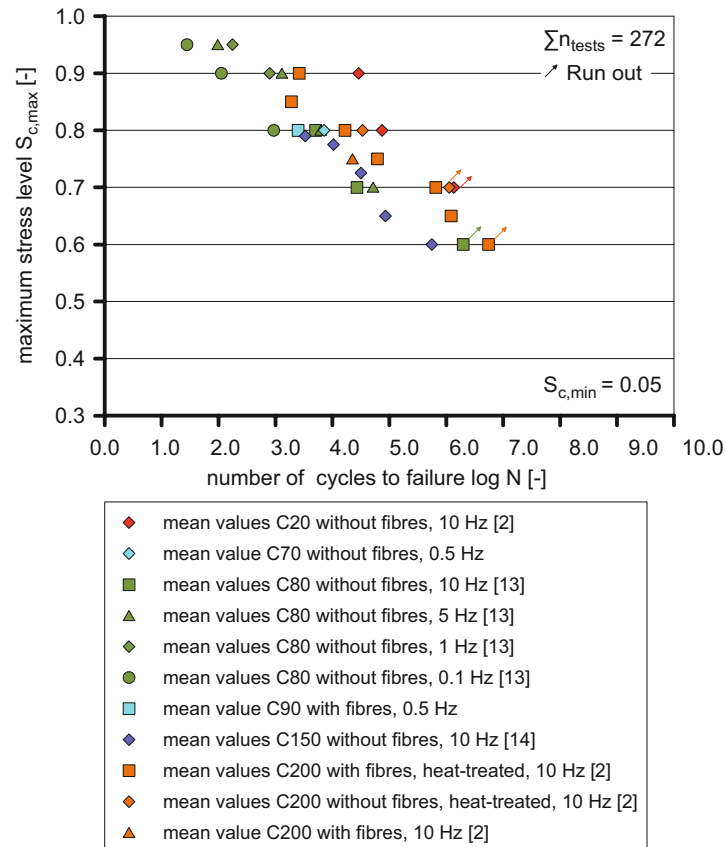


Figure 4.4. Data with varying concrete strength as presented in [Lohaus et al., 2012].

The tests were performed at different frequencies ranging from 0.1Hz – 10Hz and on concrete with and without fibres and heat treatment. The stress ratios were found relative to the mean compressive strength which was found using three specimens.

To extract the data from figure 4.4 the program "GetDataGraphDigitizer" was used and the recovered data is shown on figure 4.5. The data is also listed in table B.4 in appendix B.

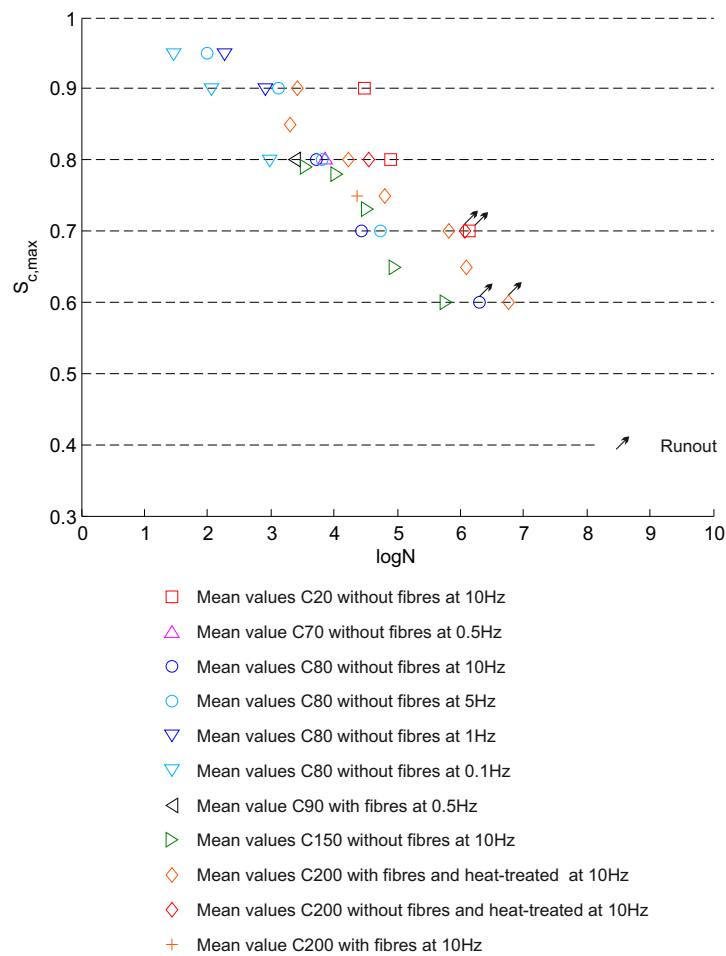


Figure 4.5. Data from tests on different concrete strength retrieved from [Lohaus et al., 2012].

4.2 Data series 3

In this section *data series 3* acquired from [Sørensen] is presented. The relevant data covers 26 test results on high strength concrete. The material that was used for the test specimens was a commercially available product based on a high performance cementitious binder material. It contained microsilica and other mineral additions and it was prepared at ultra low water to cementitious material ratio facilitated by a high dose of superplasticizing admixture. The aggregate consisted of natural sand with a grain size up to a maximum of 4 mm. The fatigue tests were made on cylindrical specimens with a diameter of 60 mm and a height of 120 mm that were stored in mould at 20 °C for one day, then demoulded and stored in water at 20 °C until testing.

Before testing, the static compressive strength of the high strength concrete was determined using 6 specimens at a loading rate of 0.88 MPa/s. At all tests the compressive strength were virtually constant at 170 MPa [Sørensen]. The tests in dry environment were performed at two different $S_{c,max}$ of 60 % and 76 % and at three different frequencies of 0.35 Hz, 5 Hz and 10 Hz. For all tests $S_{c,min}$ was kept constant at 4.2 % and the load was applied sinusoidally. The results of the

tests performed by Sørensen were available in a table in [Sørensen] and the relevant data for this report is plotted on figure 4.6. The data is also listed in table B.5 in appendix B. In the table it can be seen that a lot of points coincide at $2 \cdot 10^6$ cycles which is difficult to see on figure 4.6.

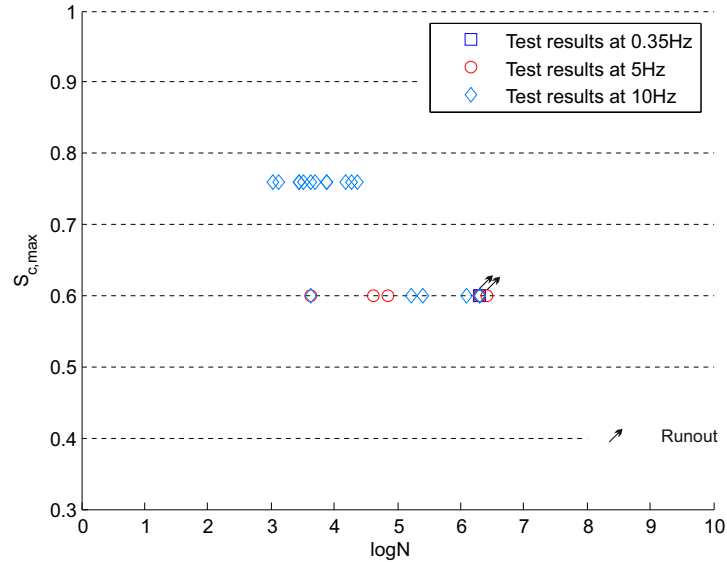


Figure 4.6. Data on high strength concrete from tests performed by Sørensen.

4.3 Comparing Data with Material Models from Codes

To evaluate the mean failure surfaces that are incorporated in the investigated codes from chapter 3, a comparison is made with some of the acquired data. On figure 4.7 a comparison is made at $S_{c,min} = 0.05$ where relevant data are taken from *data series 1* and all data series 2 is used. On figures 4.8 and 4.9 a comparison is shown at $S_{c,min} = 0.20$ and $S_{c,min} = 0.40$ where relevant data from *data series 1* is used.

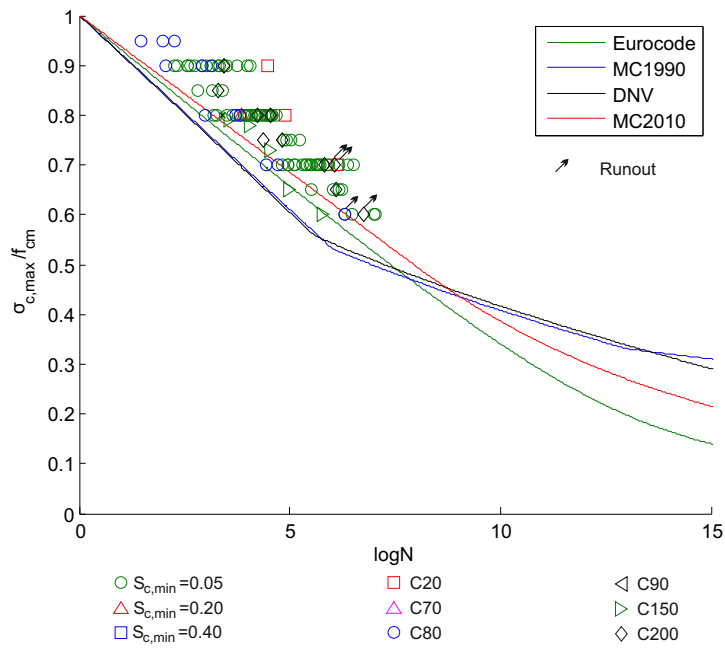


Figure 4.7. Comparison between acquired data and mean SN-curves from the investigated codes at $S_{c,min} = 0.05$.

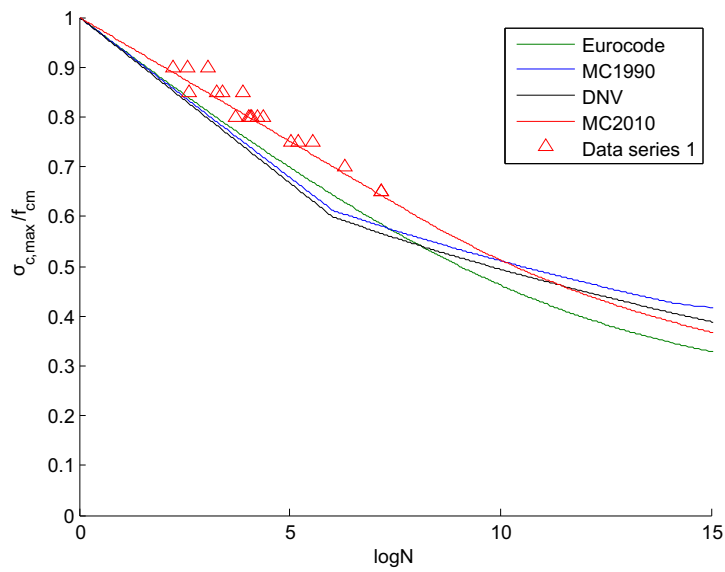


Figure 4.8. Comparison between acquired data and mean SN-curves from the investigated codes at $S_{c,min} = 0.20$.

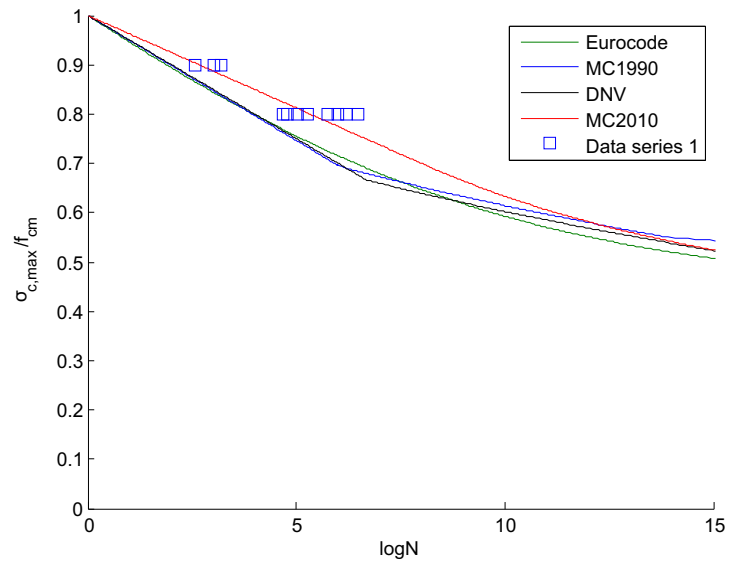


Figure 4.9. Comparison between acquired data and mean SN -curves from the investigated codes at $S_{c,min} = 0.40$.

The figures indicates that mean failure surfaces in the codes are conservative compared to the data for low $S_{c,min}$. However as $S_{c,min}$ increases they become less conservative.

This indicates that a reliability analysis based on a failure surface that captures the acquired data accurately would lead to the conclusion that the codes are conservative for low $S_{c,min}$, but more accurate as $S_{c,min}$ increases.

Developing Fatigue Failure Surface of Concrete

In this chapter a failure surface is developed for concrete under uniaxial compressive fatigue loading in the $S_{c,max}$, $S_{c,min}$, $\log N$ -space. The surface is developed as it is used to assess the reliability that is obtained by designing with the investigated codes from chapter 3.

The mathematical description for the failure surface is based on *data series 1* presented in chapter 4. Due to the range of the data the failure surface is only developed between $\log N = 0$ and $\log N = 8$.

To use the failure surface some boundaries are adopted which are presented in this chapter as well. At the end of the chapter the surface is validated against the available data, and compared to the surface in [Lohaus et al., 2012].

5.1 Mathematical Description of the Failure Surface

The mathematical description of the failure surface is developed by combining the theory behind the traditional SN-curve, that represent the $S_{c,max}$, $\log(N)$ -plane, and Goodman diagrams, that represent the $S_{c,max}$, $S_{c,min}$ -plane, see figure 5.1 . This enables the failure surface to account for mean stresses and not only the stress ranges. In general the derivation of the failure surface follows the derivation presented in [Lohaus et al., 2012]. However the assumptions that are used in [Lohaus et al., 2012], which are also listed in section 3.3, are revisited in order to improve the accuracy of the model. The main differences are pointed out throughout this section.

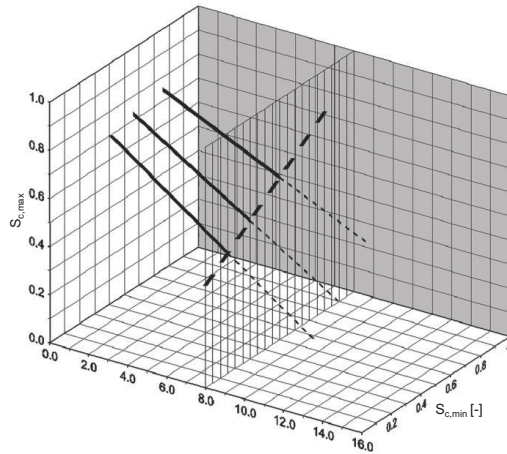


Figure 5.1. Regression lines in $\log N, S_{c,min}, S_{c,max}$ -space [Lohaus et al., 2012].

In order to develop the failure surface the following assumptions are taken into consideration:

1. Linearity of the SN -curves between $\log N = 0$ and $\log N = 8$ [Lohaus et al., 2012].
2. Failure will occur at 1 cycle for $S_{c,max} = S_{c,min} = 1$ as it corresponds to the concrete being loaded statically with its mean compressive strength.
3. The failure surface should only be defined for $S_{c,max} < 1$ as higher values would correspond to failure in the ultimate limit state.
4. The sustained compressive strength of concrete is taken as 85% of the static compressive strength [fib, 2010].

A main difference in these assumptions compared to [Lohaus et al., 2012] is that $S_{c,max} = 1$ is not bound to be at $\log N = 0$. This enables the failure surface to capture the data points more accurately, but also introduce a limitation to the surface which is presented later. The assumption about the sustained compressive strength of concrete linearity until $\log N = 8$ is incorporated in the model as deterministic values. As result it does not change the uncertainty of the model. In [Lohaus et al., 2012] the uncertainty connected with the two assumption is not investigated neither.

5.1.1 Goodman diagram

Similar to the approach in [Lohaus et al., 2012] a Goodman diagram at $\log N = 8$ is constructed using the three intersection points, where the regression lines from figure 4.2 intersect the $\log N = 8$ -plane, see figure 5.1. Furthermore assumption 4 introduces a fourth point in the plane located at $S_{c,max} = S_{c,min} = 0.85$. The four points, denoted P_1 to P_4 are shown on figure 5.2 and their values are listed in table 5.1.

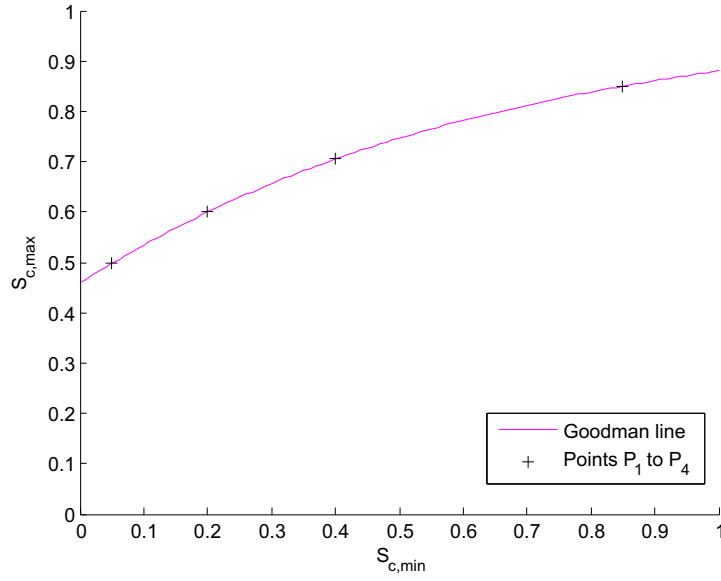


Figure 5.2. Points P_1 to P_4 shown with corresponding Goodman line at $\log N = 8$.

	$S_{c,min}$	$S_{c,max}$
P_1	0.05	0.50
P_2	0.20	0.60
P_3	0.40	0.71
P_4	0.85	0.85

Table 5.1. Values for P_1 to P_4 . P_1 to P_3 found as the intersection points between regression lines and $\log N = 8$ -plane. P_4 is found using assumption 4.

To describe the Goodman diagram in the entire plane a third order polynomial as shown in eq. (5.1) is fitted to the four points using least square error regression, which is also shown on figure 5.2. It is noted that the choice of function differs from that in [Lohaus et al., 2012], so a comparison of the two are made in appendix C.

$$S_{c,max}(S_{c,min}, \log N = 8) = a_{N8} S_{c,min}^3 + b_{N8} S_{c,min}^2 + c_{N8} S_{c,min} + d_{N8} \quad (5.1)$$

The constants of the fitted polynomial are listed in table 5.2.

a_{N8}	0.15
b_{N8}	-0.53
c_{N8}	0.80
d_{N8}	0.46

Table 5.2. Constants for the Goodman diagram at $\log N = 8$ cycles.

The tendency of the Goodman diagram shown on figure 5.2 seems appropriate compared to the tendency of the points.

5.1.2 Boundary line for $S_{c,max} = 1$

By extrapolating the regression lines from the data they will predict that $S_{c,max} > 1$ when the concrete is subjected to low cycle fatigue, see figure 5.3. As this contradicts with the ultimate limit state design, a boundary line for $S_{c,max} = 1$ is created in the $S_{c,min}, \log N$ -plane. The line is created in a similar manner as the Goodman diagram. The introduction of this boundary line makes this model significantly different from the one in [Lohaus et al., 2012], as it is based on the assumption that the failure surface will have intersection with the $\log N = 0$ plane at $S_{c,max} = 1$.

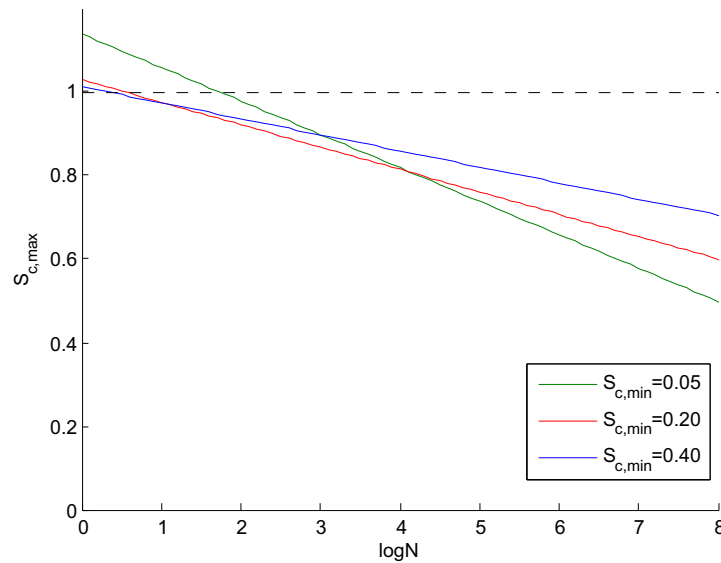


Figure 5.3. Regression lines from maximum likelihood method.

When looking at the regression lines on figure 5.3 it can be seen that the slopes are increasing when $S_{c,min}$ is increasing and that the intersection with the y-axis is increasing when $S_{c,min}$ is decreasing. An interpretation of this could be, that when $S_{c,min}$ is very low the test data does not predict low cycle fatigue very well. This could be expected as only stresses has been measured, and for very low $S_{c,min}$ and high $S_{c,max}$ some plasticity can be expected in the concrete. As result the stress measurements become insufficient, and should have been replaced with a strain analysis instead.

By extrapolating the regression lines for the data, three intersection points are found between the lines and the $S_{c,max} = 1$ -plane. A fourth point is added by using assumption 2, that failure will occur for $S_{c,min} = S_{c,max} = 1$ at one cycle. The four points, denoted Q_1 to Q_4 , are listed in table 5.3, and are shown on figure 5.4.

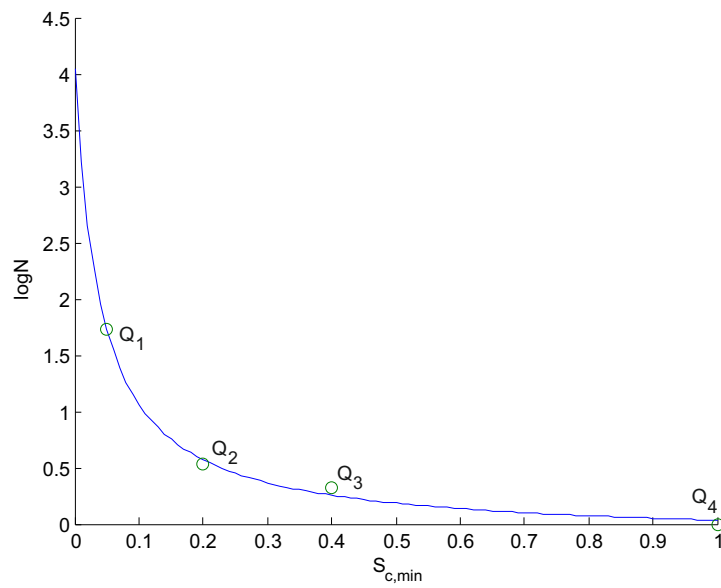


Figure 5.4. Points Q_1 to Q_4 with fitted function. The points are located in the $S_{c,max} = 1$ -plane.

	$S_{c,min}$	$\log(N)$
Q_1	0.05	1.73
Q_2	0.2	0.54
Q_3	0.4	0.32
Q_4	1	0.00

Table 5.3. Values for the points Q_1 to Q_4 . Q_1 to Q_3 are found using the regression lines from the data. Q_4 is found through assumption 2.

To approximate the boundary line for $S_{c,max} = 1$ the function shown in eq. (5.2) is fitted using least square error regression.

$$\log N(S_{c,min}, S_{c,max} = 1) = \frac{1}{(\log(S_{c,min} + 1) a_{S_{max1}} + b_{S_{max1}})} + c_{S_{max1}} \quad (5.2)$$

The best fitting line is shown on figure 5.4. The constants used for the curve are listed in table 5.4.

$a_{S_{max1}}$	13.43
$b_{S_{max1}}$	0.24
$c_{S_{max1}}$	-0.20

Table 5.4. Constants for the $S_{c,max} = 1$ boundary line.

The line describes the tendency of the points well until $S_{c,min} < 0.05$ where it gets very steep. Due to the high steepness for $S_{c,min} < 0.05$ the developed surface is expected to be unreasonable non-conservative in this area.

5.1.3 Creating the failure surface

By using assumption 1 the failure surface can be constructed by connecting straight lines at each $S_{c,min}$ between the Goodman diagram described in eq. (5.1) and the boundary line for $S_{c,max} = 1$ described in eq. (5.2). On figure 5.5 the principle is shown where the $\log N = 8$ -plane is marked with gray and the $S_{c,max} = 1$ -plane is marked with green. On the figure three straight lines are shown at $S_{c,min} = 0.05$, $S_{c,min} = 0.20$ and $S_{c,min} = 0.40$.

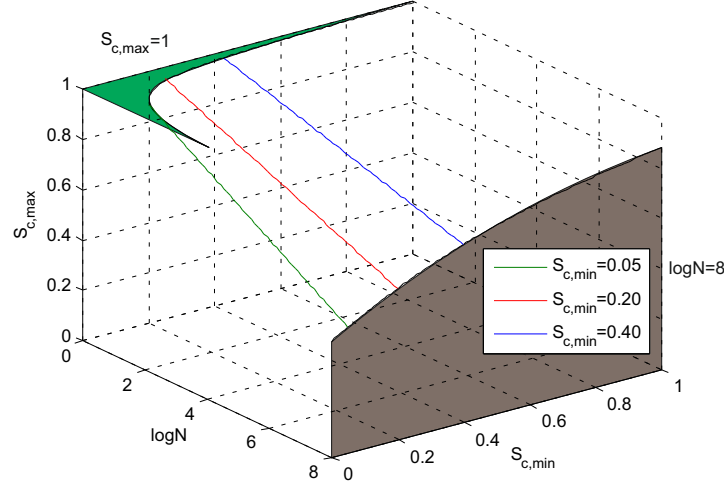


Figure 5.5. Goodman diagram and boundary shown with regression lines in $S_{c,max}$, $S_{c,min}$, $\log N$ -space.

The assumption of linearity of the SN -curves is taken from [Lohaus et al., 2012]. In the article it is pointed out that previous investigation has shown a linear correlation between $S_{c,max}$ and $\log N$ up till $\log N = 8$.

Given the previous assumptions the entire failure surface can be described by eq. (5.3).

$$\log N(S_{c,min}, S_{c,max}) = \frac{S_{c,max} - b_{surf}(S_{c,min})}{a_{surf}(S_{c,min})} \quad (5.3)$$

The slope, $a_{surf}(S_{c,min})$, of the surface is found using the Goodman diagram and the boundary line for $S_{c,max} = 1$ as shown in eq. (5.4).

$$a_{surf}(S_{c,min}) = \frac{\Delta S_{c,max}(S_{c,min})}{\Delta \log N(S_{c,min})} \quad (5.4)$$

Where

$$\left. \begin{array}{l} \Delta S_{c,max}(S_{c,min}) \\ \Delta \log N(S_{c,min}) \end{array} \right| \begin{array}{l} \text{Is found by eq. (5.5)} \\ \text{Is found by eq. (5.6)} \end{array}$$

$$\Delta S_{c,max}(S_{c,min}) = 1 - S_{c,max}(S_{c,min}, \log N = 8) \quad (5.5)$$

$$\Delta \log N(S_{c,min}) = \log N(S_{c,min}, S_{c,max} = 1) - 8 \quad (5.6)$$

As the slope is known the intersection between the failure surface and the $\log(N) = 0$ plane is found using eq. (5.7).

$$b_{surf}(S_{c,min}) = 1 - a_{surf}(S_{c,min}) \log N(S_{c,min}, S_{c,max} = 1) \quad (5.7)$$

The failure surface that has been developed is shown in figure 5.6.

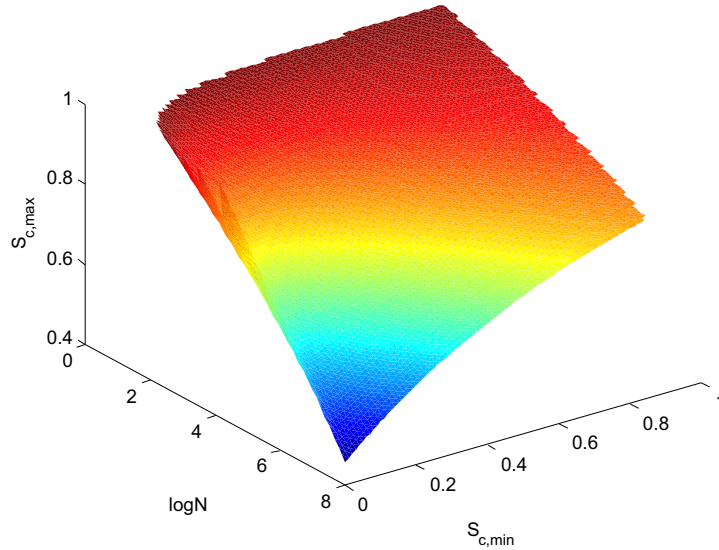


Figure 5.6. Failure surface.

Boundaries of the failure surface

The introduced failure surface has the following boundaries.

1. $0 \leq \log N \leq 8$
2. $S_{c,min} \leq S_{c,max}$
3. $S_{c,max} \leq 1$
4. $S_{c,max} \geq S_{c,max}(S_{c,min}, \log N = 8)$

these boundaries are included in figure 5.6 and the 3 first boundaries are shown more clearly on figure 5.7.

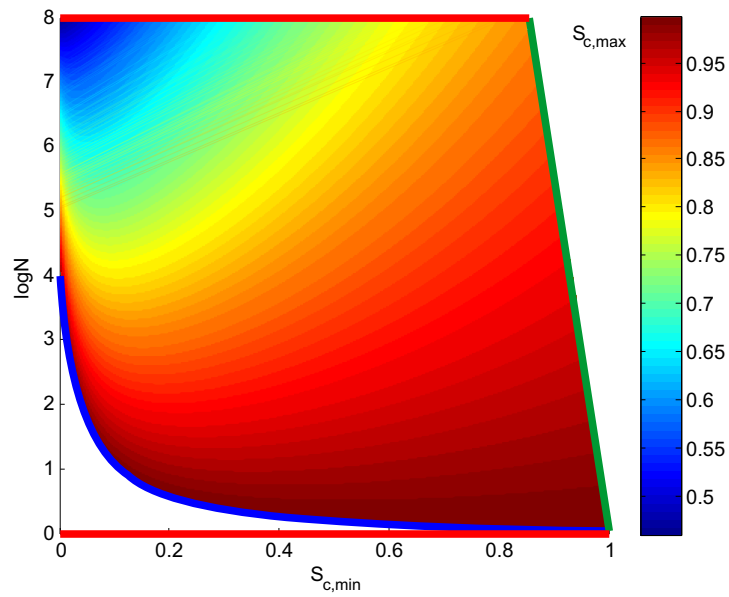


Figure 5.7. Boundaries of the failure surface. Boundary condition 1 is marked with red, 2 with green and 3 with blue.

The first boundary condition is introduced due to the range of the available data. More data should be available to investigate the non-linear effect between $\log N$ and $S_{c,max}$ that occurs for very high cycle fatigue.

The second boundary condition stems from the definition of maximum and minimum.

The third boundary condition is introduced to avoid contradiction with ultimate limit state design. This boundary condition limits the use of the mathematical model for low cycle fatigue. To account for low cycle fatigue another model intended towards low cycle fatigue could be developed based on strains instead of stresses.

To illustrate boundary condition 4 figure 5.8 shows the Goodman diagram at $\log N = 8$ and a line representing $S_{c,min} = S_{c,max}$.

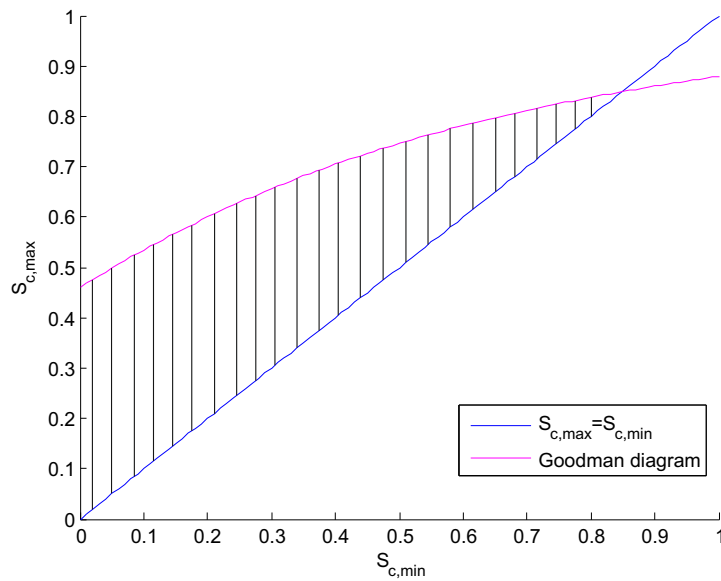


Figure 5.8. Illustration of boundary condition 4. The figure shows the $S_{c,max}, S_{c,min}$ -plane at $\log N = 8$.

All stress states below the $S_{c,min} = S_{c,max}$ line are impossible due to boundary condition 2.

The hatched area on figure 5.8 represents stress states that can not be predicted by the developed surface due to boundary condition 4. However if stress states in this region occur it could be predicted if it is assumed that the SN -curves behave linear after $\log N = 8$, see figure 5.9.

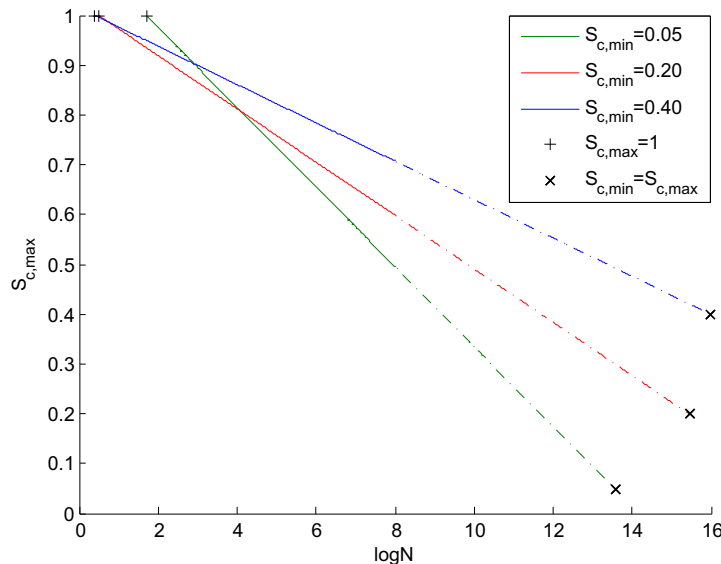


Figure 5.9. SN -curves at $S_{c,min}$ equal to 0.05, 0.20 and 0.40. The dotted lines represent linear extrapolation of the SN -curves beyond $\log N = 8$.

On figure 5.9 the SN -curves at $S_{c,min}$ equal to 0.05, 0.20 and 0.40 are drawn linear after $\log N = 8$. It is assumed that it is a conservative solution to extrapolate the

SN-curves in a linear manner. The real solution is likely to let the SN-curves go asymptotically towards $S_{c,min} = S_{c,max}$ as $\log N$ rises. This makes sense as the fatigue life should go towards infinite as the stress ranges go towards zero. This approach is also used in [Lohaus et al., 2012], however as mentioned it is not investigated in this report, due to lack of data in the appropriate $\log N$ -range. In the reliability analysis that is presented in chapter 10 the assumption of linear extrapolation is used.

5.2 Dependency of Concrete Strength

In this section it is investigated how the compressive strength of concrete will influence its fatigue behavior. This is done as some research has found that the fatigue life of concrete gets relatively lower as the concrete strength increases. This is also acknowledged in e.g. EN 1992-2, MC1990 and MC2010 where the design fatigue reference strength is reduced more the higher the compressive strength is, see chapter 3.

To find the effect of the concrete strength on fatigue behavior *data series 2 and 3* are used, as they represents varying concrete strengths. The minimum stress ratio, $S_{c,min}$ is slightly different for the two data series, however the difference is so small that it is assumed to be neglectable for the intended purpose. On figure 5.10 both *data series 2 and 3* are plotted together with its regression lines. The regression lines are obtained by MLM taking run-outs into account.

It is noted that the data from [Lohaus et al., 2012] represent mean values from a total of 272 tests whereas the data from [Sørensen] represent failure or run-out for each test specimen.

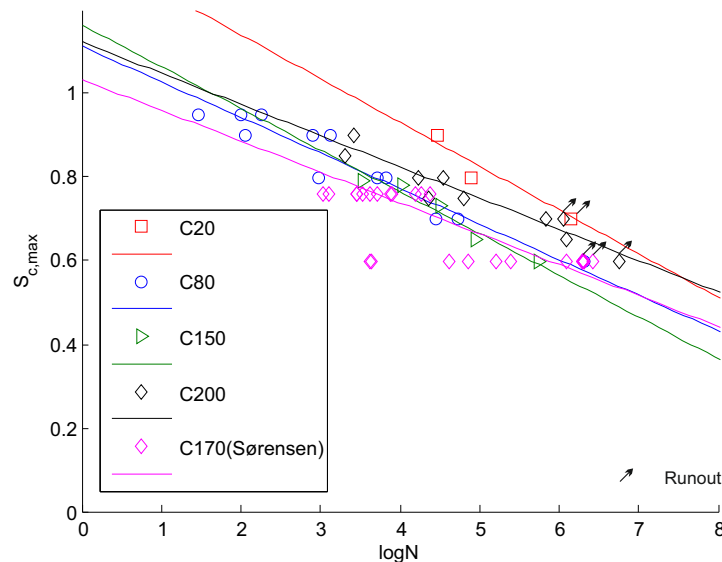


Figure 5.10. Fatigue tests with corresponding regression lines at $S_{c,min} \approx 0.05$. Run-outs are included.

The regression lines are made for all data representing the same concrete strength without taking account of different frequencies, steel fibres or heat treatment as the effect of these conditions are not investigated in this report. Furthermore

concrete strength C70 and C90 from *data series 2* are not taken into account as only one data point was available which is insufficient to make a meaningful regression line.

By looking at figure 5.10 no conclusive tendency can be seen regarding the fatigue behavior compared to the compressive strength based on the used data. This is made more clear on figure 5.11 where the intersection of the regression lines at $\log N = 8$ are shown with the compressive strength of the concrete depicted on the x -axis.

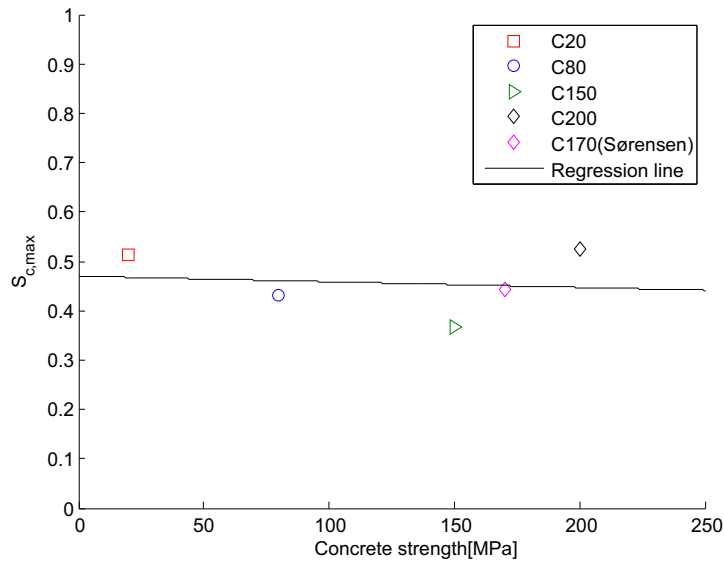


Figure 5.11. Fatigue strength of concrete at $\log N = 8$ for different concrete strength.

The points on figure 5.11 does not show the tendency adopted in the codes. A linear regression line from maximum likelihood method is also shown on figure 5.11 which follows eq. (4.4). In table 5.5 the slope, intersection with the $S_{c,max}$ -axis and standard variation of the error term is listed.

Intersection with $S_{c,max}$ -axis	0.4748
Slope	-0.0001
Standard deviation	-0.0527

Table 5.5. Parameters for regression line of concrete strength.

As the line is practically horizontal it cannot be concluded that concrete is being more sensitive to fatigue the stronger it is from the data that has been investigated in this report. However it is based on only 5 different concrete strengths and to make any general conclusions a test series should be planned specifically to investigate this effect.

As conclusion this report does not intend to include the effect of reducing the fatigue strength as the compressive strength increases, in the developed failure surface.

5.3 Validation of Failure Surface

As the developed failure surface is deviating from the one in [Lohaus et al., 2012], but is based on the same data, the two will be compared in this section. This is done to validate that the accuracy of the developed surface has improved, compared to the one in [Lohaus et al., 2012], with respect to the acquired data. On figure 5.12 the two failure surfaces are compared to the best fitting regression line using MLM, for the data at $S_{c,min} = 0.05$ from *data series 1*.

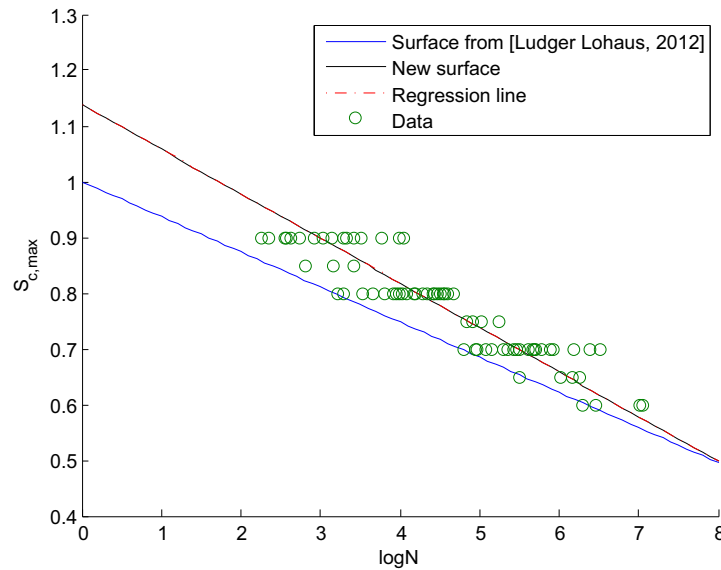


Figure 5.12. Comparison between the new surface, the one in [Lohaus et al., 2012] and *data series 1*.

On the figure it is seen that the developed failure surface capture the data more accurately than the one from [Lohaus et al., 2012]. In appendix C.3 similar figures are shown for $S_{c,min} = 0.20$ and $S_{c,min} = 0.40$ that both leads to the same conclusion of the new surface being more accurate for the acquired data. However it is noted that the developed failure surface becomes more similar to the surface from [Lohaus et al., 2012] as $S_{c,min}$ increases. This effect is also expected by looking at figure 5.4, where the $S_{c,max} = 1$ -line approaches $\log N = 0$ for higher $S_{c,min}$.

To further validate the developed surface it is plotted on figure 5.13 against *data series 2*. For comparison the surface from [Lohaus et al., 2012] and the regression line for the data is plotted on figure 5.13 as well.

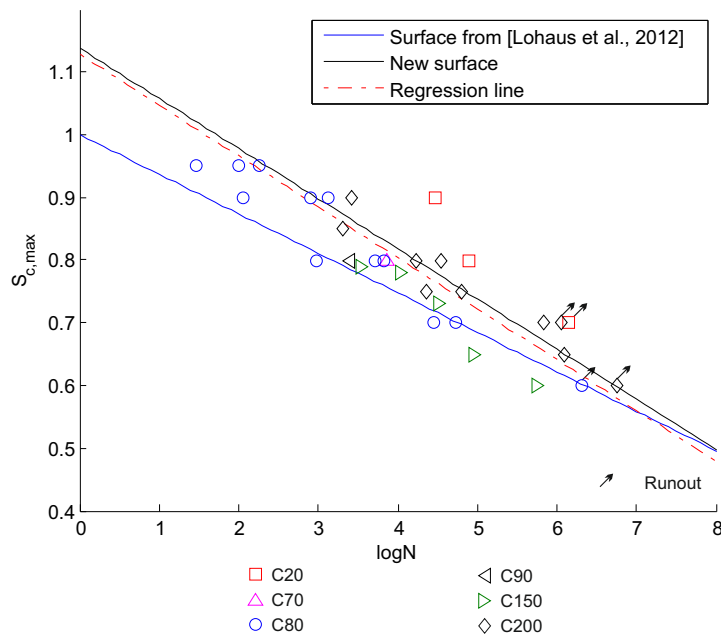


Figure 5.13. Comparison between the new surface, the one in [Lohaus et al., 2012] and data series 2.

It can be seen that the new failure surface is very close and almost parallel to the regression line, whereas the surface from [Lohaus et al., 2012] is conservative compared to both. As result it can be concluded that the new surface approximates the fatigue behavior of various concrete strengths more accurately than the one in [Lohaus et al., 2012], with respect to the data used in this report.

5.4 Comparison Between Developed Surface and those used in the Investigated Codes

To see how much the developed surface deviates from those used in the investigated codes a comparison is made. The comparison is made at $S_{c,min} = 0.05$, $S_{c,min} = 0.20$ and $S_{c,min} = 0.40$ to compare with the acquired data as well. The comparisons are shown on figures 5.14, 5.15 and 5.16.

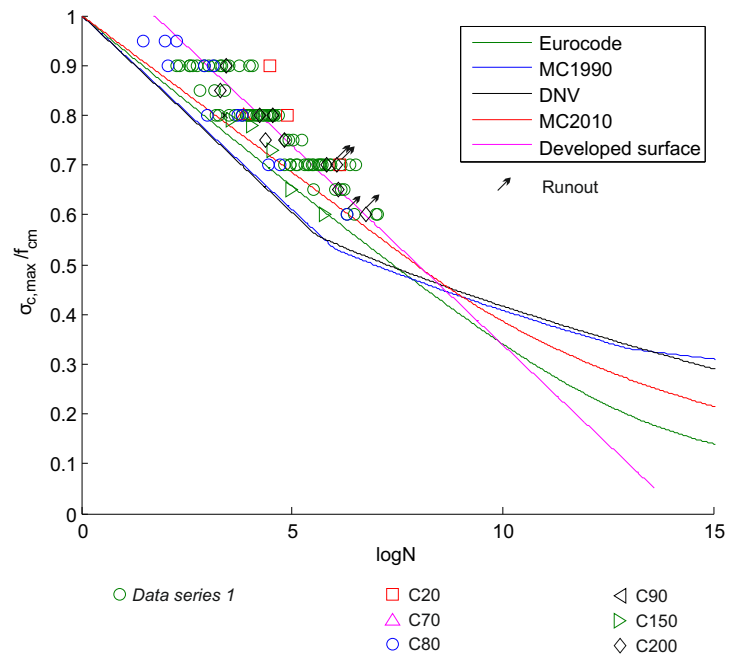


Figure 5.14. Comparison between failure surfaces at $S_{c,min} = 0.05$. Data are shown as well.

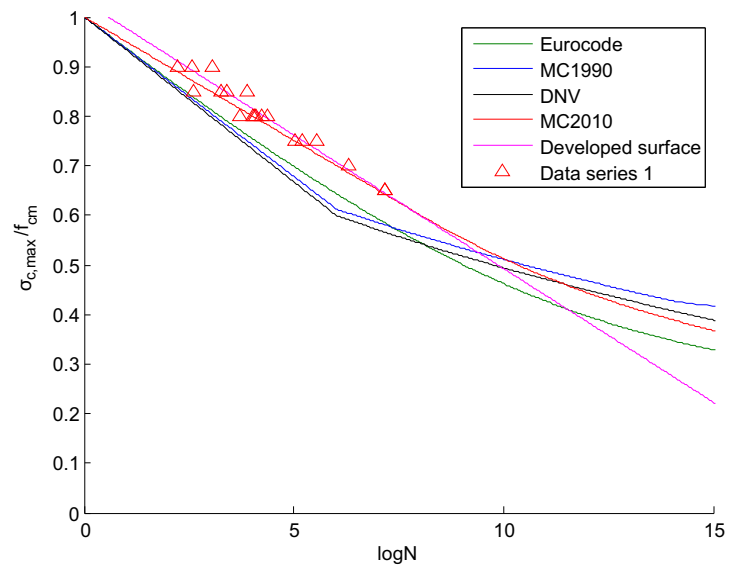


Figure 5.15. Comparison between failure surfaces at $S_{c,min} = 0.20$. Data are shown as well.

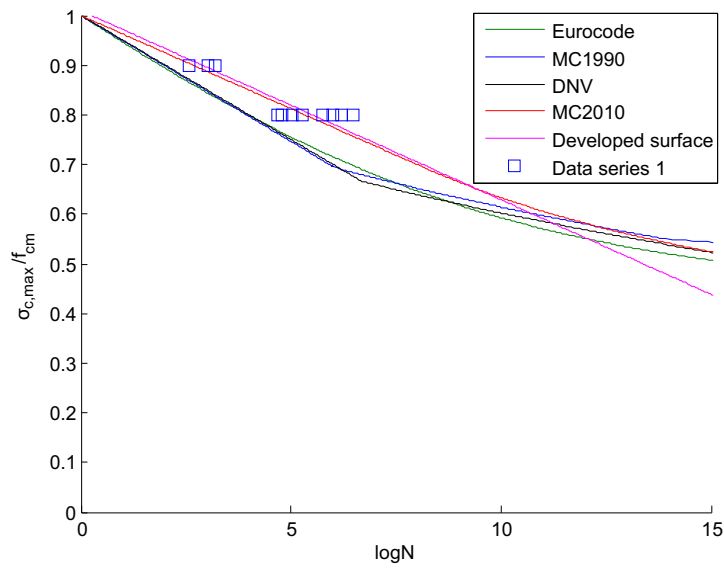


Figure 5.16. Comparison between failure surfaces at $S_{c,min} = 0.40$. Data are shown as well.

The following observations are made from the comparisons:

- The developed surface deviates from the codes but captures the data most accurately.
- for $S_{c,min} = 0.05$ the deviation is largest but it decreases fast as $S_{c,min}$ rises.
- All investigated codes tend to become asymptotic for high $\log N$.

As conclusion it can be expected that the investigated codes are conservative when evaluated against the developed surface, for design cases where low $S_{c,min}$ and low $\log N$ -values are dominating. For design cases where high $\log N$ -values are dominant the opposite is expected.

Part II

Reliability and Uncertainty

In this part of the report a reliability analysis is conducted to assess the reliability level of the codes, that are presented in part I.

To estimate the reliability level of the codes design equations are formulated for each code. The resulting design parameters are then evaluated using two different limit state equations, based on the developed failure surface from part I, and the failure surface from [Lohaus et al., 2012].

Using the limit state equations the partial safety factors of the codes are calibrated. Then a sensitivity study is carried out for the stochastic variables that are introduced in the limit state equation, to evaluate the importance of each.

Last in this part a discussion and a conclusion is presented. which sums up the investigations that are carried out throughout the report.

Reliability Theory

In this chapter a general introduction to the reliability theory, that is used in this part of the report, is presented. Generally the reliability concept arises as nothing can be determined deterministic, due to the randomness that appear in nature. Instead stochastic variables are introduced which allows uncertainties to be taken into account from e.g. the measurements and imperfect mathematical models. In general all uncertainty can be divided into four groups:

- **Physical uncertainty** from the natural randomness of a quantity.
- **Measurement uncertainty** from the uncertainty connected to measurements of e.g. strength parameters or geometrical properties.
- **Statistical uncertainty** occurs as only a limited sample size is observed for the quantity that is determined.
- **Model uncertainty** is introduced as the mathematical models that are used to describe the behavior of nature are approximate.

6.1 General reliability theory

Generally the methods that are used to measure the reliability of a structure can be divided into four groups [Sørensen, 2011b]:

- **Level I methods** The uncertain parameters are modelled by a characteristic value, and partial safety factors are introduced to calibrate the reliability. A typical example of a level I method is design codes.
- **Level II methods** The uncertainties are introduced by using stochastic variables and taking correlation between them into account. The stochastic variables are implicitly assumed to be normal distributed. An example of a level II method is the reliability index method.
- **Level III methods** The uncertain quantities are modelled as their joint distribution functions, and the probability of failure is estimated as a measure of reliability.

- **Level IV methods** Consequence and risk is taken into account. This enables different design to be compared on an economical basis, taking into account failure probabilities, costs and benefits of the structures.

Level I methods can be calibrated by level II methods and level II methods can be calibrated by level III methods etc. In this report level II-II methods are used to calibrate level I methods.

6.1.1 Failure surface

For a sample space, ω , a failure function can be formulated which divides the space into a safe region, ω_s , and a failure region, ω_f . This is shown in eq. (6.1).

$$f(\mathbf{x}) \begin{cases} > 0 & , \quad x \in \omega_s \\ \leq 0 & , \quad x \in \omega_f \end{cases} \quad (6.1)$$

Where

\mathbf{x} | Is a vector $[x_1, x_2, \dots, x_n]$ containing realizations of \mathbf{X}
 \mathbf{X} | Is a vector $[X_1, X_2, \dots, X_n]$ with n stochastic variables

This is illustrated on figure 6.1 in a 2-dimensional space for simplicity.

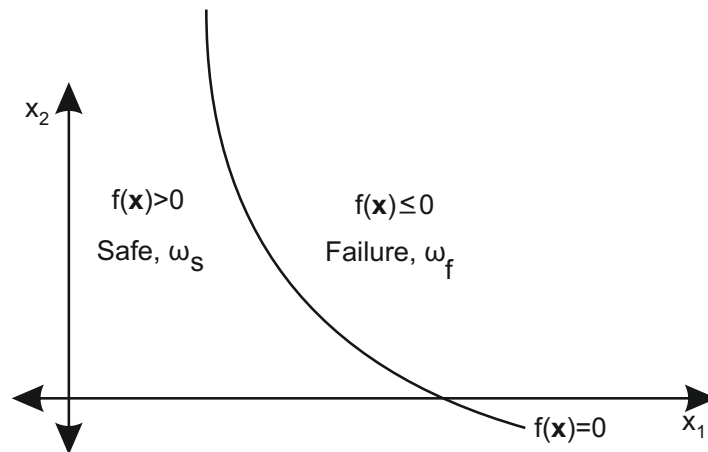


Figure 6.1. Illustration of sample space divided by a failure function in a 2-dimensional space.

When looking at figure 6.1 the probability of failure, P_f , can be obtained as the probability that the realized x_1 and x_2 corresponds to a point located in ω_f .

6.1.2 Reliability index

The reliability index, β , can be used to describe the reliability of a structure. There are several ways to define the reliability index and in this report the definition by Hasofer & Lind is used. The reliability index for uncorrelated stochastic variables is calculated by transforming the stochastic variables, \mathbf{X} , to a normalized set of stochastic variables, \mathbf{U} . This is done by the identity shown in eq.

(6.2).

$$\Phi_{U_i}(u_i) = F_{X_i}(x_i) \quad (6.2)$$

Where

X_i	Stochastic variable i in the physical domain with realization x_i
U_i	Normalized stochastic variable i in U-space with realization u_i
F_{X_i}	Distribution for X_i
Φ_{U_i}	Cumulative standard normal distribution for U_i

β can then be found as the shortest distance between origo and $f(\mathbf{u}) = 0$ in the U-space. This is illustrated in figure 6.2.

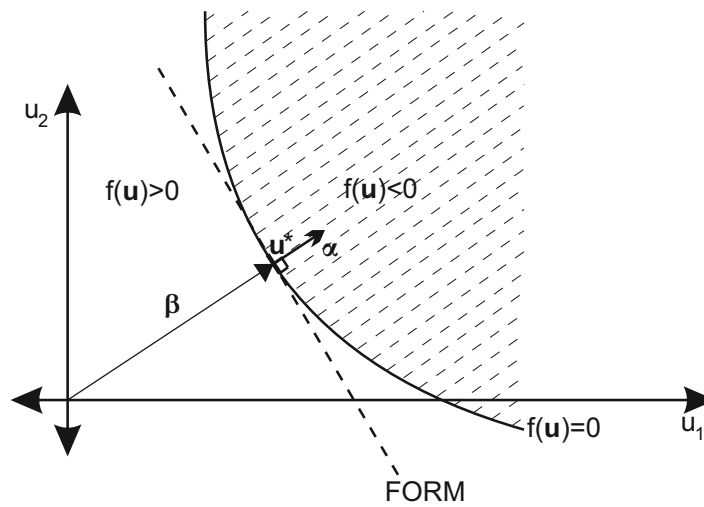


Figure 6.2. Illustration of β and FORM.

The point, u^* , on $f(\mathbf{u}) = 0$ that has the shortest distance to origo is referred to as the beta point. By transforming u^* back into the physical domain a design point, x^* , can be obtained.

6.1.3 FORM

In order to convert the reliability index into a probability of failure first order reliability method, or FORM, is used in this report. By looking at figure 6.2 it can be seen that the probability of failure can be calculated as the probability of $f(\mathbf{u}) \leq 0$. The exact solution to this would be to calculate the probability that the realisations of U_1 and U_2 , corresponds to a point in the hatched area on figure 6.2. However for non-linear failure functions this can be difficult to obtain, so in order to approximate it a linerization of the failure function is made in u^* . This is also illustrated in figure 6.2. It is then assumed that all area behind the linear tangent line corresponds to failure, and the relation between β and the probability of failure simplifies to eq. (6.3).

$$P_f = \Phi(-\beta) \quad (6.3)$$

The unit vector, α , showed in figure 6.2 is normal to the beta point, and the values of α can be interpreted as the sensitivity of β to the different variables in \mathbf{U} . The sensitivity can also be measured by the sensitivity elasticity e_p defined in eq. (6.4).

$$e_p = \frac{d\beta}{dp} \frac{p}{\beta} \quad (6.4)$$

where

p | Stochastic moment to be investigated

The interpretation of e_p is that if p is changed 1% then β is changed $e_p\%$.

6.1.4 Correlated variables

In some cases the different stochastic variables that are investigated will be correlated, which has to be taken into account to give a reasonable estimate of the reliability. For normal distributed variables this can be done by Choleski triangulation which is briefly explained.

The correlated stochastic variables \mathbf{X} are transformed into correlated normalized variables \mathbf{Y} , see eq. (6.5).

$$Y_i = \frac{X_i - \mu_{X,i}}{\sigma_{X,i}} \quad (6.5)$$

The correlation matrix, ρ , will be the same for \mathbf{X} and \mathbf{Y} [Sørensen, 2011b]. The normalized variables in \mathbf{Y} are then transformed into normalized non-correlated variables \mathbf{U} by a lower triangular matrix \mathbf{T} , see eq. (6.6).

$$\mathbf{U} = \mathbf{T}\mathbf{Y} \quad (6.6)$$

\mathbf{T} can be obtained by eq. (6.7) [Sørensen, 2011b].

$$\mathbf{T}\mathbf{T}^T = \rho \quad (6.7)$$

The non-correlated normalized stochastic variables \mathbf{U} can then be used in a reliability analysis using FORM as described earlier. Lastly it is recognized that the described transformation for normal distributions can be used for lognormal distributions by using the relation that if $A = \ln(B)$ and B is lognormal distributed then A will be normal distributed.

6.1.5 Target reliability

When designing a structure it is important to know what reliability it should reach, in order to have adequate safety. This is referred to as the target reliability index, β_t .

The reliability of a structure is time dependent, e.g. the probability of failure for a structure is higher in a 100year reference period than in a 10year reference period. It is therefore important to clearly state the time reference for the target

reliability. In this report annual target reliabilities for a certain year is used. These are found using the relationship described in eq. (6.8).

$$\beta_{annual,n} = \beta_n - \beta_{n-1} \quad (6.8)$$

Where

$\beta_{annual,n}$		Is the n'th year annual reliability
β_n		Is the reliability for a reference period of n years
β_{n-1}		Is the reliability for a reference period of n-1 years

6.1.6 Reliability in codes

In order to assess the reliability of a design based on codes, a design equation as shown in eq. (6.9) is introduced.

$$G(\mathbf{p}, z, \mathbf{x}_c, \boldsymbol{\gamma}) = 0 \quad (6.9)$$

Where $\mathbf{x}_c = (x_{c1}, x_{c2}, \dots, x_{cn})$ are n characteristic values corresponding to $\mathbf{X} = (X_1, X_2, \dots, X_n)$, $\mathbf{p} = (p_1, p_2, \dots, p_k)$ are k deterministic quantities and $\boldsymbol{\gamma} = (\gamma_1, \gamma_2, \dots, \gamma_m)$ are m partial safety factors. The partial safety factors are derived to ensure sufficient safety when using \mathbf{x}_c as basis for the design. Using the design equation a value for the design parameter, z , is found. The design parameter could e.g. be the cross-sectional area of a bar or the first moment of area for a beam.

The optimal design parameter is then used in a limit state equation defined as in eq. (6.10).

$$g(\mathbf{p}, z, \mathbf{X}) = 0 \quad (6.10)$$

To estimate the reliability FORM can be used on the limit state equation. This can be compared to the target reliability that the code should reach in order to determine whether or not the code is conservative in the given design.

Loads

To evaluate the design from the different codes that has been presented in chapter 3 two fatigue limit state cases are investigated. A foundation for an onshore wind turbine and a bridge subjected to traffic load.

The loads are divided into two case for the bridge. First loads used for the design equations are determined as deterministic loads, secondly the loads used for the limit state equation are found where an uncertainty of the weight of the vehicles is included.

7.1 Bridge

The static system of the bridge can be seen on figure 7.1.

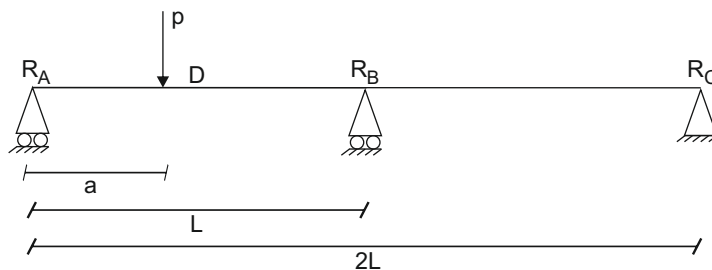


Figure 7.1. Static system of the bridge.

As seen on figure 7.1 the bridge is assessed as a continuous simple supported two span beam. In this report two loads acting on the bridge are taken into account namely dead load from the bridge itself and traffic load. The point of interest, D, is mid span at $\frac{L}{4}$.

7.1.1 Traffic Load

In this section the traffic loads working on the bridge will be estimated. The traffic loads are modelled as recommended in EN 1991-2, which offers several traffic models for fatigue:

- *Load Model 1*

- *Load Model 2*
- *Load Model 3*
- *Load Model 4*
- *Load Model 5*

Load Model 1 and *Load Model 2* are used to check if the fatigue life is unlimited and thus will not be used further in this project.

Load Model 3 models a single lorry passing over the bridge.

Load Model 4 models a set of standard lorries passing over the bridge, however it does not model more than one lorry crossing the bridge simultaneously. EN 1991-2 states that *Load Model 4* simulates real traffic more accurately than *Load Model 3* thus *Load Model 3* will not be investigated further.

Load Model 5 is modelled through traffic measurement, which is not available in this project and thus *Load Model 5* cannot be used.

First the number of lorries passing over the bridge in a year has to be specified, the traffic acting on the bridge is assumed to be in Traffic category 2 and the number of lorries passing over the bridge in a year is assumed to be $N_{obs} = 0.5 \cdot 10^6$. EN 1991-2 specifies the distribution of the lorries, and how they are modelled, through different traffic types, where traffic type 2 is chosen in this report.

Furthermore the weight of each single lorry is randomized by a stochastic scaling factor which is assumed lognormal distributed with a mean of 1 and a coefficient of variation of 0.1 [Lohaus et al., 2012].

Convergence Analysis

When introducing the stochastic scaling factor it is important that it has converged for the amount of simulated lorries. Figure 7.2 shows the convergence analysis for the mean value of the scaling factor, and figure 7.3 shows the convergence analysis for the standard deviation of the scaling factor.

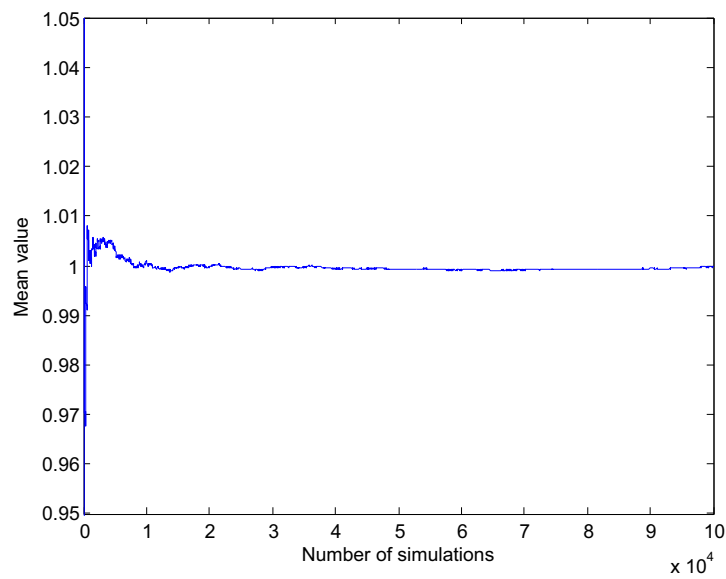


Figure 7.2. Convergence analysis of the mean value of the scaling factor.

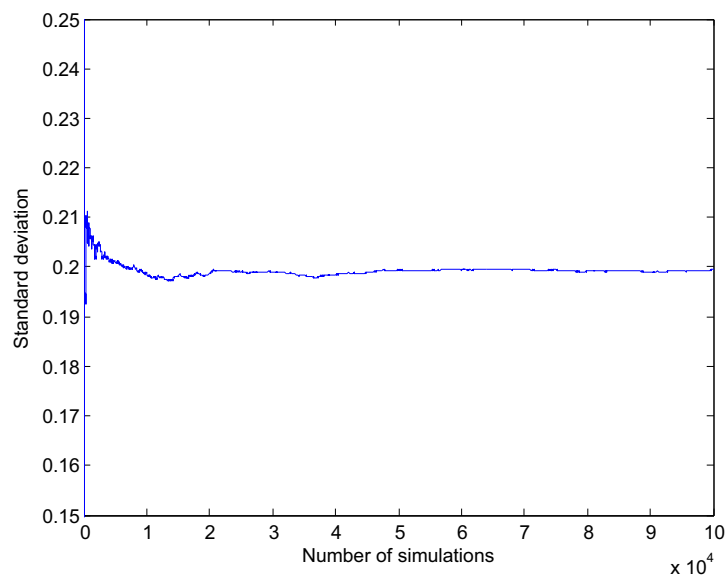


Figure 7.3. Convergence analysis of the standard deviation of the scaling factor.

As seen on figures 7.2 and 7.3 the stochastic scaling factor converges after approximately 2000 simulations, thus the lowest number of lorries of a certain type has to be greater than 2000. The amount of different lorry types is displayed in table 7.1 corresponding to traffic category 2 and traffic type 2 over a 1 year period.

Lorry type	amount
1	200000
2	50000
3	150000
4	75000
5	25000

Table 7.1. Amount of different types of lorries.

It can be concluded that the amount of simulated lorries for a 1 year period are sufficient, for convergence to occur.

Influence line

To find the load from *Load Model 4* acting at point *D* on figure 7.1 an influence line is calculated, see eq. (7.1). The moment is calculated positive clockwise.

$$M_D(a) = \begin{cases} -p\left(\frac{L}{2} - a\right) + \frac{(4pL^3 - 5pL^2a + pa^3)}{8L^2} & \text{if } 0 \leq a \leq \frac{L}{2} \\ \frac{(4pL^3 - 5pL^2a + pa^3)}{8L^2} & \text{if } \frac{L}{2} < a \leq L \\ \frac{(p(2L-a)^3 - L^2p(2L-a))}{8L^2} & \text{if } L < a \leq 2L \end{cases} \quad (7.1)$$

Where

p | Point load
 a | Distance between R_A and p , see figure 7.1

The influence line can be seen on figure 7.4.

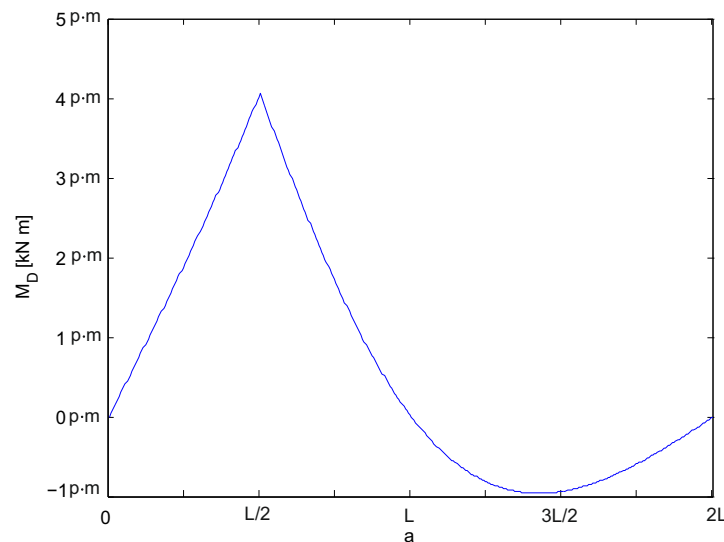


Figure 7.4. Influence line for the point *D*.

As the axles of the lorries pass the bridge it is assumed that only elastic deformations will occur. This implies that superposition can be used to find the total

load in point D when more than one axle from the lorry is positioned on the bridge.

7.1.2 Dead Load

To model the dead load a cross-section has to be estimated. The cross section is set to have a width of 10 m and a height of 1.2 m. It is assumed that the density of reinforced concrete is $2500 \frac{\text{kg}}{\text{m}^3}$. The dead weight of the bridge can then be modelled as a line load of $q_{dead} = 294.6 \frac{\text{kN}}{\text{m}}$ where the gravitational acceleration is assumed $9.82 \frac{\text{m}}{\text{s}^2}$. To find the influence of the line load in point D the line load is discretized into point loads. This is an approximation but as the discretization gets finer it will converge towards the true solution.

7.1.3 Total load

Figure 7.5 shows the simulated load in point D from 5 trucks passing over the bridge with 1 m/s. Superposition is used, so the dead load is added to the load from the trucks, which offsets the load. This is illustrated on figure 7.5.

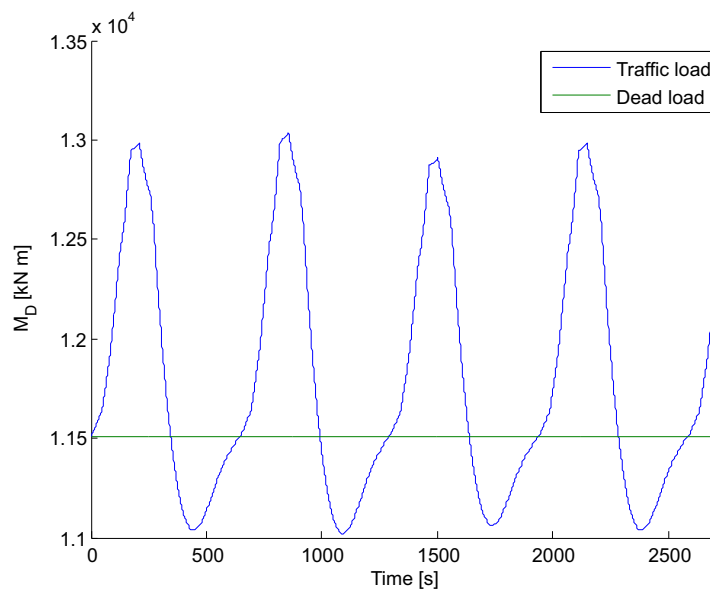


Figure 7.5. Time series of the load in point D for five trucks together with the dead load.

The entire time series for N_{obs} trucks moving at 1 m/s can be seen on figure 7.6 where only the extremes are shown.

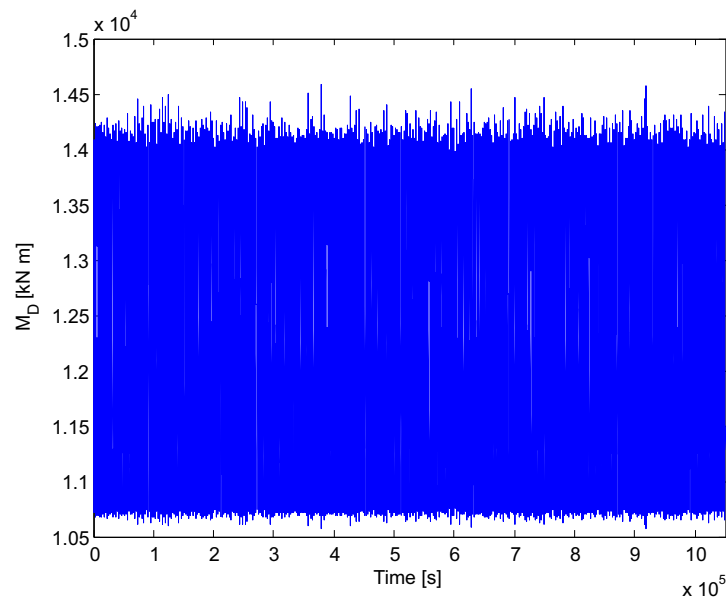


Figure 7.6. Entire time series.

After simulating one year of traffic, Rainflow counting is performed to extract the load cycles, represented by mean stresses and amplitudes. A histogram of the results are shown on figure 7.7 where the loads has been divided into 50 times 50 bins.

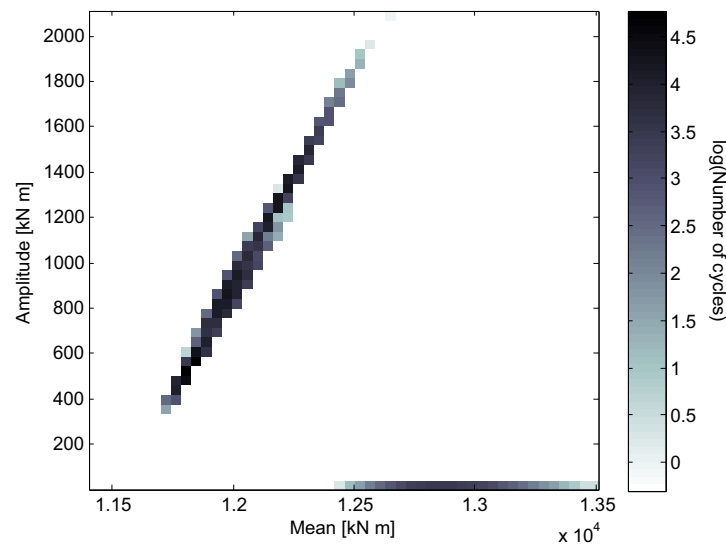


Figure 7.7. Histogram of the load cycles acting in point *D*.

Due to the results of the convergence analysis it is assumed that the histogram is representative for any year in the bridges lifetime. Hence for a n year period the amount of load cycles in each bin should be multiplied with n .

The entire time series of the loads for the design equations can be seen on figure 7.8, where the scaling factor is removed.

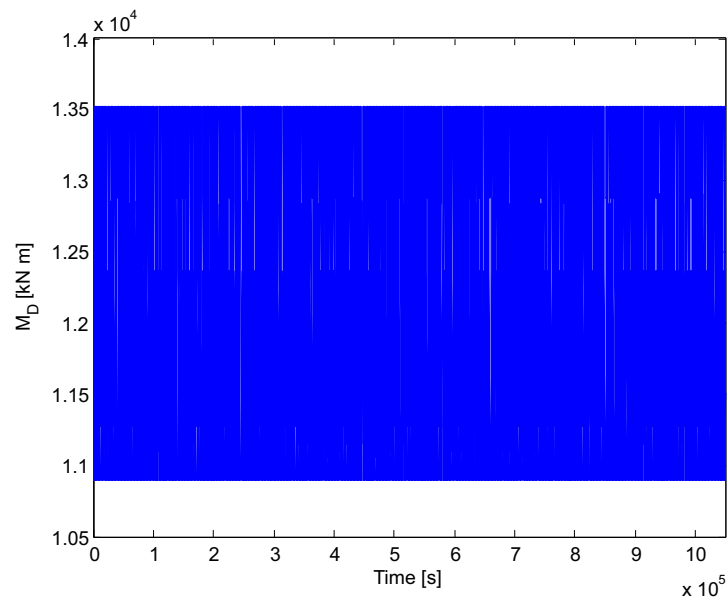


Figure 7.8. Time series for the design equation.

7.2 Wind Turbine Foundation

A time series of the moment working on the foundation of a wind turbine for a year, were provided by the project supervisors. This time series will be referred to as a Markov matrix. The Markov matrix contains both positive and negative moment, corresponding to compression and tension. Due to the scope of the report, all the moments which cause tension will be set to zero, e.g. if M_{max} is positive for a given cycle and M_{min} is negative then M_{min} will be set as zero. If both M_{max} and M_{min} is negative the entire cycle is dismissed. A histogram of the maximum and the minimum moments can be seen on figure 7.9.

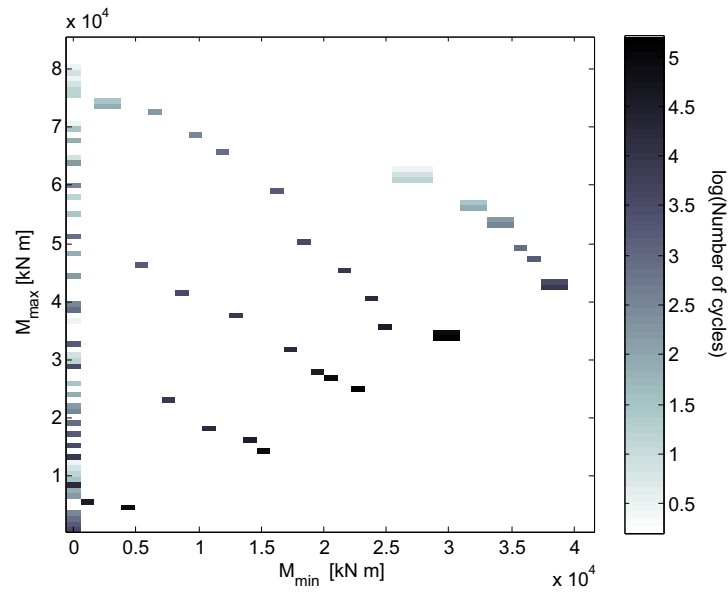


Figure 7.9. Histogram of the moments for the wind turbine foundation.

It can be seen on figure 7.9, that a part of the spectrum that is described has a M_{min} of zero. This is because all tensile stresses is set as zero, and thus all negative momentum is also set as zero. It can be seen that the failure surface presented in chapter 5, is non-conservative at low $S_{c,min}$. Due to this is can be expected that the reliability level of the codes for this case will be high, and in turn the calibrated partial safety factors will be low.

Design Equations

In this chapter the design equations used for the reliability assessment will be presented. All the design equations are based on the codes presented in chapter 3. Two main design cases are investigated in this report, namely the bridge and the wind turbine foundation, both of these uses the same design equations, but with different partial safety factors and lifetimes.

The loads acting on the bridge and the wind turbine foundation are found as moments in chapter 7. For the design equations stresses are used, thus the first moment of area needs to be found. This will be the design parameter, z_d , in the design equations.

In all the investigated design codes, Miners rule is used for damage accumulation, with a damage threshold of 1.0. The design equation is used to design to the limit which leads to the general design equation in eq. (8.1).

$$G(z_d, \mathbf{p}, \boldsymbol{\gamma}, \mathbf{M}_{min}, \mathbf{M}_{max}) = 1.0 - t \sum_{i=1}^k \frac{n_i}{N_i(z_d, \mathbf{p}, \boldsymbol{\gamma}, M_{min,i}, M_{max,i})} = 0 \quad (8.1)$$

Where

n_i	Actual stress cycles for stress state i pr. year
N_i	Allowed stress cycles for stress state i found differently depending on the investigated code
t	Lifetime of the structure [year]
k	Number of stress states
$\boldsymbol{\gamma}$	Vector containing partial safety factors
\mathbf{p}	Vector containing coefficients e.g. C_1 in DNV
\mathbf{M}_{min}	Vector containing minimum moments of the stress cycles
\mathbf{M}_{max}	Vector containing maximum moments of the stress cycles

In all the design equations the mean compressive cylinder concrete strength is assumed to be 125 MPa with a COV as presented in chapter 9, which yields a characteristic strength of 98.2 MPa.

In the background document draft CD 61400-1 ed 4 it is stated that a wind turbine normally should be designed for a lifetime of 20-25 years. In this report it is assumed that the wind turbine foundation is designed for a 25 year lifetime.

As DK NA EN 1993-2 states that a 100 year reference period should be used for steel bridges it is assumed the same can be applied for the concrete bridge in this report.

8.1 Effects that are not Considered in Design Equations

The codes presented in chapter 3, includes several effect which the data presented in chapter 4, and in turn the developed failure surface, does not take into account. These effect are divided into three categories.

- Stress gradient effects, modelled in codes by η and α .
- Time depended effects, modelled in the codes by f_{cn} , k_1 and β_{cc} .
- Relatively lower fatigue life for stronger concrete, modelled in the codes by α_{fat} and C_5 .

Because these effects are not modelled in the developed failure surface, they are removed from the design equations used to obtain the design parameters. As result the reliability analysis is only aimed towards the failure surfaces and partial safety factors that are adopted in the different codes.

In the following a short description is made about why the effects are not considered.

8.1.1 Stress gradient effects

The effect from having a stress gradient in the cross section is included in MC1990 MC2010 and DNV. However the data that is used in this report only covers uniform compression, which therefore also applies to the developed failure surface.

8.1.2 Time dependent effects

The acquired data that is used in this report does not include information about different ageing times of the test specimens. Therefore time dependent effects can not be investigated with respect to this data, and it is therefore not included in the developed failure surface. It is noted however that the time dependent effects modelled by k_1 and β_{cc} in Eurocode, MC1990 and MC2010 will negate each other if the fatigue loading starts after sufficiently long time.

8.1.3 Fatigue sensitivity dependent of concrete strength

The fatigue reduction in fatigue strength from α_{fat} and C_5 is neglected in the design equation as it was not observed on the acquired data. This was found in chapter 5, and is also observed in [Lohaus et al., 2012].

8.2 Eurocode

In this section it is described how N_i in the design equation is found for Eurocode. The design parameter is introduced as shown in eq. (8.2) and eq. (8.3).

$$\sigma_{cd,max,i} = \gamma_{F,fat} \frac{M_{max,i}}{z} \quad (8.2)$$

$$\sigma_{cd,min,i} = \gamma_{F,fat} \frac{M_{min,i}}{z} \quad (8.3)$$

These equations will replace equations (3.10) and (3.11). As α_{fat} , k_1 and β_{cc} are excluded from the design equations in the reliability analysis eq. (8.4) will replace eq. (3.2) and then the procedure described in chapter 3 is followed.

$$f_{cd,fat} = f_{cd} \quad (8.4)$$

As the required safety for the bridge and wind turbine differs different partial safety factors are used. The assumptions that are made are described below.

8.2.1 Bridge

As EN 1992-2 is intended for concrete bridges the recommendations specified in the code with national annexes are used, where the following assumptions are taken into consideration:

- The construction is made of reinforced in situ casted concrete, thus $\gamma_{C,fat} = 1.1 \cdot 1.45 \gamma_3$.
- The construction is in normal control class, thus $\gamma_3 = 1$.
- $\alpha = 1.0$ as recommended in DK NA EN 1992-2.
- The partial safety factor for the load is set to $\gamma_{F,fat} = 1.0$ as recommended in EN 1992-1-1.

The design parameter for the bridge using Eurocode can be found in table 8.1.

	z_d
Bridge	0.283 m ³

Table 8.1. Design parameters for the bridge found through Eurocode where α_{fat} , k_1 and β_{cc} are excluded.

8.2.2 Wind turbine foundation

There is no Eurocode available specifically intended for wind turbines. Therefore it is chosen to adopt the partial safety factor for the load from IEC 61400-1. This is done as it is assumed that the Markov matrix for the wind load is obtained as suggested in IEC. The material partial safety factor is taken from Eurocode as its failure surface is used.

It is noted that the partial safety factor for loads in IEC 61400-1 is 1.0 which is

the same as the partial safety factor for loads in EN 1992-2. As such the wind turbine is designed with the exact same partial safety factors as the bridge. This leads to an expectation that the reliability of the wind turbine will be too high for the chosen combination.

The following assumptions are taken into consideration for the wind turbine foundation:

- The partial safety factor for the concrete $\gamma_{c,fat}$ is set to $1.2 \cdot \gamma_n$ which corresponds to γ_m for FLS from IEC 61400-1.
- The foundation is assumed to be in component class two, thus $\gamma_n = 1.15$.
- α is found through EN 1992-2 and is similar to the bridge design.
- The partial safety factor for loads $\gamma_{F,fat}$ is set to 1.0 corresponding to $\gamma_F = 1.0$ for FLS in IEC 61400-1.

The design parameter for the wind turbine foundation is shown in table 8.2.

Z_d	
Wind turbine foundation	1.809 m ³

Table 8.2. Design parameters for the wind turbine foundation found through Eurocode where α_{fat} , k_1 and β_{cc} are excluded.

8.3 MC1990 and MC2010

In this section it is described how N_i is obtained for the design equations based on MC1990 and MC2010. The design parameter is introduced as shown in eq. (8.5) and eq. (8.6).

$$S_{cd,max,i} = \frac{\gamma_{Sd} \frac{M_{max,i}}{z}}{f_{cd,fat}} \quad (8.5)$$

$$S_{cd,min,i} = \frac{\gamma_{Sd} \frac{M_{min,i}}{z}}{f_{cd,fat}} \quad (8.6)$$

It is noted that γ_{Sd} is replaced by γ_{Ed} when MC2010 is considered. Furthermore it should be noticed that η_c is removed from the equations compared to equations (3.18) and (3.19).

To exclude α_{fat} , k_1 and β_{cc} the fatigue design reference strength is estimated by eq. (8.7).

$$f_{cd,fat} = \frac{f_{ck}}{\gamma_{c,fat}} \quad (8.7)$$

Equations (8.5) and (8.6) are then replaced with equations (3.18) and (3.19). Furthermore the design follows the general procedure described in chapter 3. Some assumptions has to be made for using the design equation, for the two considered design cases. These are described in the following.

8.3.1 Bridge

As both MC1990 and MC2010 are intended for the design of civil engineering works in general, the bridge is designed with the recommendations from these codes. The following assumptions are taken into consideration:

- The partial safety factor for the concrete is $\gamma_c = \gamma_{c,fat} = 1.5$ as recommended in the two codes.
- The partial safety factor for loads, $\gamma_{Sd} = \gamma_{Ed}$, is assumed to follow the recommended value of 1.1.

The design parameters for the bridge according to MC1990 and MC2010 are listed in table 8.3.

	Z_d
MC1990	0.310 m ³
MC2010	0.278 m ³

Table 8.3. Design parameters for the bridge from MC1990 and MC2010 where both η_c , α_{fat} , β_{cc} and k_1 are excluded.

8.3.2 Wind turbine foundation

To design the wind turbine foundation the draft CD IEC 61400-6 is included in the design as it is intended specifically for wind turbine foundations. Furthermore the draft CD IEC 61400-6 explicitly recommends the use of the failure surface from MC1990, and it is therefore assumed that it can be combined with MC2010 as well.

The draft CD IEC 61400-6 states that the partial safety factors for materials and loads should be found through IEC 61400-1 when designing for fatigue.

The following assumptions are taken into consideration when designing the wind turbine foundation using the material models from MC1990 and MC2010:

- The partial safety factor for the concrete $\gamma_c = \gamma_{c,fat}$ is set to $1.2 \cdot \gamma_n$ which corresponds to γ_m from IEC 61400-1.
- The foundation is assumed to be in component class two, thus $\gamma_n = 1.15$.
- The partial factor for loads $\gamma_{Sd} = \gamma_{Ed}$ is set to 1.0 corresponding to $\gamma_F = 1.0$ in IEC 61400-1.

The design parameters for the wind turbine foundation using the material model from MC1990 and MC2010 are listed in 8.4.

	Z_d
MC1990	1.656 m ³
MC2010	1.546 m ³

Table 8.4. Design parameters for the wind turbine foundation using MC1990 and MC2010 where α_{fat} , β_{cc} , k_1 and η_c are excluded.

8.4 DNV

In this section it is presented how N_i is estimated in the design equation for DNV. The design parameter is introduced as shown in equations (8.8) and (8.9).

$$\sigma_{cd,max,i} = \gamma_F \frac{M_{max,i}}{z} \quad (8.8)$$

$$\sigma_{cd,min,i} = \gamma_F \frac{M_{min,i}}{z} \quad (8.9)$$

Furthermore f_{cn} is replaced by f_{ck} , α is excluded and C_5 is neglected. This leads to f_{rd} being determined by eq. (8.10).

$$f_{rd} = \frac{f_{ck}}{\gamma_c} \quad (8.10)$$

Equations (8.8), (8.9) and eq. (8.10) are then replacing equations (3.26), (3.27) and equation (3.28). Furthermore the design follows the procedure described in chapter 3. When designing the bridge and the wind turbine two different DNV standards are taken into consideration. This is described in the following.

8.4.1 Bridge

When designing the bridge DNV-OS-C502 is used. It is specified in the code that it applies for deep water foundation of bridges, however it is assumed that by choosing an appropriate C_1 and Δ it can be used for this design as well. The following assumptions are taken into consideration when designing the bridge:

- The partial safety factor for the concrete γ_c is set to 1.5 which corresponds to reinforced concrete with normal tolerances.
- The bridge is assumed to be above the splash zone so $\Delta = 1$.
- The bridge is assumed to be located in air so $C_1 = 12$.
- The partial safety factor for loads $\gamma_F = 1.0$ as recommended in DNV-OS-C502 for FLS.

Table 8.5 shows the determined design parameter, using the listed assumptions.

	z_d
Bridge	0.270 m ³

Table 8.5. Design parameter for the bridge using DNV without taking α , f_{cn} and C_5 into account.

8.4.2 Wind turbine foundation

To design the wind turbine foundation DNV-OS-J101 is used as reference, as it is intended specifically for offshore wind turbines. As the foundation designed in this report is considered onshore, it is assumed that an appropriate choice of C_1 and Δ can compensate for the code being specified for offshore structures.

In DNV-OS-J101 it is recommended that the material model from DNV-OS-C502 is used together with the partial safety factors from DNV-OS-J101. Therefore When designing the wind turbine foundation the following assumptions are taken into account:

- The partial safety factor for the concrete γ_c is set to 1.5 which corresponds to reinforced concrete with normal tolerances according to DNV-OS-J101.
- The foundation is assumed to be above the splash zone so $\Delta = 1$.
- The foundation is assumed to be located in air so $C_1 = 12$.
- The partial safety factor for loads is $\gamma_F = 1.0$, as recommended in DNV-OS-J101 for FLS.

As this results in the bridge and wind turbine foundation using the same partial safety factors for DNV, it is expected that the foundation will obtain a conservative reliability level. The design parameter for the wind turbine foundation according to DNV is shown in table 8.6.

	Z_d
Wind turbine foundation	2.022 m ³

Table 8.6. Design parameters for the wind turbine using DNV without the effect from stress gradients and fatigue strength relative to compressive strength.

8.5 Comparison

All the design parameters from the different codes are listed in table 8.7 for comparison.

	Bridge	Wind turbine foundation
Eurocode	0.283 m ³	1.809 m ³
MC1990	0.310 m ³	1.656 m ³
MC2010	0.278 m ³	1.546 m ³
DNV	0.270 m ³	2.022 m ³

Table 8.7. Design parameters for the bridge and wind turbine obtained the presented design equations.

The following observations are made for the design parameters for the bridge:

- The design parameters are generally within reasonable ranges of each other.
- Compared to figure 3.12 the design parameter from Eurocode, MC1990 and MC2010 are as expected.
- DNV has the slightly most non-conservative design parameter which is not expected from figure 3.12. This is probably due to the combined partial safety factor, $\gamma_M \gamma_F$, being lower in DNV compared to the other codes.

The results from DNV for the bridge indicates that the assumptions made in section 3.6 about f_{cn} , α and C_5 neglects some safety, that is incorporated in the partial safety factors used in the other codes.

To further investigate this the design parameter from DNV is obtained using the partial safety factors from MC1990 and MC2010. The result is shown in table 8.8.

z	
Bridge	0.2975 m ³

Table 8.8. Design parameter for the bridge combining failure surface from DNV with partial safety factors from MC1990 and MC2010.

The acquired design parameter is as expected from figure 3.12 which further indicates that the assumptions used for DNV neglects some safety. As a result of this it is expected that the reliability analysis for DNV will yield non-conservative results for the bridge, compared to the other codes.

For the wind turbine foundation the following observations are made:

- The deviation of the design parameters obtained for the wind turbine foundation are significantly higher than for the bridge.
- The relation between the design parameters from MC1990 and MC2010 are as expected from figure 3.12.
- Eurocode and DNV are more conservative than MC1990 and MC2010 which is not expected from figure 3.12.

The high deviation of the design parameters is a result of the deviations of the used partial safety factors. DNV and Eurocode use the same as for the bridge, which also leads to them being the most conservative for the wind turbine foundation as expected.

Uncertainty Modeling and Limit State Equations

In this chapter, two different limit state equations are derived based the developed failure surface from chapter 5 and the failure surface from [Lohaus et al., 2012], which is also incorporated in MC2010 . The limit state equations are used to carry out the reliability analysis of the presented codes.

First a description is made of the general uncertainties that are used in both limit state equations. This covers the uncertainty related to Miner's rule, the uncertainty of the concrete strength itself and the uncertainty connected to how stresses are obtained.

After the introduction to the general uncertainties, the first limit state equation, LSE 1, is presented. The first limit state equation is based on the failure surface from chapter 5.

Last in this chapter the second limit state equation, LSE 2, is presented which is based on the failure surface from [Lohaus et al., 2012].

9.1 General Stochastic Variables

In both limit state equations some stochastic variables will reoccur. These stochastic variables are listed below and a description of each is given in this section.

- Δ , Miner's rule.
- X_{scf} , stress concentration factor.
- X_w , uncertainty considering the modelled wind.
- f_c , concrete strength.

9.1.1 Miner's rule

Miner's rule will be modelled as a lognormal distribution with a mean of 1.0 and a COV of 0.3 which is in accordance with [JCSS, 2014] for welded connections

in steel. It is recognized that this might be a crude estimation as it is used for concrete in this investigation, thus the *COV* of Miner's rule is subjected to a sensitivity study in section 10.4.

9.1.2 Factors affecting stresses

The stress concentration factor models the uncertainty related to assessment of stresses for a detail. It is assumed to be modelled as a lognormal distribution with a mean value of 1.0 and a *COV* of 0.1. The assumption is based on [Sørensen and Toft, 2014] which estimates the *COV* for tubular steel joints to range between 0.00 and 0.20.

As the *COV* for X_{scf} is applied to stresses in concrete in this investigation, a sensitivity study is made in section 10.4.

When investigating the reliability for the wind turbine foundation an uncertainty considering the modelling error of the wind itself and wind turbine structural dynamics is introduced. Therefore when assessing the wind turbine foundation X_w is introduced. It is modelled as presented in the background document draft CD IEC 61400-1 ed 4 as a lognormal distribution with a mean value of 1.0 [Dalsgaard and Toft, 2014]. The *COV* for X_w is found from eq. (9.1).

$$COV_{load} = \sqrt{COV_{wind}^2 + COV_{scf}^2} \quad (9.1)$$

Where COV_{load} should be at least 0.15 which corresponds to $COV_{wind} \approx 0.1$.

Application of X_{scf} and X_w

Two application of X_{scf} and X_w are considered in this report. In the first application the uncertainties are multiplied on both the stress ranges and the mean stresses as shown in eq. (9.2) and eq. (9.3).

$$S_{c,min} = \frac{X_{scf} X_w \sigma_{min}}{f_c} = \frac{X_{scf} X_w (\sigma_{mean} - \sigma_{ampl})}{f_c} \quad (9.2)$$

$$S_{c,max} = \frac{X_{scf} X_w \sigma_{max}}{f_c} = \frac{X_{scf} X_w (\sigma_{mean} + \sigma_{ampl})}{f_c} \quad (9.3)$$

Where

σ_{mean}		Mean stress of a given stress cycle
σ_{ampl}		Amplitude of a given stress cycle

For the bridge this implies that the effect of the dead load and the load from the passing vehicles have the same uncertainty. Similar for the wind turbine it corresponds to the mean wind and turbulence having the same uncertainty.

However it can also be assumed that the effect of the dead load and mean wind, is much more certain than the traffic load and turbulence, so eq. (9.2) and eq. (9.3) can be replaced with eq. (9.4) and eq. (9.5).

$$S_{c,min} = \frac{(\sigma_{mean} - X_{scf} X_w \sigma_{ampl})}{f_c} \quad (9.4)$$

$$S_{c,max} = \frac{(\sigma_{mean} + X_{scf} X_w \sigma_{ampl})}{f_c} \quad (9.5)$$

Both placements of \mathbf{X}_{scf} and \mathbf{X}_w are investigated in the reliability analysis where the first placement is referred to as application 1 and the second placement is referred to as application 2. It is noted that \mathbf{X}_w is neglected when the bridge design case is investigated.

9.1.3 Concrete strength

As the strength of concrete, f_c , is subjected to both aleatory and epistemic uncertainty it is included as a stochastic variable. The concrete strength is assumed to be lognormal distributed with a mean value, f_{cm} , and a standard deviation, σ_{fc} . According to DS/INF 172 the coefficient of variation for compressive strength of concrete can be found by eq. (9.6).

$$V_{fc} = \sqrt{V_m^2 + V_2^2} \quad (9.6)$$

Where

V_{fc}	Coefficient of variation for the compressive strength of concrete
V_m	Uncertainty for the strength parameter, found by eq. (9.7)
V_2	Uncertainty for the mathematical model used in the calculations

It is noted that V_2 will not be included in the uncertainty of V_{fc} in this investigation, as a model uncertainty is explicitly included, which is described in detail later in this chapter. The model uncertainty will cover the same uncertainty as V_2 however it will be based on the obtained data from chapter 4 compared with the used failure surfaces.

$$V_m = \sqrt{V_{m0}^2 + V_{mp}^2} \quad (9.7)$$

Where

V_{m0}	Coefficient of variation for the compressive strength of concrete, found by the running control made by the producer of the concrete.
V_{mp}	Uncertainty for the strength parameter, that stems from difference in laboratory tests and the final construction.

Values for COV can be found in DS/INF 172. In this report it is assumed that the concrete is reinforced and in situ cast. The relevant values from DS/INF 172 are listed in table 9.1.

	V_{m0}	V_{mp}	V_{fc}
Value from DS/INF 172	0.1	0.1	0.14

Table 9.1. Coefficients of variation from DSINF172 for in situ cast reinforced concrete.

When determining the coefficient of variation for the compressive strength of concrete it has to be noted that some literature assumes a constant standard deviation. This is e.g. the case in [Jensen, 2008] which is shown in appendix D.

9.2 Limit State Equation

Generally the basis of the limit state equations used to assess the reliability can be seen in eq. (9.8).

$$g(z, \mathbf{M}_{min}, \mathbf{M}_{max}, \mathbf{X}, \mathbf{p}) = \Delta - t \sum_{i=1}^k \frac{n_i}{N_i(z, M_{min,i}, M_{max,i}, \mathbf{X}, \mathbf{p})} \quad (9.8)$$

N_i is obtained differently depending on the limit state equation which will be described below.

9.2.1 Limit state equation LSE 1

In LSE 1 two different approaches are used to estimate the model uncertainty. These will be denoted uncertainty model I and uncertainty model II.

In uncertainty model I the mean failure surface presented in chapter 5 is treated deterministic, and the model uncertainty is modelled by a stochastic variable, $\mathbf{X}_{1,I}$. This is done by comparing data and model predictions.

In uncertainty model II the uncertainty of the developed surface will be introduced in the regression lines shown on figure 4.2 that are used as basis for the entire surface.

Uncertainty model I

In uncertainty model I N_i is obtained by eq. (9.9).

$$\log N_i = f_I (M_{max,i}, M_{min,i}, z, \mathbf{f}_c, \mathbf{X}_{scf}, \mathbf{X}_{1,I}) \quad (9.9)$$

Where

$$f_I = \frac{S_{c,max,i} - \left(1 - \frac{Y_1}{Y_2-8} Y_2\right)}{\frac{Y_1}{Y_2-8}} + \mathbf{X}_{1,I}$$

Where

$\mathbf{X}_{1,I}$	Model uncertainty for LSE 1 using uncertainty model I
Y_1	Found by eq. (9.10)
Y_2	Found by eq. (9.11)

$$Y_1 = 1 - (a_{N8} S_{c,min,i}^3 + b_{N8} S_{c,min,i}^2 + c_{N8} S_{c,min,i} + d_{N8}) \quad (9.10)$$

$$Y_2 = \frac{1}{\log(S_{c,min,i} + 1) a_{Smax1} + b_{Smax1}} + c_{Smax1} \quad (9.11)$$

Estimating $\mathbf{X}_{1,I}$

In uncertainty model I the model uncertainty is added to $\log N_i$. The uncertainty is modelled normal distributed with a mean of $\mu_{X_{1,I}}$ and a standard deviation of $\sigma_{X_{1,I}}$. These are found by comparing test results with the prediction from the failure surface, see figure 9.1 and 9.2, and by using maximum likelihood method

to optimize the parameters of $X_{1,I}$.

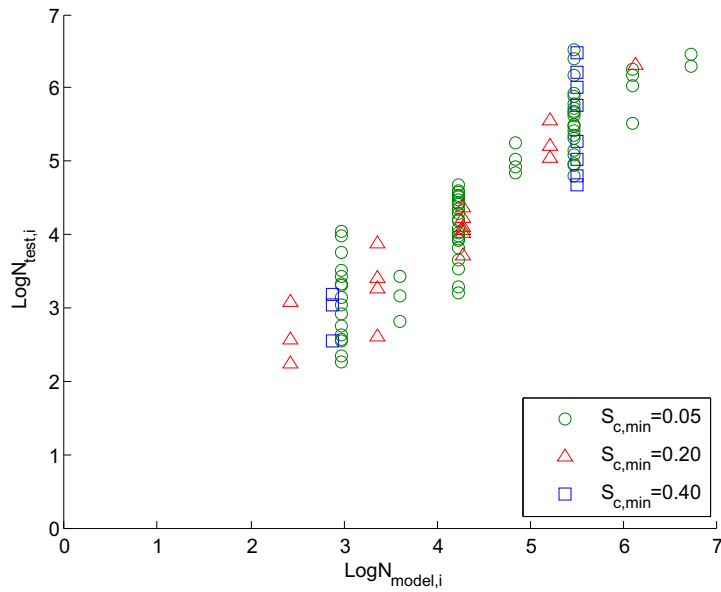


Figure 9.1. data series 1 plotted against model predictions.

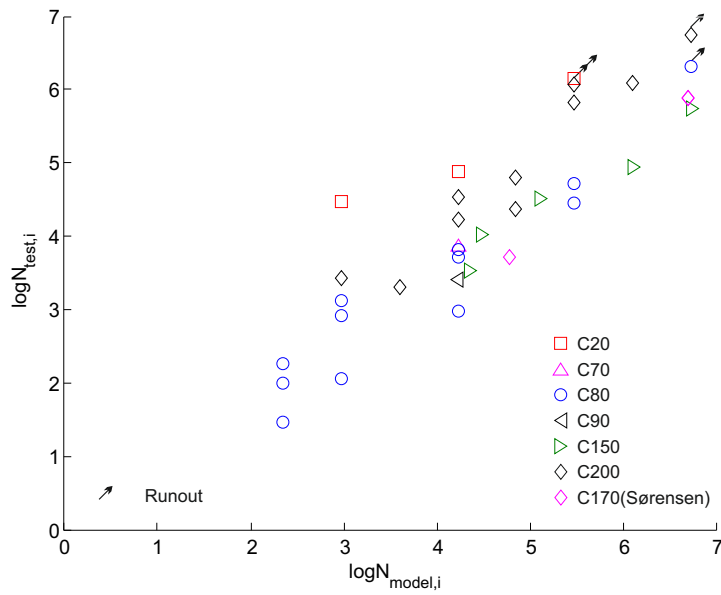


Figure 9.2. data series 2 and 3 plotted against model predictions.

To estimate $X_{1,I}$ all data that is presented in chapter 4 is used. As the failure surface is developed from *data series 1*, this data is included to take the scatter of the data into account. *data series 2 and 3* are included as well to take account for data with different strengths to make the uncertainty more general.

data series 3 is represented by its mean values to be in compliance with *data series 2*.

As there are run-out tests included in *data series 3* the mean values can not be estimated directly from the data by classic statistics. If classic statistics is used the run-out tests would be accounted for as tests with failure and as a result the mean value would be smaller than expected. Instead the mean values are estimated by the regression line shown on figure 5.10, as it include the effect of run-out tests by the use of MLM.

In table 9.2 the mean value and standard deviation for $X_{1,I}$ are shown by using the following data combinations for both the developed surface and the one presented in [Lohaus et al., 2012]:

1. All data.
2. *data series 2 and 3*, representing data with various concrete strengths.
3. All data for concrete stronger than 50 MPa.
4. *data series 2 and 3* for concrete strengths above 50 MPa.

The first two combinations are chosen to see how well the models predicts the fatigue behavior of concrete, both with and without *data series 1* from which they are constructed. The last two combinations are included to see how much effect the C20 concrete has on the uncertainty as the models are based on high strength concrete.

For combinations 1 and 3, it has to be noted that the amount of data is not equally distributed between the different concrete strengths. Hence *data series 1* will contribute with more than half the total amount of data points, and therefore this is weighted more than the two other data series when using MLM.

Combination	$\mu_{X_{1,I}}$	$\sigma_{X_{1,I}}$
1	0.10	0.51
2	-0.40	0.60
3	-0.11	0.49
4	-0.48	0.47

Table 9.2. Mean values and standard deviations for $X_{1,extI}$ for different data combinations.

From the results it can be seen that combination 2 and 4 has significantly larger mean values. This is because *data series 2 and 3* accounts for different concrete strengths compared to *data series 1*. Furthermore *data series 1* is used to develop the failure surface and therefore it is expected that the surface predicts those with a higher accuracy. On figure 9.3 the model uncertainty is illustrated for data combination 1.

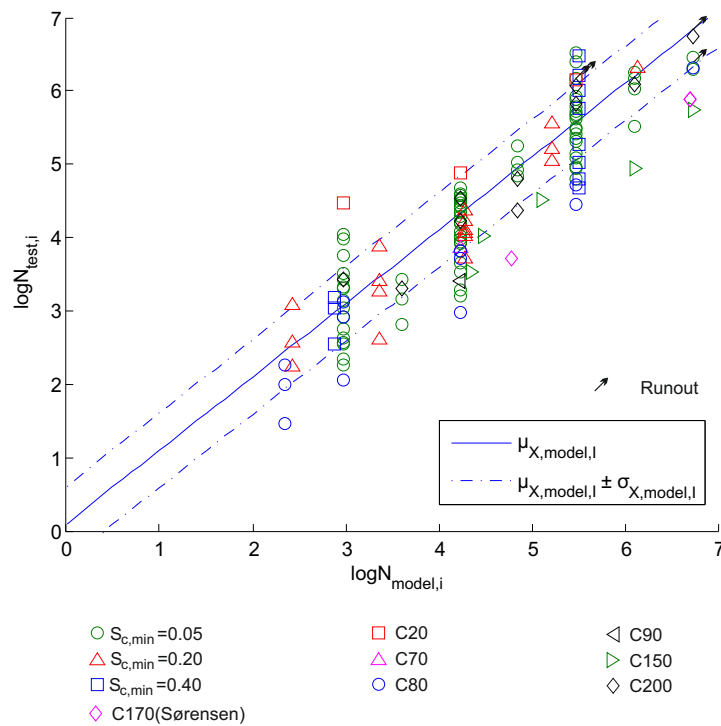


Figure 9.3. Model uncertainty using data combination 1 for the developed surface.

In appendix D the model uncertainty for the other data combinations are graphically shown as well. Generally it is seen that the mean and standard deviations are well estimated.

As the scope of the investigations in this report is high strength concrete the model uncertainty from combination 3 is used for further analysis, as it excludes the C20 concrete.

Estimating $X_{1,II}$

The general idea with uncertainty model II is to account for *data series 1* and *data series 2 and 3* separately. This is intended as *data series 1* is used as basis for the failure surface while *data series 2* and *3* are not taken into account when developing the failure surface.

Furthermore *data series 1* is represented by single tests while *data series 2* is represented by mean values from tests. Therefore it is expected that the equal weighting of the data that is used in uncertainty model I is underestimating the standard deviation, which is indicated by figure 9.3.

To account for the scatter in *data series 1* the *SN*-curves that were used as basis for the surface in chapter 5, are treated stochastic. To include the residual uncertainty from *data series 2 and 3* a model uncertainty is introduced which is added to $\log N_i$. This is done by comparing model predictions with *data series 2* and mean values of *data series 3*.

As *data series 2 and 3* are represented by mean values it is assumed that the scatter of the data is not taken into account twice.

In uncertainty model II $\log N_i$ is found by eq. (9.12).

$$\log N_i = f_{II}(M_{max,i}, M_{min,i}, z, f_c, \mathbf{X}_{1,II}, k_{2,0.05}, k_{2,0.20}, k_{2,0.40}, \epsilon_{0.05}, \epsilon_{0.20}, \epsilon_{0.40}) \quad (9.12)$$

As it can be seen, uncertainty model II contains more stochastic variables than uncertainty model I. This is due to the parameters k_2 and ϵ being modelled stochastic in the SN -curves that were used as basis for the developed surface. The function f_{II} is defined as eq. (9.13).

$$f_{II} = \frac{S_{c,max,i} - \left(1 - \frac{Y_1}{Y_2-8} Y_2\right)}{\frac{Y_1}{Y_2-8}} + \mathbf{X}_{1,II} \quad (9.13)$$

by seeing eq. (9.13), uncertainty model II may seem identical to uncertainty model I, this is however not the case. To illuminate the difference of the two, a point by point procedure of how uncertainty model II is constructed is presented below.

- Based on the data used to develop the surface the SN -curves used as basis for the developed failure surface are modelled stochastic to include the uncertainty related to the scatter of *data series 1*.
- A realization of the SN -curves at $S_{c,min} = 0.05$, $S_{c,min} = 0.20$ and $S_{c,min} = 0.40$ is made based on the values in table 9.3.
- The realized SN -curves are used to identify the points P_1 to P_3 and Q_1 to Q_3 using the same approach as in chapter 5.
- The Goodman line, and the $S_{c,max} = 1$ line are fitted to the points P_1 to P_4 and Q_1 to Q_4 . This alters the constants in Y_1 and Y_2 compared to uncertainty model I.
- By linear interpolation between the Goodman line and the $S_{c,max} = 1$ line the entire failure surface is created, similar to how the failure surface was developed in chapter 5.
- To include the residual uncertainty from *data series 2 and 3* the model uncertainty $X_{1,II}$ is introduced.
- *data series 3* is converted to mean values. Then both *data series 2 and 3* are represented by mean values, which is assumed to avoid taking scatter into account twice.

The expressions used to construct the Goodman line and the $S_{c,max} = 1$ line in chapter 5 are made to fit the points P_1 to P_4 and Q_1 to Q_4 , for the mean SN -curves. When modeling the failure surface stochastic it is not certain that the realized P_1 to P_3 and Q_1 to Q_3 corresponds to the mean curves from which the expressions in eq. (5.1) and eq. (5.2) fits. From this a problem of the fitted curves can arise, which is treated in appendix D.

The SN -curves are as mentioned treated stochastic in this model. As seen in appendix D each SN -curve is constructed as eq. (9.14).

$$\log N = k_1 S_{c,max} + \mathbf{k}_2 + \boldsymbol{\epsilon} \quad (9.14)$$

Where the moments for \mathbf{k}_2 and $\boldsymbol{\epsilon}$ for each SN -curves can be seen in table. 9.3.

	k_1		\mathbf{k}_2 (Norm. dist.)		$\boldsymbol{\epsilon}$ (Norm. dist.)		
	μ	σ	μ	σ	μ	σ	σ_σ
$S_{c,min} = 0.05$	-12.50	-	14.23	0.05	0	0.46	0.04
$S_{c,min} = 0.20$	-18.65	-	19.19	0.07	0	0.32	0.05
$S_{c,min} = 0.40$	-26.02	-	26.35	0.17	0	0.56	0.12

Table 9.3. Values for the parameters of the SN -curves at $S_{c,min}$ 0.05, 0.20 and 0.40.

It is assumed that \mathbf{k}_2 is fully correlated across the different SN -curves likewise is the error term $\boldsymbol{\epsilon}$. The assumption is based on the fact that it seem appropriate to believe that a concrete that is e.g. strong at one $S_{c,min}$ will also be so at any other $S_{c,min}$. However to validate the assumption tests at different $S_{c,min}$ could be made using test specimens from the same batch of concrete. This has not been investigated further in this report.

The standard deviations σ_{k_2} and $\sigma_{\sigma,\epsilon}$ are expressions of the statistical uncertainty.

The model uncertainty $\mathbf{X}_{1,II}$ is assumed normal distributed. It is found by MLM using *data series 2 and 3*. For simplicity the mean failure surface is chosen as being representative for all realizations of the SN -curves when estimating $\mathbf{X}_{1,II}$. This assumption is investigated and justified in appendix D. Using this assumption $\mathbf{X}_{1,II}$ is found by comparing the mean surface predictions with *data series 2 and 3*. However this is exactly what was done when finding $\mathbf{X}_{1,I}$ in combination 2 and 4. Therefore the results for $\mathbf{X}_{1,II}$ with and without the C20 concrete can be found directly in table 9.2.

As the scope of the report is high strength concrete combination 4 is chosen for further analysis due to the exclusion of the C20 concrete.

Comparison of model I and II

In this section a comparison is made between how the uncertainty of the developed failure surfaces is modelled in uncertainty model I and II.

- Uncertainty model I

In the first uncertainty model all uncertainty is included in the stochastic variable $\mathbf{X}_{1,I}$. As result uncertainty model I has the same uncertainty all over the surface. However the results in table 9.3 proves this to be a crude assumption.

When finding the parameters of $\mathbf{X}_{1,I}$ MLM is used, which weighs the data equally. However for combination 1 and 3 both single data points and data points representing means are evaluated. Due to this the estimated model

uncertainty may be imprecise.

As uncertainty model I treats all model uncertainty through one stochastic variable it is very simple to use compared to model uncertainty II.

- Uncertainty model II

In uncertainty model II the uncertainty from *data series 1* is included directly in the *SN*-curves and statistical uncertainty is taken into account. As a result the uncertainties from this data series may vary across the surface. This makes uncertainty model II able to alter the shape of the surface instead of only offsetting it on the $S_{c,max}$ -axis as model I.

As the Goodman diagram and the curve at $S_{c,max} = 1$ are optimized to capture the mean *SN*-curves their accuracy decrease as the realized *SN*-curves deviate from this, see appendix D.

$\mathbf{X}_{1,II}$ is included to account of the uncertainty from *data series 2 and 3* separately from *data series 1*. This way of modeling the uncertainties separate the data points that represents mean values and those representing single tests.

As uncertainty model II includes more stochastic variables than uncertainty model I it is more complicated to use and takes a longer time to calculate numerically.

9.3 Limit State Equation LSE 2

A second limit state equation, LSE 2, is included which is based on the failure surface from [Lohaus et al., 2012]. This limit state equation is introduced to make a comparison of the reliabilities that are found through the failure surface developed in this report and one incorporated in a current code.

To estimate the model uncertainty, X_2 , of LSE 2 the same approach as for $X_{1,I}$ is used. The results can be seen in table 9.4.

Combination	$\mu_{X,model,I}$	$\sigma_{X,model,I}$
1	0.71	0.66
2	0.57	0.80
3	0.69	0.64
4	0.47	0.67

Table 9.4. Mean values and standard deviations for \mathbf{X}_2 for different data combinations.

It can be seen that the standard deviations and mean values for LSE 2 are higher than for LSE 1, which is due to the assumption that the failure surface from [Lohaus et al., 2012] should cross $\log N = 0$ at $S_{c,max} = 1$. Figure 9.4 shows the predicted data and the observed data, together with the estimated uncertainty.

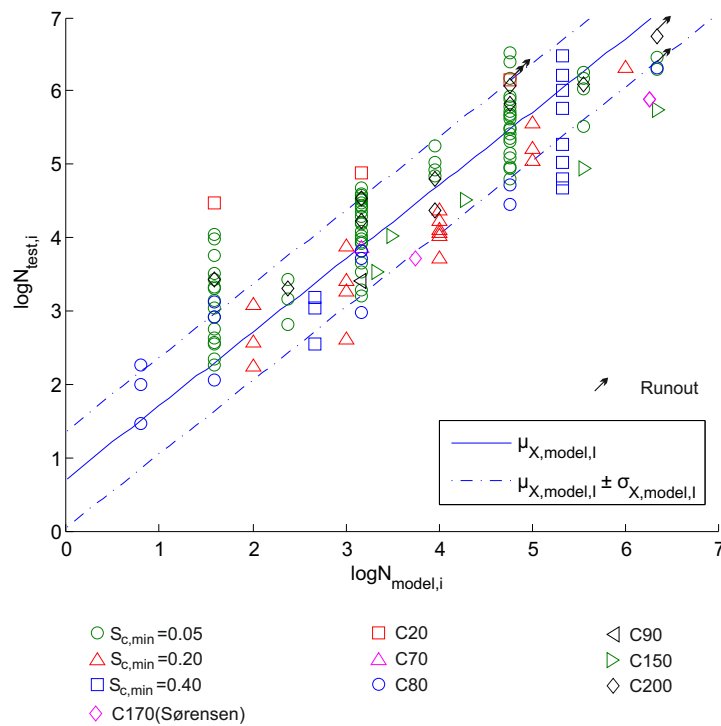


Figure 9.4. Model uncertainty using data combination 1 for the surface in [Lohaus et al., 2012].

As it can be seen on figure 9.4 and in table 9.4, the mean value is different from zero.

However as it was assumed in chapter 3 that the mean failure surface from MC2010 was without a bias this is investigated in the reliability analysis as well. This investigation is conducted to evaluate how much safety the bias accounts for.

The figures below illustrates the model uncertainty and how well it describes the data points. It can be seen that the assumption of removing the bias of the model uncertainty can be reasonable at high $S_{c,min}$ values, where the biased model uncertainty becomes non-conservative compared to the data points. However at low $S_{c,min}$ the unbiased uncertainty becomes less accurate and more conservative than the biased. The figures illustrate data combination 3.

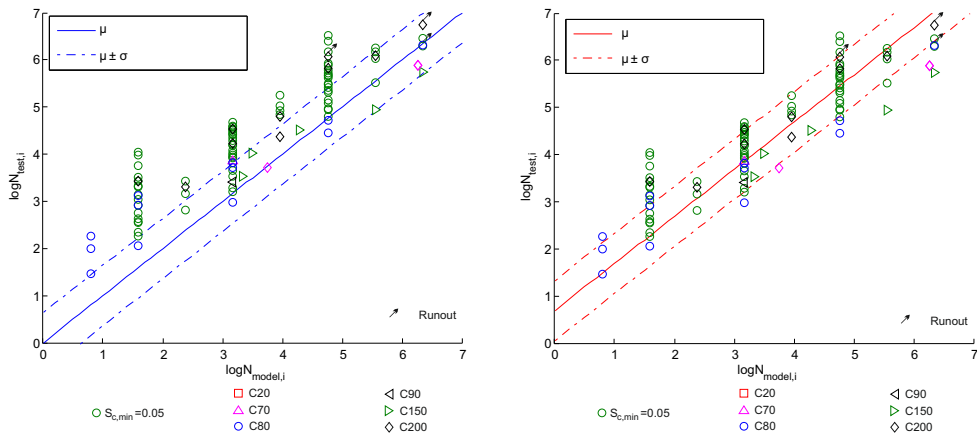


Figure 9.5. Illustration of model uncertainty for data at $S_{c,min} = 0.05$. Where the figure on the left is without bias and the right is with bias.

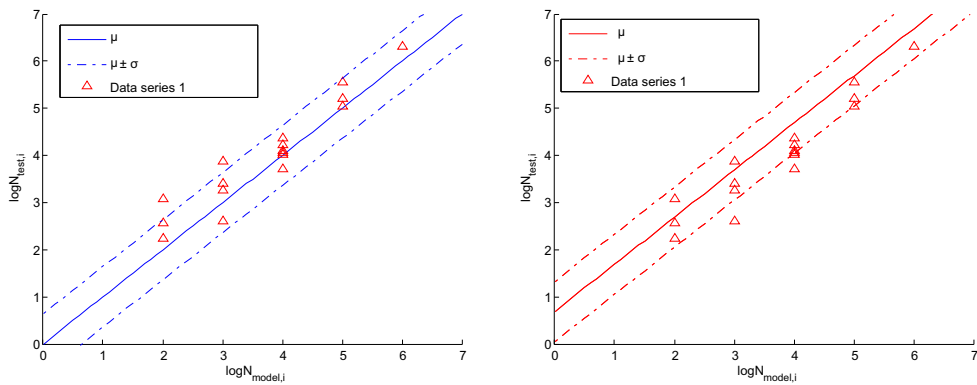


Figure 9.6. Illustration of model uncertainty for data at $S_{c,min} = 0.20$. Where the figure on the left is without bias and the right is with bias.

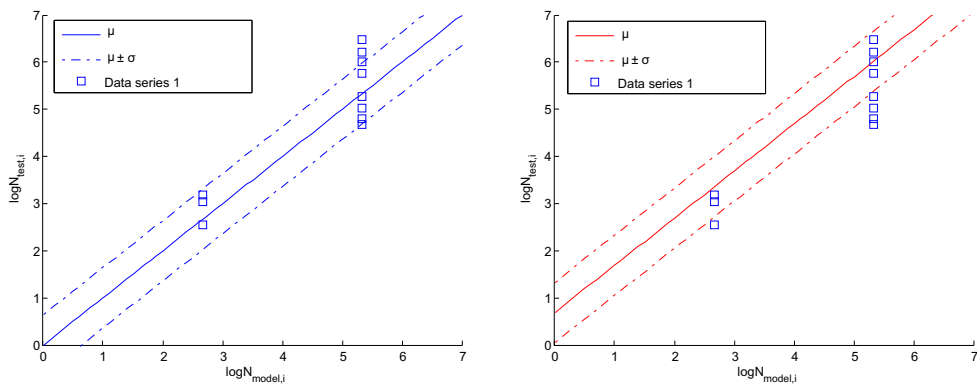


Figure 9.7. Illustration of model uncertainty for data at $S_{c,min} = 0.40$. Where the figure on the left is without bias and the right is with bias.

Reliability Analysis

In this chapter a reliability analysis is made for the presented codes in chapter 3. The reliability analysis is made using the limit state equations presented in chapter 9, and the design equations presented in chapter 8.

When designing the bridge an annual target reliability of $\beta_t = 5.2$ is assumed as minimum throughout its lifetime of a 100 years. This assumption is based on DK NA EN 1993-2 for steel bridges, where this annual target reliability is proposed corresponding to high safety class.

When designing the wind turbine foundation using IEC an annual target reliability of $\beta_t = 3.3$ is assumed as minimum throughout its lifetime of 25 years. This assumption is based on the background document draft CD 61400-1 ed 4 where this target annual reliability is proposed for unmanned structures.

When designing the wind turbine foundation according to DNV an annual target reliability of $\beta_t = 3.7$ is assumed as minimum throughout its lifetime. This is in accordance with DNV-OS-J101 where it is specified that the annual probability of failure should not exceed $P_f = 10^{-4}$ for unmanned structures.

In the end of the chapter a sensitivity study is conducted for the used limit state equations.

Throughout the chapter FORM is used to evaluate the reliabilities. In appendix D.5 a comparison is made between reliabilities found through FORM and Monte Carlo simulation to validate the use of FORM. Furthermore it is assumed that the minimum annual reliability level is obtained in the last year of the lifetime.

10.1 Reliability Level in Codes

In this section the annual reliability indices that are obtained through the design parameters from chapter 8 are presented and commented.

10.1.1 Bridge

The reliability levels for the bridge are presented in table 10.1. The number of the limit state equation is noted with 1 and 2, the used uncertainty model is noted

with I and II, and the application of \mathbf{X}_{scf} and \mathbf{X}_w is noted with app. 1 and app. 2.

	LSE 1,I, app.1	LSE 1,I, app.2
Eurocode	5.35	6.01
MC1990	5.76	6.55
MC2010	5.26	5.90
DNV	5.15	5.75
	LSE 1,II, app.1	LSE 1,II, app.2
Eurocode	5.25	5.88
MC1990	5.67	6.41
MC2010	5.17	5.77
DNV	5.06	5.63
	LSE 2, app.1 w. bias	LSE 2, app.2 w. bias
Eurocode	5.45	6.13
MC1990	5.87	6.67
MC2010	5.37	6.02
DNV	5.25	5.88
	LSE 2, app.1 wo. bias	LSE 2, app.2 wo. bias
Eurocode	5.30	5.94
MC1990	5.72	6.48
MC2010	5.22	5.84
DNV	5.11	5.69

Table 10.1. Annual reliability indices for the bridge design case using z_d found in table 8.7.

The following observations are made for the obtained reliabilities for the bridge:

- The annual reliability indices correspond well with the obtained design parameters.
- For application 1 of \mathbf{X}_{scf} the obtained reliability indices are close to β_t , except for MC1990.
- For application 2 of \mathbf{X}_{scf} the obtained reliability indices are higher than for application 1.
- The obtained reliability indices for LSE 1 and LSE 2 are very similar.
- The obtained reliability indices for LSE 1,I and LSE 1,II are very similar.
- LSE 2 with bias obtains slightly higher annual reliabilities than LSE 2 without bias.

The observations indicate that based on the data used in this report the partial safety factors could used in Eurocode, MC2010 and DNV could be applied for high strength concrete. However for application 2, where mean stresses are estimated with a higher certainty than the stresses from the passing vehicles, a reduction might be appropriate. The results also indicates that the material model that is incorporated in MC1990 generally should be combined with a lower material partial safety factor, with respect to the data used in this report.

Furthermore the results indicates that most of the fatigue damage is accumulated for a relatively high $S_{c,min}$ -value. This is investigated appendix D.7 where it is estimated that practically all fatigue damage stems from a stress state with $S_{c,min} \approx 0.6$, so the results are as expected.

It is noted that LSE 1,II had problems converging towards a solution using FORM. Therefore the results from LSE 1,II are assumed to be less reliable than the rest. However the obtained results from LSE 1,II indicates that modelling the model uncertainty with uncertainty model 1 i conservative compared to uncertainty model 2 for the bridge. As such it would be slightly conservative to use the results from uncertainty model 1.

Due to the convergence problems LSE 1,II is not considered further in the reliability analysis of the bridge as the results are too unreliable. The convergence problem is shown and explained in appendix D.6.

Wind turbine foundation

The reliability levels for the wind turbine foundation are presented in table 10.2.

	LSE 1,I, app.1	LSE 1,I, app.2
Eurocode	5,45	5.97
MC1990	5.09	5.70
MC2010	4.82	5.41
DNV	6.33	6.12
	LSE 1,II, app.1	LSE 1,II, app.2
Eurocode	5.08	5.07
MC1990	4.74	4.97
MC2010	4.47	4.84
DNV	5.34	5.22
	LSE 2,I, app.1 w. bias	LSE 2,I, app.2 w. bias
Eurocode	4.56	5.18
MC1990	4.23	4.75
MC2010	3.99	4.43
DNV	4.99	5.73
	LSE 2,I, app.1 wo. bias	LSE 2,I, app.2 wo. bias
Eurocode	4.31	4.84
MC1990	4.25	4.43
MC2010	3.77	4.13
DNV	4.72	5.38

Table 10.2. Reliability indices for the wind turbine foundation z_d found in table 8.7.

The following observations are made for the obtained annual reliability indices for the wind turbine foundation:

- The obtained annual reliabilities correspond well with the obtained design parameters.
- Generally the obtained annual reliability indices are higher than the target annual reliability indices.
- Generally the annual reliability indices are higher for application 2 of \mathbf{X}_{scf} and \mathbf{X}_w , than for application 1.
- The annual reliability indices obtained through LSE 1,I are higher than for LSE 2.
- LSE 2 with bias obtain slightly higher annual reliabilities than LSE 2 without bias.

The observations indicate that the material partial safety factors used for fatigue in concrete for wind turbines can be reduced with respect to the data used in this report. Furthermore the results indicate that the fatigue damage is accumulated at a low $S_{c,min}$ -value since LSE 1 obtains significantly higher annual reliabilities

than LSE 2. This is expected as LSE 1 is based on the developed surface which is non-conservative at low $S_{c,min}$ -values. In appendix D.7 it is estimated that practically all fatigue damage stems from stress states with $S_{c,min} = 0.0$ so the results are as expected.

As for the bridge LSE 1,II had problems converging towards a solution using FORM. Therefore the results from LSE 1,II are assumed to be less reliable than the rest. However the obtained results from LSE 1,II indicates that modelling the model uncertainty with uncertainty model 1 is conservative compared to uncertainty model 2 for the wind turbine foundation.

Due to the convergence problems LSE 1,II is not considered further in the reliability analysis of the wind turbine foundation as the results are too unreliable.

10.2 Target Design Parameters

In this section it is investigated what target design parameters, z_t , would lead to the specified target reliabilities for the different limit state equations. The target design parameters are obtained by altering z in the limit state equations until the target annual reliability indices are acquired. The results of the investigation are listed in table 10.3.

	LSE 1,I, app.1	LSE 1,I, app.2
$\beta_t = 3.3$	0.992	0.937
$\beta_t = 3.7$	1.133	1.043
$\beta_t = 5.2$	0.274	0.245
	LSE 2, w. bias app. 1	LSE 2, w. bias app. 2
$\beta_t = 3.3$	1.230	1.169
$\beta_t = 3.7$	1.415	1.304
$\beta_t = 5.2$	0.267	0.239
	LSE 2, wo. bias app. 1	LSE 2, wo. bias app. 1
$\beta_t = 3.3$	1.318	1.247
$\beta_t = 3.7$	1.515	1.396
$\beta_t = 5.2$	0.276	0.247

Table 10.3. z_t for the different models to obtained the target reliabilities.

For the obtained target design parameters it can be seen that, for the wind turbine foundation LSE1,I is more non-conservative than LSE2. This is as expected due to the low $S_{c,min}$ and corresponds well to the results in table 10.2. It can also be seen that the design parameters for the bridge are similar to each other, this is because that at high $S_{c,min}$ values the investigated failure surfaces are similar.

10.3 Calibrating Partial Safety Factors

In this section the partial safety factors from the codes are calibrated with respect to the used limit state equations. It is chosen to calibrate the material partial safety factor, γ_M , while keeping the partial safety factors for the loads, γ_F , as they are.

To calibrate γ_M it is changed in the design equations until z_t is obtained. The calibrated partial safety factors are referred to as $\gamma_{M,t}$.

10.3.1 Bridge

The results of the calibration for the bridge are listed in table 10.4.

	LSE 1,I, app.1	LSE 1,I, app.2	γ_M from Code
Eurocode	1.54	1.38	1.60
MC1990	1.32	1.18	1.5
MC2010	1.48	1.32	1.5
DNV	1.52	1.47	1.5
	LSE 2,I, app.1 w. bias	LSE 2, app.2 w. bias	γ_M from code
Eurocode	1.51	1.35	1.6
MC1990	1.29	1.16	1.5
MC2010	1.44	1.29	1.5
DNV	1.48	1.33	1.5
	LSE 2,I, app.1 wo. bias	LSE 2, app.2 wo. bias	γ_M from code
Eurocode	1.56	1.39	1.60
MC1990	1.34	1.20	1.50
MC2010	1.49	1.34	1.50
DNV	1.53	1.37	1.50

Table 10.4. Calibrated partial safety factors for the bridge and the partial safety factors from the codes.

The following observations are made for the calibrated partial safety factors for the bridge:

- Generally the obtained $\gamma_{M,t}$ are close to the partial safety factors currently used in the codes for Eurocode, MC2010 and DNV.
- For MC1990 $\gamma_{M,t}$ is generally lower than the partial safety factor used in the code.
- The calibrated partial safety factors for application 2 of \mathbf{X}_{scf} are lower than for application 1.
- The calibrated partial safety factors for LSE 2 without bias are slightly higher than for LSE 2 with bias.

The observations indicate that the partial safety factors currently used in Eurocode, MC2010 and DNV could be applied for high strength concrete, with respect to the data used in this report. However for MC1990 the results indicate that a reduction of the material partial safety factor to e.g. 1.4 would be appropriate.

Furthermore the data in this report indicates that a reduction in the partial safety factor should be applied if the mean stresses of a bridge can be estimated with high certainty.

10.3.2 Wind turbine foundation

The results for the calibration of the wind turbine foundation is shown in table 10.5.

	LSE 1,I, app.1	LSE 1,I, app.2	γ_M from code
Eurocode	0.88	0.83	1.60
MC1990	0.83	0.78	1.38
MC2010	0.89	0.84	1.38
DNV	0.84	0.77	1.50
	LSE 2,I, app.1 w. bias	LSE 2, app.2 w. bias	γ_M from code
Eurocode	1.08	1.03	1.60
MC1990	1.03	0.97	1.38
MC2010	1.10	1.05	1.38
DNV	1.05	0.97	1.50
	LSE 2,I, app.1 wo. bias	LSE 2, app.2 wo. bias	γ_M from code
Eurocode	1.16	1.10	1.60
MC1990	1.10	1.04	1.38
MC2010	1.18	1.12	1.38
DNV	1.12	1.04	1.50

Table 10.5. Calibrated partial safety factors for the wind turbine foundation and the partial safety factors from the codes.

The following observation are made for the calibrated partial safety factors for the wind turbine foundation:

- The calibrated partial safety factors obtained through LSE 1 are all below 1.0.
- All calibrated partial safety factors are significantly lower than those currently used in the codes.
- All partial safety factors using application 2 of \mathbf{X}_{scf} and \mathbf{X}_w are only slightly lower than for application 1.

It is very uncommon that material partial safety factors are below 1.0 as found in LSE 1. The low values are obtained because at small $S_{c,min}$ -values the failure surface used in LSE1 is very non-conservative as seen on figure 5.14. Therefore the results from LSE 1 are not very reliable for this design case.

The results from LSE 2 indicates that the material partial safety factor for wind turbines could be reduced to e.g. 1.2 in all the investigated codes, compared to the data used in this report.

10.4 Sensitivity Analysis

In this section a sensitivity analysis of LSE 1,I and LSE 2 is preformed. This sensitivity analysis contains the α vectors for accumulated reliability in the last year of service for different β_t . Some visualizations of the sensitivity and the elasticity sensitivity are presented from the same β_t as the α vectors.

10.4.1 LSE 1,I

Table 10.6 shows the α vector for LSE 1,I with application 1 of \mathbf{X}_{scf} .

	$\beta_t = 5.2$, Bridge	$\beta_t = 3.3$, Wind turbine	$\beta_t = 3.7$, Wind turbine
\mathbf{X}_{scf}	0.57	0.47	0.47
Δ	-0.03	-0.09	-0.09
f_c	-0.81	-0.66	-0.66
$\mathbf{X}_{model,I}$	-0.12	-0.33	-0.34
\mathbf{X}_w	-	0.47	0.47

Table 10.6. α vector for LSE 1,I with application 1 of \mathbf{X}_{scf} .

It can be seen from table 10.6 that LSE 1,I is far most sensitive towards the strength of the concrete. However it becomes less sensitive towards it, as β_t decreases. It can be seen that as β_t decreases the limit state equation becomes more sensitive towards the model uncertainty.

Table 10.7 shows the α vector for LSE 1, I with second application of \mathbf{X}_{scf} .

	$\beta_t = 5.2$, Bridge	$\beta_t = 3.3$, Wind turbine	$\beta_t = 3.7$, Wind turbine
\mathbf{X}_{scf}	0.13	0.30	0.31
Δ	-0.04	-0.11	-0.11
f_c	-0.98	-0.80	-0.79
$\mathbf{X}_{model,I}$	-0.15	-0.41	-0.42
\mathbf{X}_w	-	0.30	0.31

Table 10.7. α vector for LSE 1,I with application 2 of \mathbf{X}_{scf} .

Table 10.7 depict the same as table 10.6, except the sensitivity towards the concrete strength has increased. To compensate for the increase of the sensitivity

towards the concrete strength, the limit state equation becomes less sensitive towards the variables effecting the loads e.g. X_{scf} .

The sensitivity towards change in the standard deviation, for LSE 1,I with application 1 of X_{scf} , is shown visually on figure 10.1. The wind turbine foundation is the design case used in figure 10.1, $\beta_t = 3.3$ and the corresponding z_t can be found in table 10.3.

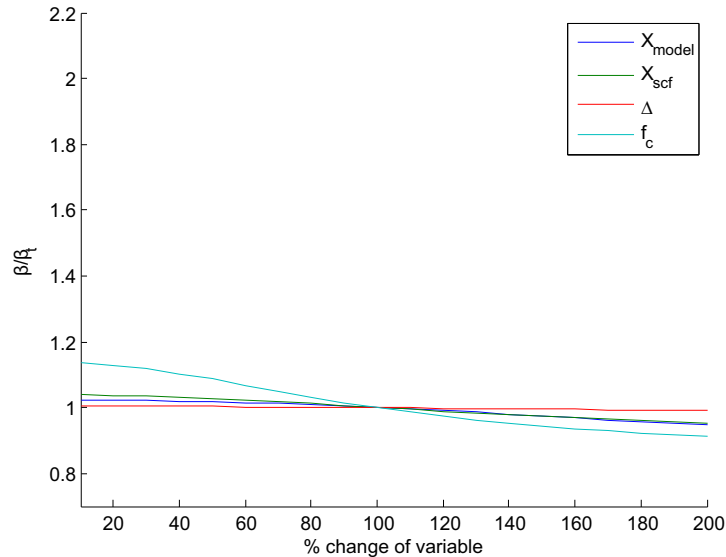


Figure 10.1. Sensitivity of model I, wind turbine foundation design case, first application of X_{scf} .

Figure 10.1 depicts the same tendencies as seen in table 10.6. Figure 10.1 can be interpreted as the elasticity sensitivity of the standard deviations for the stochastic variables.

The elasticity sensitivity corresponding to figure 10.1 can be seen in table 10.8.

	X_{model}	X_{scf}	Δ	f_c
e_p	-0.04	-0.06	-0.01	-0.14

Table 10.8. e_p for the standard deviation for the given variables.

The elasticity sensitivity from table 10.8 corresponds well with figure 10.1. It can be seen in table 10.8 that the reliability index is most sensitive towards change in the standard deviation of the concrete strength.

Figure 10.2 shows the sensitivity of LSE 1,I with application 1 of X_{scf} , with the bridge design case where $\beta_t = 5.2$ the corresponding z_t can be found in table 10.3.

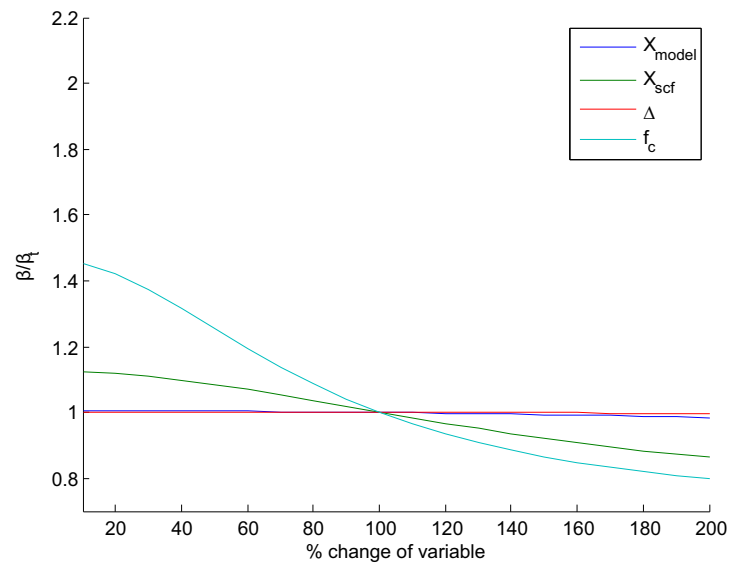


Figure 10.2. Sensitivity of model I, bridge design case, first application of X_{scf} .

By comparing figure 10.2 to figure 10.1, it can be seen that the case depicted in figure 10.2 is more sensitive towards change in the standard deviation for f_c and X_{scf} . Table 10.9 shows the elasticity sensitivity corresponding to figure 10.2.

	X_{model}	X_{scf}	Δ	f_c
e_p	-0.01	-0.17	0.00	-0.38

Table 10.9. e_p for the standard deviation for the given variables.

The results in table 10.9 are as expected by comparing to figure 10.2. Figure 10.3 shows the sensitivity for LSE 1,I with application 2 of X_{scf} , for the wind turbine foundation design case with the target reliability and target design parameter is as previous, towards change in the standard deviations.

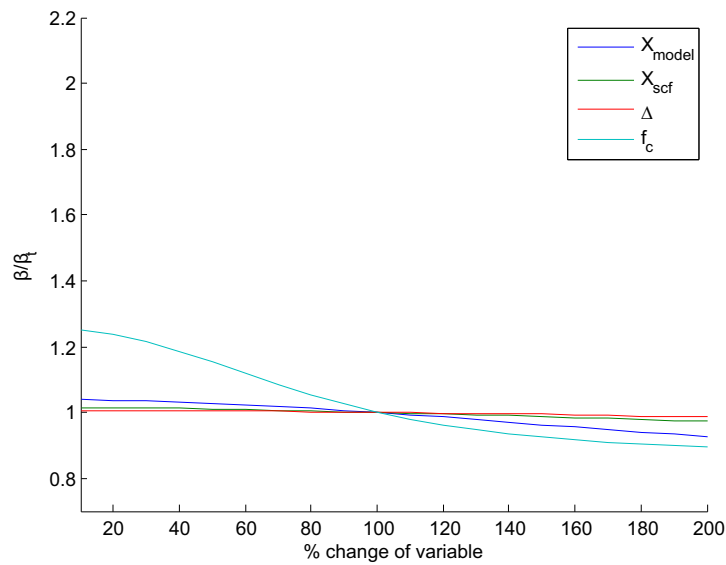


Figure 10.3. Sensitivity of model I, wind turbine foundation design case, second application of X_{scf} .

It can be seen on figure 10.3 that the limit state equation is more sensitive towards σ_{f_c} , than the case depicted in figure 10.1.

The corresponding sensitivity elasticity coefficients to figure 10.3 can be seen in table 10.10.

	X_{model}	X_{scf}	Δ	f_c
e_p	-0.07	-0.02	-0.01	-0.22

Table 10.10. e_p for the standard deviation for the given variables.

The elasticity sensitivity found in table 10.10 corresponds as expected by comparing to figure 10.3.

Figure 10.4 shows the sensitivity for LSE 1, I with second application of X_{scf} , for the bridge design case with the target reliability and target design parameter is as previous, towards change in the standard deviations.

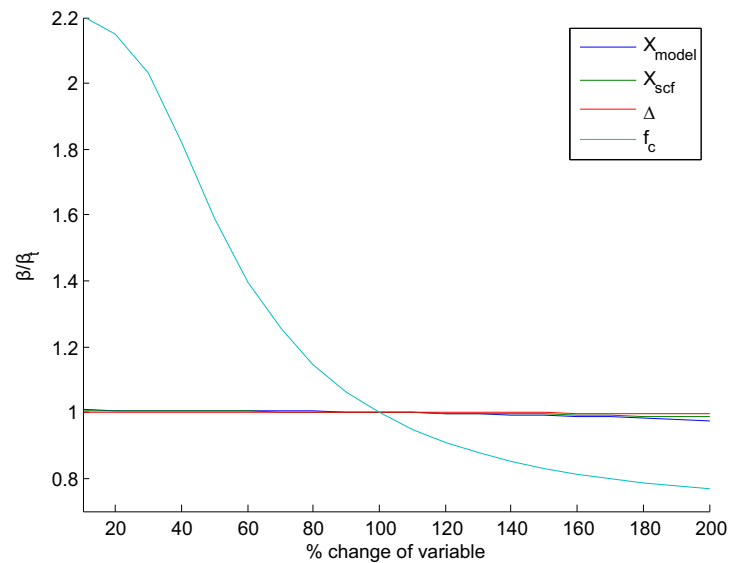


Figure 10.4. Sensitivity of model I, bridge design case, X_{scf} alternative placement.

It can be seen on figure 10.4, that the case under investigation is very sensitive towards σ_{f_c} . The corresponding sensitivity elasticity coefficients to figure 10.4 can be seen in table 10.11.

	X_{model}	X_{scf}	Δ	f_c
e_p	-0.02	-0.01	0.00	-0.57

Table 10.11. e_p for the standard deviation for the given variables.

Generally it can be seen from the figures and tables that LSE 1, I is most sensitive towards the concrete strength and that σ_{Δ} is of little to none importance. The elasticity sensitivity depict well the tendency shown on the figures, which corresponds to the presented α vectors. Due to this only the α vectors are shown for LSE 2.

10.4.2 LSE 2

LSE 2, is modelled with and without bias included in the model uncertainty and with both application of X_{scf} .

With bias

The α vector for LSE 2 with bias and with first application of X_{scf} , for different design cases can be seen in table 10.12.

	$\beta_t = 5.2$, Bridge	$\beta_t = 3.3$, Wind turbine	$\beta_t = 3.7$, Wind turbine
\mathbf{X}_{scf}	0.57	0.48	0.48
δ	-0.03	-0.05	-0.05
f_c	-0.81	-0.68	-0.68
$\mathbf{X}_{model,I}$	-0.14	-0.27	-0.27
\mathbf{X}_w	-	0.48	0.48

Table 10.12. α vector for LSE 2 with bias with first application of \mathbf{X}_{scf} .

The α vector for LSE 2 with bias and with application 2 of \mathbf{X}_{scf} , for different design cases can be seen in table 10.13.

	$\beta_t = 5.2$, Bridge	$\beta_t = 3.3$, Wind turbine	$\beta_t = 3.7$, Wind turbine
\mathbf{X}_{scf}	0.13	0.31	0.32
δ	-0.04	-0.07	-0.07
f_c	-0.97	-0.83	-0.83
$\mathbf{X}_{model,I}$	-0.18	-0.33	-0.33
\mathbf{X}_w	-	0.31	0.32

Table 10.13. α vector for LSE 2 with bias, second application of \mathbf{X}_{scf} .

Without bias

The α vector for LSE 2 without bias and with application 1 of \mathbf{X}_{scf} , for different design cases can be seen in table 10.14.

	$\beta_t = 5.2$, Bridge	$\beta_t = 3.3$, Wind turbine	$\beta_t = 3.7$, Wind turbine
\mathbf{X}_{scf}	0.57	0.48	0.48
δ	-0.03	-0.06	-0.06
f_c	-0.80	-0.68	-0.67
$\mathbf{X}_{model,I}$	-0.16	-0.29	-0.29
\mathbf{X}_w	-	0.48	0.48

Table 10.14. α vector for LSE 2 without bias, first application of \mathbf{X}_{scf} .

The α vector for LSE 2 without bias and with second application of \mathbf{X}_{scf} , for different design cases can be seen in table 10.15.

	$\beta_t = 5.2, \text{ Bridge}$	$\beta_t = 3.3, \text{ Wind turbine}$	$\beta_t = 3.7, \text{ Wind turbine}$
\mathbf{X}_{scf}	0.14	0.31	0.31
δ	-0.04	-0.07	-0.07
f_c	-0.97	0.82	-0.82
$\mathbf{X}_{\text{model,I}}$	-0.20	-0.35	-0.36
\mathbf{X}_w	-	0.31	-0.31

Table 10.15. α vector for LSE 2 without bias, second application of \mathbf{X}_{scf} .

The α vectors found for LSE 2 with and without bias are very similar, and shows the same tendency as the alpha vectors for LSE 1,I.

Discussion

In this chapter a discussion regarding the choices made throughout the report is presented. Improvements and further analysis that could have been taken into account are also mentioned.

Several effects that are expected to have an impact on the fatigue life of concrete is presented in the report however only some of these are taken into account. To make the results of the report more general all the effects should have been investigated. Especially the effect of stress gradients would have been interesting to investigate, as it is very important in design for MC1990, MC2010 and DNV, while it is not included at all in Eurocode. However due to the lack of relevant data this was not done.

Throughout the report the mean failure surfaces for the codes are assumed to be obtained by replacing the characteristic strength of concrete with the mean strength of concrete, in the expression for the failure surfaces. This assumption could have been investigated further, by getting more insight into how the failure surfaces from the different codes were developed. Furthermore the knowledge about f_{cn} was sparse and therefore some crude assumption were made to compare the DNV with the other codes. To get more reliable results it should have been investigated exactly what safety the transformation between f_{ck} and f_{cn} covers.

The data that is collected in *data series 1* and *data series 2* was recovered by digitalizing plots. This lead to some deviation between the original data and the retrieved data which could have been improved by having the actual dataset available.

The data that was obtained and used in this report, stems from different concrete mixes, testing frequencies etc. As result it can be expected that some deviation of the data points stems from these differences. This has not been taken into further consideration even though it could influence the results in the report.

To improve the developed failure surface it would have been optimal to have data for more $S_{c,min}$. This could have improved the accuracy of the developed failure surface for low $S_{c,min}$, and subsequently the reliability analysis for the wind turbine foundation. Furthermore data for $\log N > 8$ values could have been used to investigate if an asymptotic behavior towards $S_{c,min}$ is valid for high $\log N$.

Generally two design cases were analysed in part II of the report. This could have been increased by other design cases. For example other areas of the bridge

could have been investigated. It was also found that the chosen design cases had all fatigue damage at very few stress states. For the wind turbine the important stress states were at $S_{c,min} = 0$ which was an area the developed surface predicted non-conservatively. Therefore it could have been interesting to introduce a design case, where more stress states were important.

When the design equations that are used in the reliability analysis are estimated several effects are neglected, as they were assumed to be secondary effects to be investigated separately. This could have been investigated further to validate if this assumptions was reasonable, as it would change the results of the report significantly, if these effects were to be partly covered by γ_M

The COV of the two stochastic variables X_{scf} and X_w were estimated based on analyses that were made on steel. To improve the limit state equations a throughout investigation could have been made, regarding how the COV should be modelled for concrete.

Furthermore it could have been interesting to develop a limit state equation where the mean stress is varied while the stress amplitudes are kept constant. This would represent a case where prestress of the concrete is altered as this could be a viable solution in design. When the model uncertainties are found for the limit state equations through uncertainty model I mean data and single data points are weighted equally. This was expected to result in a too low standard deviation, which in turn lead to non-conservative reliabilities. As such it could have been investigated further if this effect could have been avoided by e.g. including the mean values multiple times in MLM. Furthermore statistical uncertainty could have been taken into account for uncertainty model I. However due to amount of data the statistical uncertainty would probably be very small.

As LSE 1,II had problems converging when using FORM it was neglected in most of the reliability analysis. This could have been avoided by using Monte Carlo simulation, however this way of obtaining the reliability required a lot of computational power, which was not available.

In the sensitivity study it is investigated how the standard deviation of the different stochastic variables influence the reliability results. This could have been extended to include mean value as well, to obtain a more throughout analysis of the sensitivity.

Conclusion

In this report the fatigue behavior of high strength concrete has been investigated, and the reliability of selected codes has been evaluated. This was done using a failure surface that is incorporated in a current code and a failure surface developed based on data representing over 400 fatigue tests of high strength concrete.

The codes that were selected in this report included Eurocode, MC1990, MC2010 and DNV, where it was found that the fatigue design varies between the codes. The variations was found to be greatly influenced by how stress gradients and α_{fat} is taken into account. An important observation here was that Eurocode is the only investigated code that does not include stress gradients. As this effect lead to great reduction in design for the other codes it should be investigated if this effect could be included in Eurocode as well. Furthermore it was found that Eurocode, MC1990 and MC2010 were very comparable to each other while DNV was difficult to compare to any of the other codes.

A failure surface was developed in this report based on the traditional theory behind SN -curves. The developed surface was shown to be more accurate than the one that is used in MC2010, with respect to the data used in this report. However due to the ranges of the data the failure surface used linear extrapolation after $\log N = 8$. Furthermore the developed surface showed a tendency to behave too non-conservative for very low $S_{c,min}$ -values. Therefore it is not recommended to use the developed failure surface for $S_{c,min} < 0.05$.

The design equations used in this report were made on background of the investigated codes. However stress gradients, time dependent effects and α_{fat} were excluded from the design equations. This was done so the design equations and limit state equations were comparable to each other. To exclude the effects some crude assumptions were made for DNV which in turn may have lead to an imprecise reliability analysis for DNV. Several limit state equations were evaluated where it was found that LSE 1,II was unstable when using FORM. As result LSE 1,I and LSE 2 gave the most reliable results.

When the safety of the bridge design case was evaluated it was found that the partial safety factors used in Eurocode, MC2010 and DNV was appropriate for the design case and data used in this report. However if the mean stresses of a bridge could be determined with high certainty it was suggested to make a reduction to the partial safety factor. For MC1990 the results indicated that a new partial safety factor, γ_M , of 1.4 would lead to sufficient safety, based on the data

in this report. Due to the stress states that were evaluated in the bridge design case, it is concluded that LSE 1 is the most accurate as it captured the data most accurately.

When assessing the wind turbine foundation design case, it was generally found that the investigated codes were conservative. Therefore a material partial safety factor of 1.2 is suggested for all investigated codes, with respect to the data used in this report. As application 1 and 2 of \mathbf{X}_{scf} and \mathbf{X}_w yielded very similar results no reduction should be applied for the wind turbine foundation, if the mean stresses can be determined with high certainty. As the fatigue damage was accumulated for stress states with $S_{c,min} = 0$ for the wind turbine foundation the results from LSE 1 were not very reliable. Therefore only the results from LSE 2 should be considered to ensure sufficient safety.

In the sensitivity analysis it was seen that the developed limit state equations, was most sensitive towards the compressive strength of the concrete.

Bibliography

- , 2015. *Maximum Likelihood Estimation (MLE)*. URL: https://files.nyu.edu/mrg217/public/mle_introduction1.pdf, 2015.
- Dalsgaard and Toft, 2014.** John Dalsgaard and Henrik Steensgaard Toft. *Safety Factors IEC 61400-1*. ISBN: 978-87-93278-08-0. 2014.
- DANSKE, 2015.** DEN STORE DANSKE. *beton(Historie)*. URL: http://www.denstoredanske.dk/It,_teknik_og_naturvidenskab/Teknik/Murerarbejde_og_-_v%C3%A6rkt%C3%B8j/beton/beton_%28Historie%29, 2015.
- DNV, 2015.** DNV. *OFFSHORE STANDARD DET NORSKE VERITAS DNV-OS-C502*, 2015.
- EuroLightCon, 2000.** EuroLightCon. *Fatigue of normal weight concrete and lightweight concrete*. ISBN: 90-376-02-78-9. 2000.
- fib, 2010.** fib. *fib Model Code for Concrete Structures 2010*. ISBN: 978-3-433-60409-0, 1. edition. Wilhelm Ernst and Sohn, 2010.
- fip, 1990.** fip. *CEB-FIP MODEL CODE 1990*. ISBN: 0-7277-1696-4. 1990.
- IEC, 2005.** IEC. *IEC61400-1*. 2005.
- IEC, 2015.** IEC. *IEC 61400-6 Draft*. Committee draft, 2015.
- JCSS, 2014.** JCSS. *JCSS Probabilistic Model Code*. URL: http://www.jcss.byg.dtu.dk/Publications/Probabilistic_Model_Code, 2014.
- Jensen, 2008.** Bjarne Chr. Jensen. *Betonkonstruktioner efter DS/EN 1992-1-1*. ISBN: 978-87-571-2668-6, 1. edition. Nyt Teknisk Forlag, 2008.
- Kim and Kim, 1996.** Jin-Keun Kim and Yun-Yong Kim. *EXPERIMENTAL STUDY OF THE FATIGUE BEHAVIOR OF HIGH STRENGTH CONCRETE*. Cement and Concrete Research, Volume 26, 1996.
- Lohaus, Oneschkow, and Wefer, 2012.** Ludger Lohaus, Nadja Oneschkow, and Maik Wefer. *Design model for the fatigue behaviour of normal-strength, high-strength and ultra-high-strength concrete*. Structural Concrete, Volume 13, 2012. Journal of the fib.

- Manufacturers, 2015.** Americas Cement Manufacturers. *Ultra-High Performance Concrete*. URL: <http://www.cement.org/for-concrete-books-learning/concrete-technology/concrete-design-production/ultra-high-performance-concrete>, 2015.
- Sørensen.** Eigil V. Sørensen. *Fatigue life of high performance grout in dry and wet environment for wind turbine grouted connections*.
- Sørensen, 2011a.** John Dalsgaard Sørensen. *Statistical analysis using the Maximum-Likelihood method*. Lecture Notes, 2011.
- Sørensen, 2011b.** John Dalsgaard Sørensen. *Notes in Structural Reliability Theory and Risk Analysis*. Lecture Notes, 2011.
- Sørensen and Toft, 2014.** John Dalsgaard Sørensen and Henrik Stensgaard Toft. *Safety Factors - IEC 61400-1 ed- 4 background documentg*, 2014.
- Storebaelt, 2015.** Storebaelt. *Fakta og histoire om storebaelt*. URL: <http://www.storebaelt.dk/omstorebaelt/fakta>, 2015.

Appendix

Maximum likelihood method

In this appendix maximum likelihood method, or MLM, will be outlined as it is used numerous times throughout the main report.

Typically the interest is to estimate parametric models as shown in eq. (A.1)

$$X \sim f(\boldsymbol{\theta}, x) \quad (\text{A.1})$$

Where

$\boldsymbol{\theta}$ | Is a vector with parameters e.g. mean value and standard
 f | Is a functional form e.g. a density function

In general MLM is a systematic way of finding the most likely parameters, $\boldsymbol{\theta}$, for a distribution, f , given a number of observations, $[x_1, \dots, x_n]$. It is noted that the distribution may vary between a lot of different choices but it has to be estimated before MLM can be used.

To find the parameters of a distribution based on observations is also known as the *inverse probability problem* which can not be solved directly [MLE, 2015].

A.1 Bayes' theorem

Bayes' theorem is a fundamental part of solving an inverse probability problem. In eq. (A.2) Bayes' theorem is shown.

$$p(\boldsymbol{\theta}|x) = \frac{p(\boldsymbol{\theta}) p(x|\boldsymbol{\theta})}{p(x)} \quad (\text{A.2})$$

Where

$p(\boldsymbol{\theta}|x)$ | Posterior probability of $\boldsymbol{\theta}$
 $p(\boldsymbol{\theta})$ | Prior probability of $\boldsymbol{\theta}$
 $p(x|\boldsymbol{\theta})$ | The likelihood of $\boldsymbol{\theta}$
 $p(x)$ | The unconditional probability of x

$p(x)$ is a function of the data only. As it only makes sense to compare the same data set in MLM $p(x)$ will have the same value for all observations. This reduces equation (A.2) to eq. (A.3).

$$p(\boldsymbol{\theta}|x) \propto p(\boldsymbol{\theta}) p(x|\boldsymbol{\theta}) \quad (\text{A.3})$$

Where

$\frac{1}{p(x)}$ | Is the constant of proportionality

As $p(\boldsymbol{\theta})$ is fixed before the observations eq. (A.3) may be written as eq. (A.4).

$$p(\boldsymbol{\theta}|x) = k(x) p(x|\boldsymbol{\theta}) \quad (\text{A.4})$$

Where

$k(x)$ | Is equal to $\frac{p(\boldsymbol{\theta})}{p(x)}$

As $k(x)$ is not a function of $\boldsymbol{\theta}$ it can be treated as an unknown positive constant, i.e. $k(x)$ remains the same for all values of $\boldsymbol{\theta}$.

A.2 Likelihood

Eq. (A.4) can not be calculated without making assumptions about the prior probability of $\boldsymbol{\theta}$. This problem can be avoided by introducing the likelihood, $L(\boldsymbol{\theta}|x)$, which can be calculated by eq. (A.5) [MLE, 2015].

$$L(\boldsymbol{\theta}|x) = k(x) p(x|\boldsymbol{\theta}) \propto p(x|\boldsymbol{\theta}) \quad (\text{A.5})$$

As seen the likelihood is proportional to the probability of the observations. As such the maximum probability for $\boldsymbol{\theta}$ given x can be calculated from $p(x|\boldsymbol{\theta})$. It has to be noted that likelihoods can only be compared for the same data set and the same prior.

To find the optimal parameters different estimators, $\hat{\boldsymbol{\theta}}$, are used. The optimal parameters are then the value of $\hat{\boldsymbol{\theta}}$ that maximizes the likelihood.

For a data set with more observation, $[x_1, \dots, x_n]$, that are all independent the likelihood for the entire sample can be calculated as the product of the individual likelihoods, see eq. (A.6).

$$L = L_1 \cdot L_2 \cdot \dots \cdot L_n = \prod_{i=1}^n L_i \quad (\text{A.6})$$

Given that MLM tries to maximize the likelihood the log-likelihood function can be used instead which is shown in eq. (A.7).

$$\ln L = \ln L_1 + \ln L_2 + \dots + \ln L_n = \sum_{i=1}^n \ln L_i \quad (\text{A.7})$$

This holds as all likelihoods are positive as such the likelihood and the log-likelihood will have the maxima the same place.

To estimate the value of $\hat{\boldsymbol{\theta}}$ that maximizes the probability analytical solutions can be found however it is more common to use numerical methods which is also done in the investigations in this report.

A.3 Variation of the MLM parameters

By taking the derivatives of the likelihood with respect to the parameters the Hessian matrix, H , is obtained, see eq. (A.8) [Sørensen, 2011a].

$$H_{i,j} = \frac{\partial^2 \ln L}{\partial \theta_i \partial \theta_j} \quad (\text{A.8})$$

By taking the inverse to the Hessian matrix the covariance matrix for the estimator is obtained, see eq. (A.9).

$$C_{\theta_1, \dots, \theta_n} = [-H]^{-1} = \begin{bmatrix} \sigma_{\theta_1}^2 & \rho_{\theta_1 \theta_2} \sigma_{\theta_1} \sigma_{\theta_2} & \cdots & \rho_{\theta_1 \theta_n} \sigma_{\theta_1} \sigma_{\theta_n} \\ \rho_{\theta_1 \theta_2} \sigma_{\theta_1} \sigma_{\theta_2} & \sigma_{\theta_2}^2 & \cdots & \rho_{\theta_2 \theta_n} \sigma_{\theta_2} \sigma_{\theta_n} \\ \vdots & \vdots & \ddots & \vdots \\ \rho_{\theta_1 \theta_n} \sigma_{\theta_1} \sigma_{\theta_n} & \rho_{\theta_2 \theta_n} \sigma_{\theta_2} \sigma_{\theta_n} & \cdots & \sigma_{\theta_n}^2 \end{bmatrix} \quad (\text{A.9})$$

Lastly it can be shown that for large samples MLM will be very efficient as no better unbiased estimator is possible [MLE, 2015].

A.4 Parameter estimation for regression lines

MLM can be used to estimate the parameters of a regression line in a m -dimensional space given a set of observation $(x, y) : (x_1, y_1), \dots, (x_n, y_n), \dots, (x_N, y_N)$ where tests $1 : n$ represents failure and tests $n + 1 : N$ represent run-out tests. If it is assumed that the lack of fit, modelled by a stochastic variable ϵ , is normal distributed the likelihood can be found as eq. (A.10).

$$L(\alpha_0, \alpha_1, \dots, \alpha_m, \mu_\epsilon, \sigma_\epsilon) = \prod_{i=1}^n \frac{1}{\sqrt{2\pi} \sigma_\epsilon} e^{-\frac{1}{2} \left(\frac{y_{obs,i} - y_{model,i} - \mu_\epsilon}{\sigma_\epsilon} \right)^2} \cdot \prod_{i=n+1}^{n+N} \Phi \left(\frac{y_{obs,i} - y_{model,i} - \mu_\epsilon}{\sigma_\epsilon} \right) \quad (\text{A.10})$$

Where

$(\alpha_0, \alpha_1, \dots, \alpha_m, \mu_\epsilon, \sigma_\epsilon)$	Parameters to be estimated by MLM
$y_{obs,i}$	Observation of y at test i
$y_{model,i}$	Is a function of $(\alpha_0, \alpha_1, \dots, \alpha_m, x_1, \dots, x_v)$ in the m -dimensional space
Φ	Cumulative normal distribution

The optimal parameters are then found by maximizing the likelihood.

Data

In this chapter the data used in the report is shown.

B.1 Data from Structural Concrete

In this section the data acquired from [Lohaus et al., 2012] is presented. *data series 1* which is used to create the failure surface, is shown in table B.1, B.2 and B.3.

$\log(N)$	$S_{c,max}$	$\log(N)$	$S_{c,max}$	$\log(N)$	$S_{c,max}$	$\log(N)$	$S_{c,max}$
2.26	0.90	3.21	0.80	4.57	0.80	5.61	0.70
2.34	0.90	3.28	0.80	4.44	0.80	5.66	0.70
2.57	0.90	3.52	0.80	4.67	0.80	5.71	0.70
2.63	0.90	3.66	0.80	4.59	0.80	5.69	0.70
2.75	0.90	3.81	0.80	4.84	0.75	5.79	0.70
2.56	0.90	3.91	0.80	4.92	0.75	5.89	0.70
2.92	0.90	3.95	0.80	5.02	0.75	5.92	0.70
3.03	0.90	3.99	0.80	5.25	0.75	6.18	0.70
3.15	0.90	4.03	0.80	4.81	0.70	6.39	0.70
3.30	0.90	4.09	0.80	4.94	0.70	6.52	0.70
3.34	0.90	4.18	0.80	4.97	0.70	5.51	0.65
3.42	0.90	4.20	0.80	5.08	0.70	6.03	0.65
3.51	0.90	4.29	0.80	5.14	0.70	6.16	0.65
3.76	0.90	4.34	0.80	5.31	0.70	6.25	0.65
3.99	0.90	4.42	0.80	5.36	0.70	6.30	0.60
4.05	0.90	4.47	0.80	5.42	0.70	6.47	0.60
2.80	0.85	4.50	0.80	5.47	0.70	7.01	0.60
3.16	0.85	4.54	0.80	5.50	0.70	7.04	0.60
3.42	0.85						

Table B.1. Extracted data from [Lohaus et al., 2012] at $S_{c,min} = 0.05$.

$\log(N)$	$S_{c,max}$	$\log(N)$	$S_{c,max}$
2.24	0.90	4.10	0.80
2.57	0.90	4.23	0.80
3.07	0.90	4.38	0.80
2.61	0.85	5.04	0.75
3.27	0.85	5.20	0.75
3.41	0.85	5.55	0.75
3.87	0.85	6.31	0.70
3.71	0.80	7.16	0.65
4.01	0.80	7.19	0.65
4.06	0.80		

Table B.2. Extracted data from [Lohaus et al., 2012] at $S_{c,min} = 0.20$.

$\log(N)$	$S_{c,max}$	$\log(N)$	$S_{c,max}$
2.56	0.90	5.28	0.80
3.03	0.90	5.76	0.80
3.19	0.90	6.01	0.80
4.68	0.80	6.21	0.80
4.79	0.80	6.48	0.80
5.03	0.80		

Table B.3. Extracted data from [Lohaus et al., 2012] at $S_{c,min} = 0.40$.

data series 2 is shown in table B.4.

$\log N$	$S_{c,max}$	Runout	Other info
4.48	0.90	No	C20 without fibers 10 Hz
4.88	0.90	No	C20 without fibers 10 Hz
6.14	0.70	Yes	C20 without fibers 10 Hz
3.86	0.80	No	C70 without fibers 0.5 Hz
1.46	0.95	No	C80 without fibers 0.1 Hz
2.06	0.90	No	C80 without fibers 0.1 Hz
2.98	0.80	No	C80 without fibers 0.1 Hz
2.26	0.95	No	C80 without fibers 1 Hz
2.91	0.90	No	C80 without fibers 1 Hz
2.00	0.95	No	C80 without fibers 5 Hz
3.13	0.90	No	C80 without fibers 5 Hz
3.82	0.80	No	C80 without fibers 5 Hz
4.73	0.70	No	C80 without fibers 5 Hz
3.72	0.80	No	C80 without fibers 10 Hz
4.44	0.70	No	C80 without fibers 10 Hz
6.31	0.60	Yes	C80 without fibers 10 Hz
3.41	0.80	No	C80 with fibers 0.5 Hz
3.53	0.79	No	C150 without fibers 10 Hz
4.02	0.78	No	C150 without fibers 10 Hz
4.51	0.73	No	C150 without fibers 10 Hz
4.94	0.65	No	C150 without fibers 10 Hz
5.75	0.60	No	C150 without fibers 10 Hz
3.42	0.90	No	C200 with fibers, Heat-treated, 10 Hz
3.31	0.85	No	C200 with fibers, Heat-treated, 10 Hz
4.22	0.80	No	C200 with fibers, Heat-treated, 10 Hz
4.81	0.75	No	C200 with fibers, Heat-treated, 10 Hz
5.83	0.70	No	C200 with fibers, Heat-treated, 10 Hz
6.09	0.65	No	C200 with fibers, Heat-treated, 10 Hz
6.75	0.60	Yes	C200 with fibers, Heat-treated, 10 Hz
4.54	0.80	No	C200 without fibers, Heat-treated, 10 Hz
6.06	0.70	Yes	C200 without fibers, Heat-treated, 10 Hz

Table B.4. Mean values from test shown in [Lohaus et al., 2012] at $S_{c,min} = 0.05$.

B.2 Data from Sørensen

In this section *data series 3* is presented in table B.5.

$\log N$	$S_{c,max}$	Runout	Other info
6.30	0.60	Yes	0.35 Hz
6.30	0.60	Yes	0.35 Hz
6.43	0.60	Yes	5 Hz
6.31	0.60	Yes	5 Hz
6.31	0.60	Yes	5 Hz
4.85	0.60	No	5 Hz
4.63	0.60	No	5 Hz
3.64	0.60	No	5 Hz
6.30	0.60	Yes	10 Hz
6.30	0.60	Yes	10 Hz
6.09	0.60	No	10 Hz
5.39	0.60	No	10 Hz
5.22	0.60	No	10 Hz
3.62	0.60	No	10 Hz
4.37	0.76	No	10 Hz
4.19	0.76	No	10 Hz
3.87	0.76	No	10 Hz
3.71	0.76	No	10 Hz
3.62	0.76	No	10 Hz
3.45	0.76	No	10 Hz
4.27	0.76	No	10 Hz
3.89	0.76	No	10 Hz
3.52	0.76	No	10 Hz
3.46	0.76	No	10 Hz
3.11	0.76	No	10 Hz
3.04	0.76	No	10 Hz

Table B.5. Data from [Sørensen] performed at $S_{c,min} = 0.042$.

Failure Surface

In this chapter the appendix for chapter 5 is presented.

C.1 Comparison of Goodman diagrams

In [Lohaus et al., 2012] the discontinuous rational function shown in eq. (C.1) is used to approximate the Goodman line at $\log N = 8$.

$$S_{c,max} = \frac{a + b S_{c,min}}{1 + c S_{c,min} + d S_{c,min}^2} \quad (\text{C.1})$$

where the parameters a, b, c and d can be found in [Lohaus et al., 2012] as the values listed in table C.1.

Constant	Value from [Lohaus et al., 2012]
a	0.45
b	1.8
c	1.8
d	-0.3

Table C.1. Values for the constants used in eq. (C.1).

This differs from the third order polynomial that is assumed in this report so a comparison of the two approaches is made. On figure C.1 the two functions are plotted against the 4 data points they are based on.

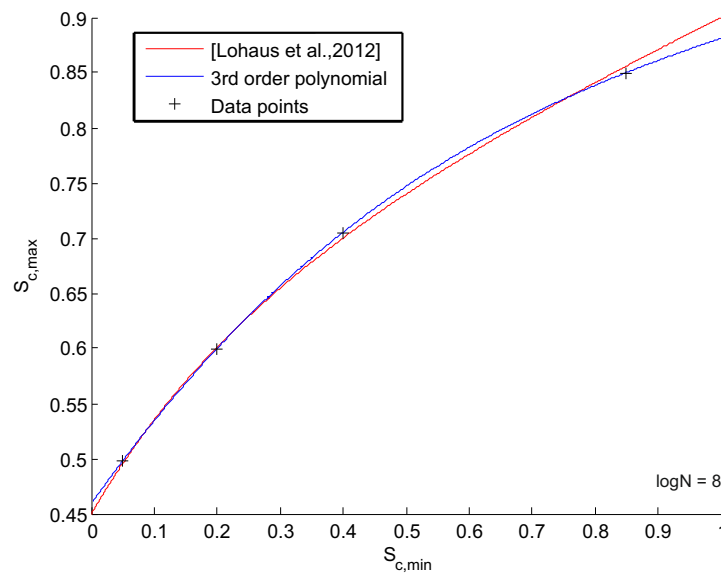


Figure C.1. Comparison between the two approaches to constructing the Goodman diagram at $\log N = 8$.

On the figure it can be seen that the two lines show a lot of similarity however the 3rd order polynomial is capturing all the data points precisely. In practice both approaches are applicable, however given the slightly improved precision of the third order polynomial this is chosen as the best fit in this report.

C.2 Dependency of Concrete Strength

In this section the intersection of the regression lines from various concrete strengths shown on figure 5.11 are shown for $\log N = 6$ and $\log N = 4$. Figure C.2 shows the intersections at $\log N = 6$ with the best fitting linear regression line using MLM and figure C.3 shows the same for $\log N = 4$.

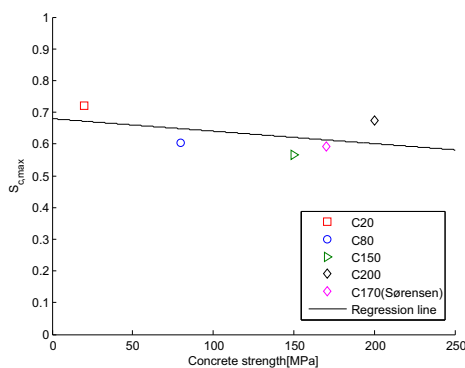


Figure C.2. Fatigue strength of concrete at $\log N = 6$ for different concrete strengths.

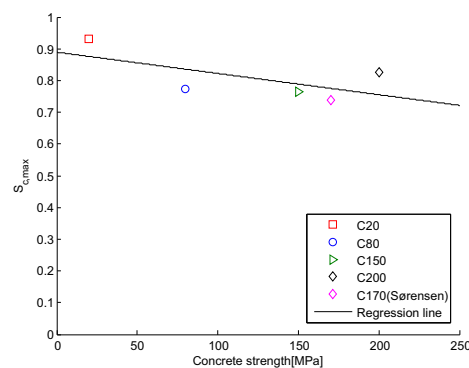


Figure C.3. Fatigue strength of concrete at $\log N = 4$ for different concrete strengths.

It can be seen that as the intersections are captured at lower $\log N$ the line get a lower slope however it has to mentioned that the regression lines are made with

very few data points. This makes the credibility of the lines quite low when they are used to predict general behavior. By looking at the data it does not seem like a clear tendency that the fatigue strength of concrete gets relatively lower as the compressive strength increases. By looking at the points it also seem like the C20 concrete contributes a lot to the lower slope of the regression lines. As this report focuses on high strength concrete the C20 concrete could be neglected which would probably flatten out the regression lines. However this has not been investigated any further.

C.3 Validation of Surface

To validate the developed surface it is compared to the one in [Lohaus et al., 2012] and to the regression lines for the data at $S_{c,min} = 0.20$ and $S_{c,min} = 0.40$ in figures C.4 and C.5.

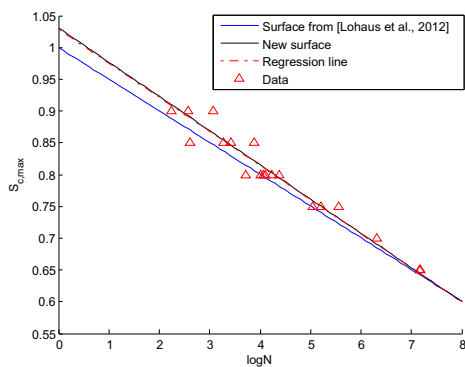


Figure C.4. Comparison between the new surface, the one in [Lohaus et al., 2012] and the regression line for the data at $S_{c,min} = 0.20$.

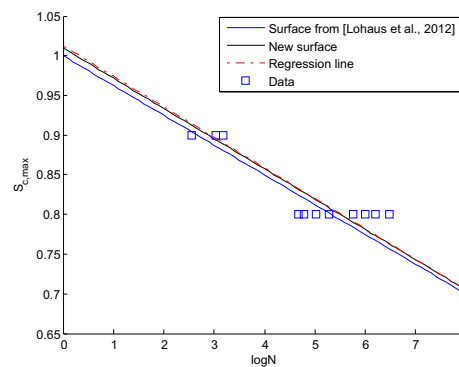


Figure C.5. Comparison between the new surface, the one in [Lohaus et al., 2012] and the regression line for the data at $S_{c,min} = 0.40$.

It can be seen on both figures that the developed surface captures the data more accurately than the surface from [Lohaus et al., 2012].

Uncertainty Modeling

In this chapter the appendix corresponding to chapter 9 in the main report is shown.

D.1 Coefficient of Variation for f_c

In [Jensen, 2008] a table is given with mean and characteristic values for the compressive cylinder concrete strength. As it is assumed that the strength is lognormal distributed and the characteristic strength is taken as the 5th percent quantil a coefficient of variation and standard deviation can be derived from the values. In table D.1 the characteristic and mean values from the table [Jensen, 2008] is shown with the derived standard deviation and coefficient of variation.

f_{ck}	12	16	20	25	30	35	40
f_{cm}	20	24	28	33	38	43	48
σ	5.82	5.59	5.45	5.33	5.25	5.19	5.14
COV	0.29	0.23	0.19	0.16	0.14	0.12	0.11
f_{ck}	45	50	55	60	70	80	90
f_{cm}	53	58	63	68	78	88	98
σ	5.10	5.08	5.05	5.03	4.99	4.97	4.94
COV	0.10	0.09	0.08	0.07	0.06	0.06	0.05

Table D.1. Values for the uncertainty on concrete strength from [Jensen, 2008].

It can be seen from the table that the coefficient of variation is varying a lot as the concrete strength varies. However a tendency is that it is getting smaller as the concrete is getting stronger. Furthermore it can be seen that the standard deviation of the concrete is almost the same for all concrete strengths, but as the COV it is also decreasing slightly as the strength increases. This shows another way of modelling the uncertainty regarding compressive strength of concrete than keeping COV constant as has been chosen in the main report.

D.2 Model I

In this section the model uncertainty for data combination 2, 3 and 4 are shown for both the developed surface and the surface from [Lohaus et al., 2012].

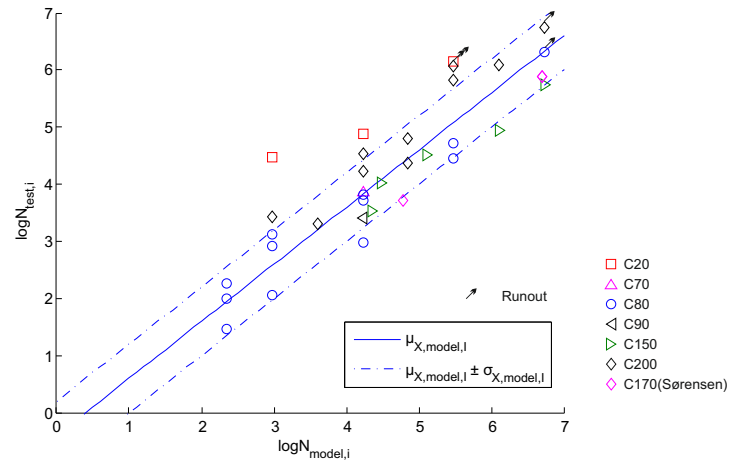


Figure D.1. Model uncertainty using data combination 2 for the developed surface.

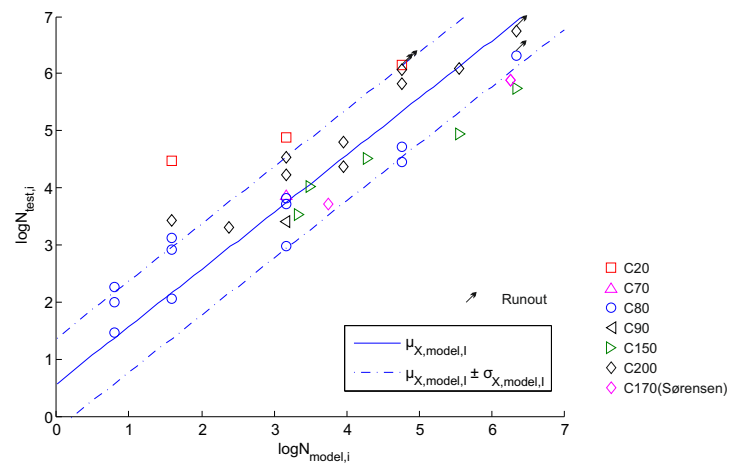


Figure D.2. Model uncertainty using data combination 2 for the surface in [Lohaus et al., 2012].

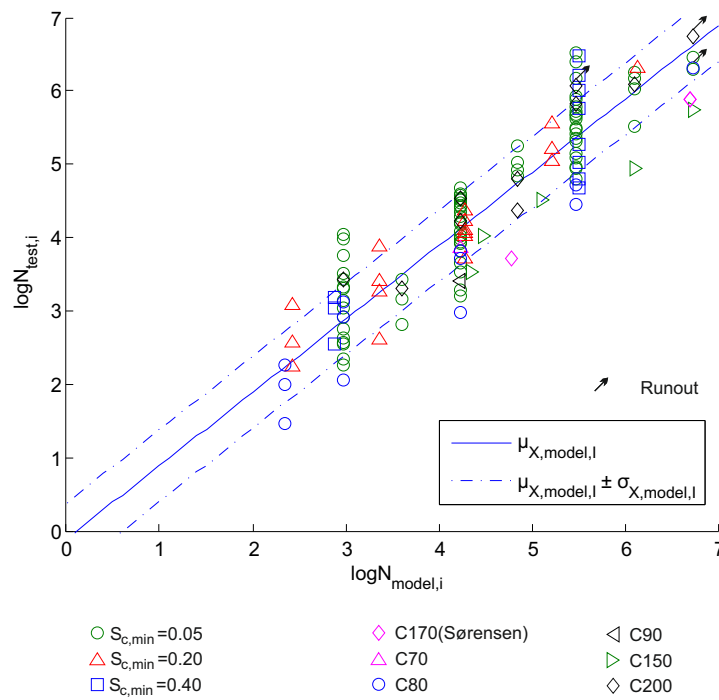


Figure D.3. Model uncertainty using data combination 3 for the developed surface.

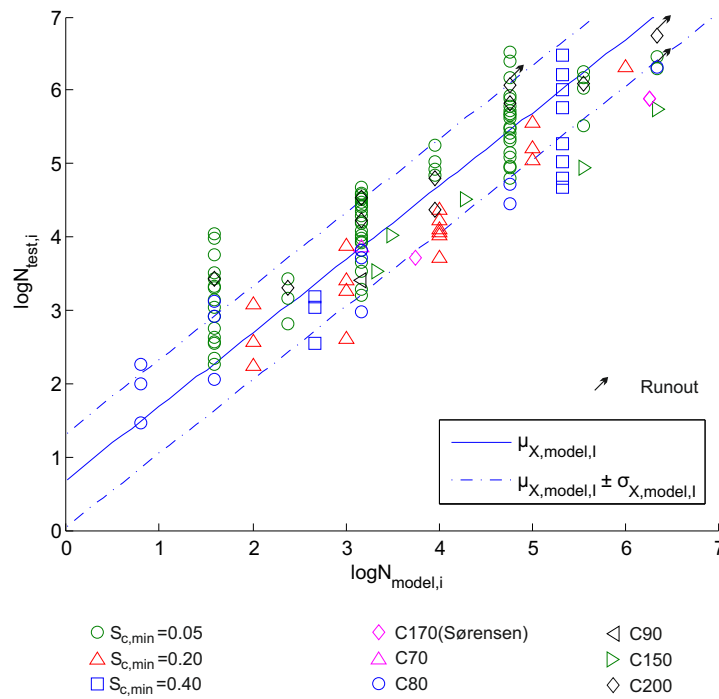


Figure D.4. Model uncertainty using data combination 3 for the surface in [Lohaus et al., 2012].

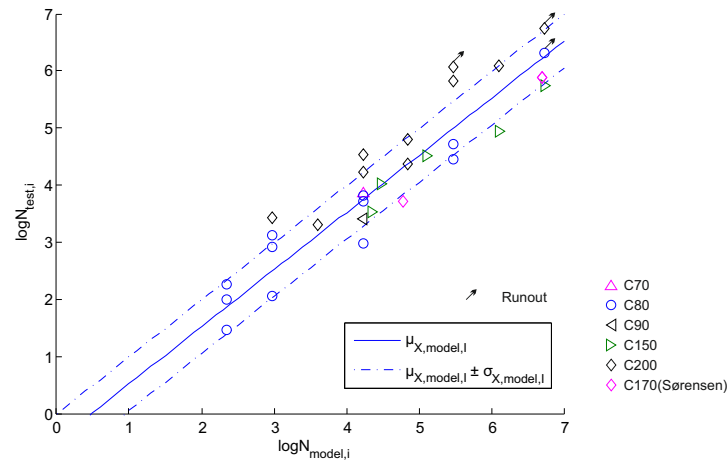


Figure D.5. Model uncertainty using data combination 4 for the developed surface.

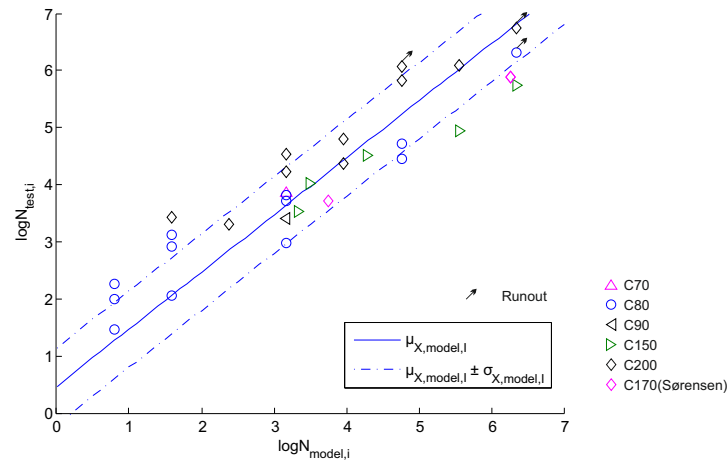


Figure D.6. Model uncertainty using data combination 4 for the surface in [Lohaus et al., 2012].

D.3 LSE 1,II

In this section the appendix associated to LSE 1,II is presented.

LSE 1,II is constructed from realizations of the SN -curves, from which the points Q_1 to Q_3 and P_1 to P_3 are found. To these points the Goodman diagram and the $S_{c,max} = 1$ line will be fitted. Due to the difference in the standard deviations for the SN -curves the points can differentiate, and it has to be investigated if the lines still act appropriately.

D.3.1 SN -curves

In chapter 4 SN -curves are derived from the data presented in appendix B using MLM. the constants from the investigation can be seen in table 4.5. The MLM investigation also yielded a hessian matrix, which can be used to obtain the

covariance matrix.

$$C = (-H)^{-1}$$

Where

C	Covariance matrix
H	Hessian matrix

Through the covariance matrix the correlation and the standard deviations for each variable is found. The results are listed in table D.2, and the correlation matrices can be seen from eq. (D.1) to eq. (D.2).

	k_1		k_2		ϵ		
	μ	σ	μ	σ	μ	σ	σ_σ
$S_{c,min} = 0.05$	-12.50	0.6	14.23	0.47	0	0.46	0.04
$S_{c,min} = 0.20$	-18.65	1.02	19.19	0.81	0	0.32	0.05
$S_{c,min} = 0.40$	-26.02	3.83	26.35	3.17	0	0.56	0.12

Table D.2. Results from the SN-curves found by MLM.

$$\rho_{0.05} = \begin{bmatrix} 1.00 & 0.99 & 0.04 \\ 0.99 & 1.00 & 0.04 \\ 0.04 & 0.04 & 1.00 \end{bmatrix} \quad (D.1)$$

$$\rho_{0.20} = \begin{bmatrix} 1.00 & 1.00 & 0.10 \\ 1.00 & 1.00 & 0.10 \\ 0.10 & 0.10 & 1.00 \end{bmatrix}$$

$$\rho_{0.40} = \begin{bmatrix} 1.00 & 1.00 & 0.14 \\ 1.00 & 1.00 & 0.14 \\ 0.14 & 0.14 & 1.00 \end{bmatrix} \quad (D.2)$$

Where

$$\rho = \begin{bmatrix} \rho_{k_1,k_1} & \rho_{k_1,k_2} & \rho_{k_1,\epsilon} \\ \rho_{k_2,k_1} & \rho_{k_2,k_2} & \rho_{k_2,\epsilon} \\ \rho_{\epsilon,k_1} & \rho_{\epsilon,k_2} & \rho_{\epsilon,\epsilon} \end{bmatrix}$$

As it can be seen the variables k_1 and k_2 are fully correlated, due to this k_1 will be set as a deterministic value found in table D.2. The MLM investigation is then done again but where k_1 is not optimized. The new values for the lines can be seen in table D.3, and the correlations can be seen in eq. (D.3) to eq. (D.4).

	k_1		k_2		ϵ		
	μ	σ	μ	σ	μ	σ	σ_σ
$SN_{0.05}$	-12.50	-	14.23	0.05	0	0.46	0.04
$SN_{0.20}$	-18.65	-	19.19	0.07	0	0.32	0.05
$SN_{0.40}$	-26.02	-	26.35	0.17	0	0.56	0.12

Table D.3. Results from the SN -curves found by MLM .

$$\rho_{0.05} = \begin{bmatrix} 1.00 & 0.00 \\ 0.00 & 1.00 \end{bmatrix} \quad (D.3)$$

$$\rho_{0.20} = \begin{bmatrix} 1.00 & 0.01 \\ 0.01 & 1.00 \end{bmatrix}$$

$$\rho_{0.40} = \begin{bmatrix} 1.00 & 0.00 \\ 0.00 & 1.00 \end{bmatrix} \quad (D.4)$$

Where

$$\rho = \begin{bmatrix} \rho_{k_2,k_2} & \rho_{k_2,\epsilon} \\ \rho_{\epsilon,k_2} & \rho_{\epsilon,\epsilon} \end{bmatrix}$$

D.3.2 Goodman diagram

The Goodman line is constructed from the points, P_1 to P_3 , where the SN -curves crosses $\log N = 8$. These points stems from a realization of the SN -curves and are therefore modelled random when the SN -curves are.

The Goodman line has to act properly for all realizations of the points, which can be problematic due to the different standard deviations of the SN -curves. To investigate the Goodman line the SN -curves are realized for different probabilities, and the points are found for each realization. The realized points to different probabilities can be seen on figure D.7. When realizing the SN -curves only the error term ϵ is realized while k_2 is set as the mean value. This is due that the standard deviation is significantly larger on the error term. The SN -curves are assumed fully correlated for this investigation.

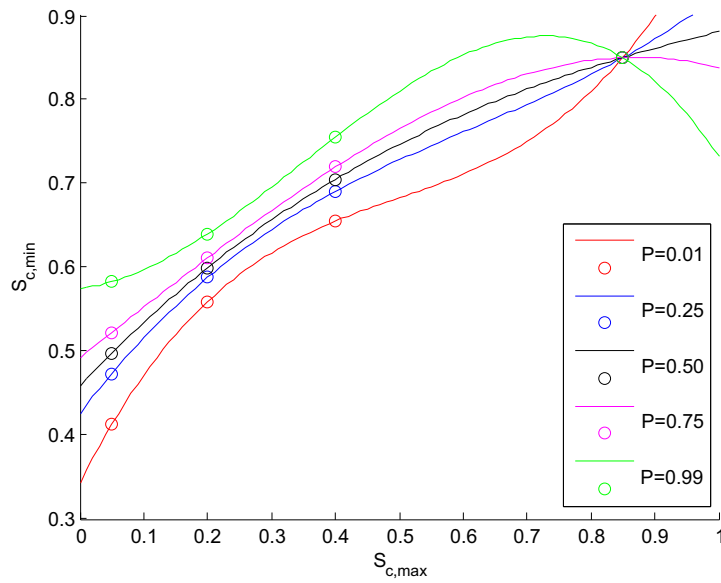


Figure D.7. Realized points and fitted 3rd. degrees polynomials.

As it can be seen on figure D.7 the points for the more extreme probabilities make the 3rd order polynomial bad at capturing the tendency of the points. To ensure that the Goodman diagram act probably some of the degrees of freedom in the polynomial are removed by restricting the constants in the function, see eq. (D.5).

$$S_{c,max}(S_{c,min}, \log N = 8) = a_{N8} S_{c,min}^3 + b_{N8} S_{c,min}^2 + c_{N8} S_{c,min} + d_{N8} \quad (D.5)$$

Figure D.8 shows the points and the Goodman diagrams where two of the degrees of freedom has been restricted, namely a_{N8} and b_{N8} which is set as the values found in table 5.2.

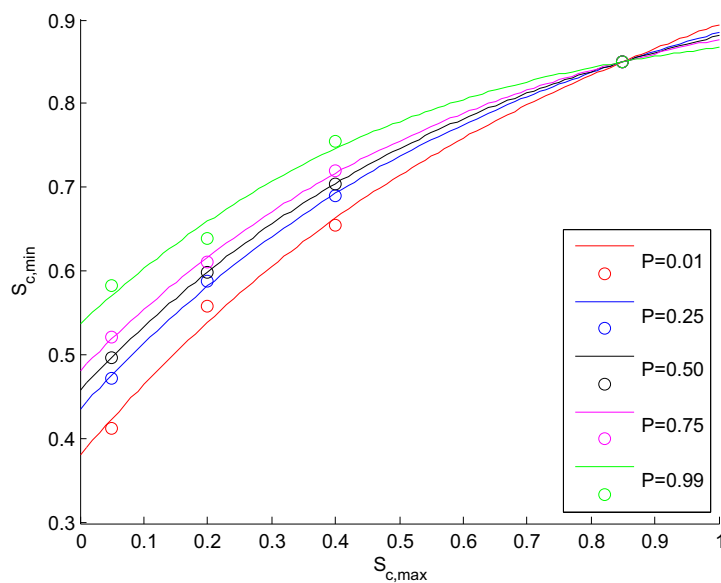


Figure D.8. Goodman diagram fitted to different quantiles.

By looking at figure D.8 it is evaluated that removing two degrees of freedom is a proper solution to the problem.

D.3.3 $S_{c,max} = 1$ line

For the line at $S_{c,max} = 1$ the same problem as presented for the Goodman line arises, which is solved in a similar manner. Eq. (D.6) shows the expression which is used to describe the line at $S_{c,max} = 1$.

$$\log N(S_{c,min}, S_{c,max} = 1) = \frac{1}{(\log(S_{c,min} + 1) a_{S_{max}1} + b_{S_{max}1})} + c_{S_{max}1} \quad (D.6)$$

The constants $a_{S_{max}1}$, $b_{S_{max}1}$ are restricted to the values found in table 5.4, figure D.9 shows the realized points and there corresponding lines.

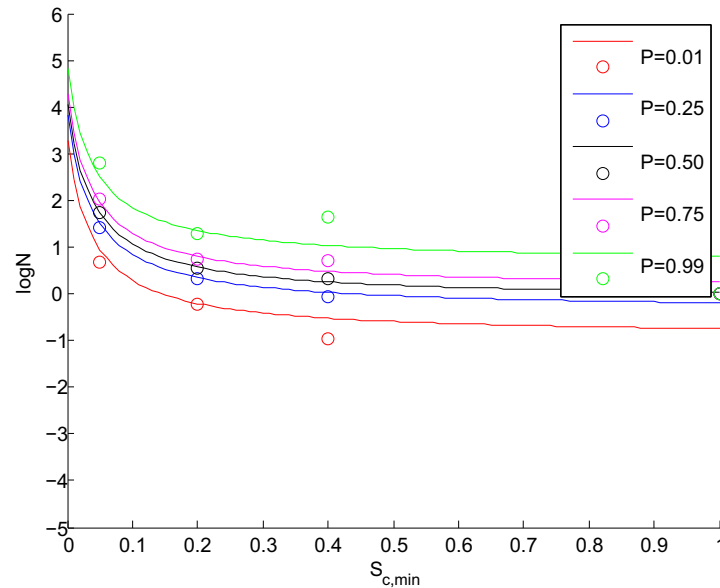


Figure D.9. $S_{c,max} = 1$ line fitted to different quantiles.

It is deemed that the expression acts properly.

D.4 $X_{1,II}$

In this section the appendix concerning the model uncertainty $X_{1,II}$ is presented. The model uncertainty used in LSE 1,II, is found by comparing the predicted values of $\log N$ to the observed values for $\log N$ for various concrete strengths. For LSE 1,II the predicted values are found from the mean failure surface, even though the failure surface is stochastic. Figure D.10 shows the mean value of the model uncertainty for different quantiles of the error term in the SN -curves.

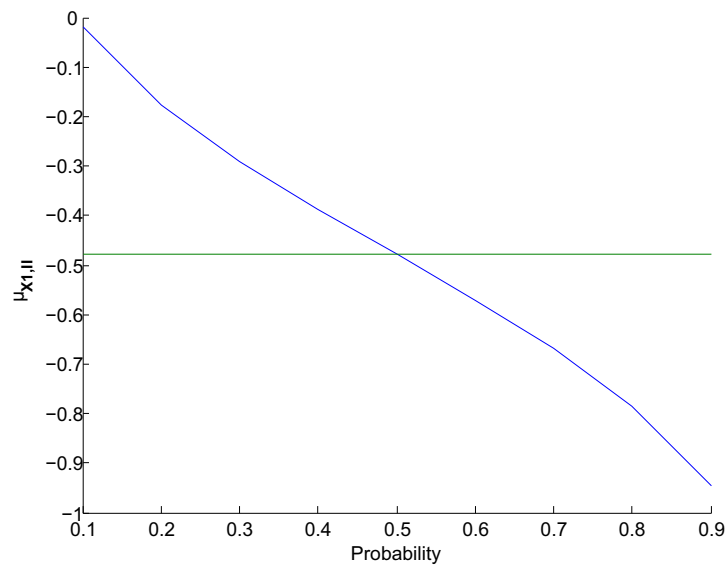


Figure D.10. Mean values of the model uncertainty to different realizations of the failure surface. The green line represent the mean value used for the model uncertainty.

The same investigation is made for the standard deviation of the model uncertainty and can be seen on figure D.11.

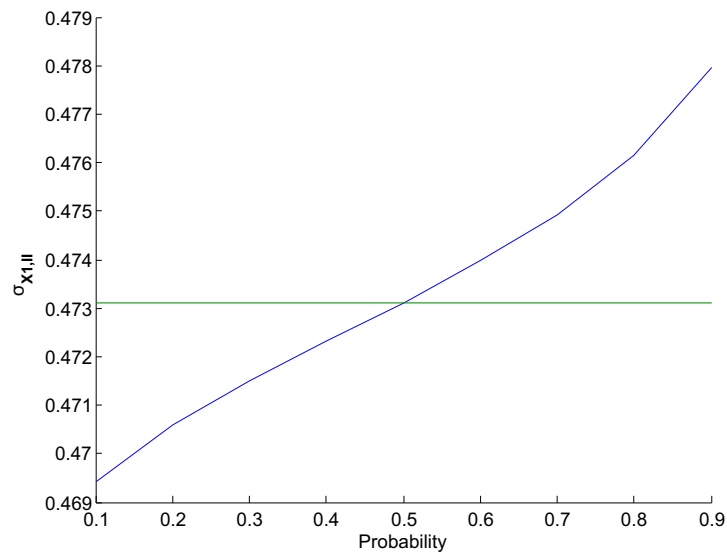


Figure D.11. Mean values of the model uncertainty to different realizations of the failure surface. The green line represent the mean value used for the model uncertainty.

By seeing figures D.10 and D.11, it is deemed adequate to model the uncertainty corresponding to the mean failure surface.

D.5 Form and Monte Carlo

In this section a comparison between a reliability index found through Monte Carlo simulation and FORM analysis is made. This is done to validate that the FORM analysis yields plausible results. table D.4 shows a cumulative reliability obtained for LSE 1, I, for a representative design case.

	Monte Carlo	FORM
β	2.13	2.14
p_f	$1.68 \cdot 10^2$	$1.61 \cdot 10^2$

Table D.4. Comparison of reliability indices for FORM and Monte Carlo, for the wind turbine foundation design case with a z of 0.992 m^3 for the 24. year.

To ensure that the Monte Carlo simulation yields correct results a convergence analysis is shown in figure D.12.

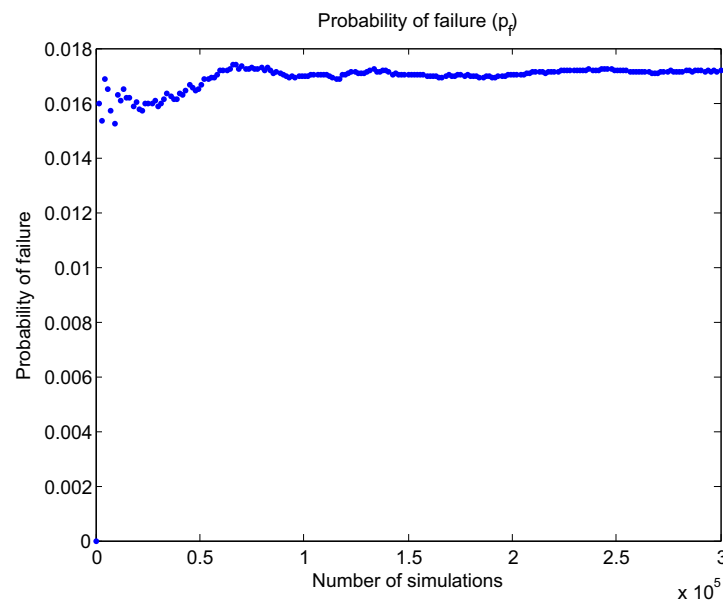


Figure D.12. Convergence analysis for Monte Carlo.

It can be seen that FORM and Monte Carlo yields similar results.

D.6 Convergence of Reliability

It is seen that for some instance the limit state equations has trouble converging, this is a frequent problem for LSE 1, II. The convergence problem stem from the construction of the limit state equation itself, where some *if* statements are present. LSE 1, II, as stated in the report are altered from each realization, this makes convergence difficult to obtain. To make sure that the reliability analysis gives a somewhat reliable result, that is more independent of the number of iterations used, the found reliability dependent of number of iterations, $\beta(itt)$ are

meaned over a given number of iterations, figure D.13 shows an representative example of this.

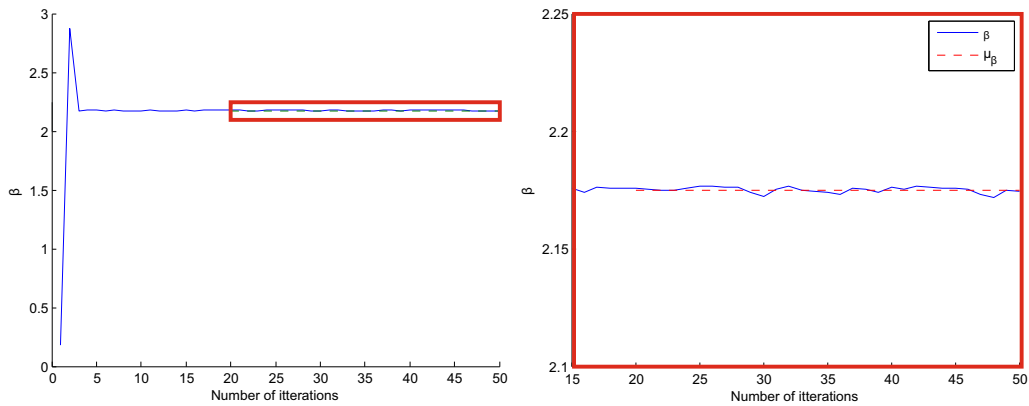


Figure D.13. Example of assumption used to find reliability when convergence is not obtained.

This seems to approximate to decent solutions. However the problem makes it difficult to make meaningful sensitivity stuides.

D.7 Stress States for the Bridge Design Case

As the reliability indices for LSE 1 and LSE 2 are very similar for the bridge design case it indicates that the fatigue damage is accumulated at high $S_{c,min}$. To see if this is the case the stress states for the bridge using Eurocode are shown on figure D.14. The stress states are found through the design equation used for Eurocode.

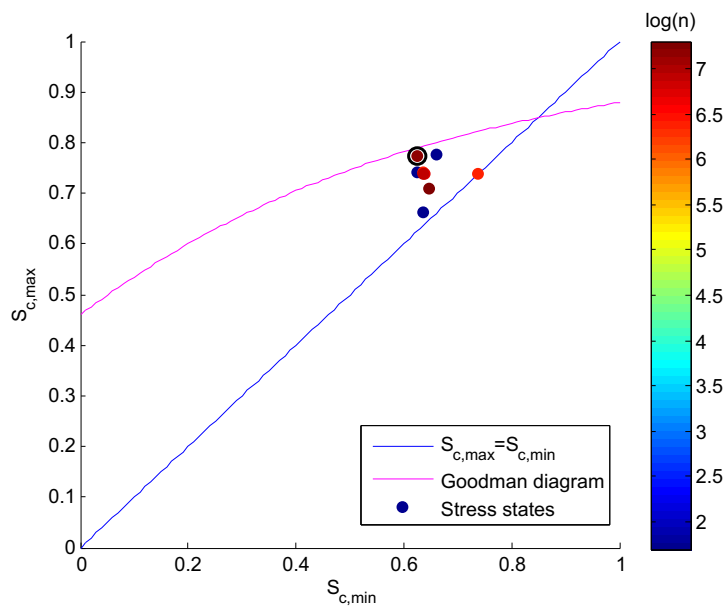


Figure D.14. Stress states applied to the bridge using Eurocode.

It is noted that the stress state marked with a back circle is estimated to account for approximately 98% of the total fatigue damage.

On the figure the $S_{c,min} = S_{c,max}$ -line and the Goodman diagram from the developed surface is shown as well. This indicates that the stress states of the bridge are in the transition where the developed surface uses linear approximation and as such some results from the bridge are expected to be slightly conservative.

D.8 Stress States for the Wind Turbine Design Case

As the reliability indices for LSE 1 and LSE 2 are very different for the wind turbine design case it indicates that the fatigue damage is accumulated at low $S_{c,min}$. To see if this is the case the stress states for the wind turbine using Eurocode are shown on figure D.15. The stress states are found through the design equation used for Eurocode.

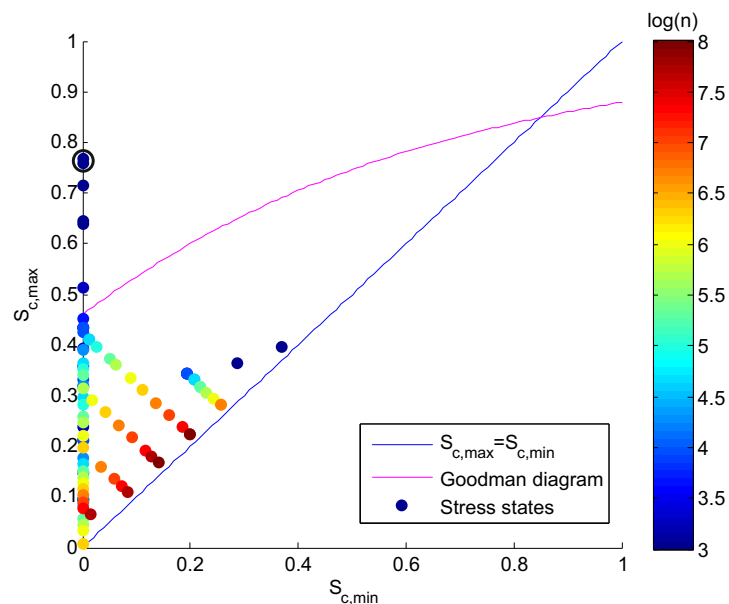


Figure D.15. Stress states applied to the wind turbine using Eurocode.

It is noted that the stress states marked with a back circle is estimated to account for approximately 90% of the total fatigue damage.

On the figure the $S_{c,min} = S_{c,max}$ -line and the Goodman diagram from the developed surface is shown as well. This indicates that the stress states that contribute to the fatigue damage of the wind turbine are outside the area of linear extrapolation for the developed surface. However the damage is accumulated at $S_{c,min} = 0$ where the developed failure surface is probably imprecise.